Development and Evaluation of Semi-open Loop Ground Source Heat Pump Systems

Hadi Farabi Asl

2017

Graduate School of Engineering and Resource Science
Akita University

Table of Contents

List of Figures

List of Tables

ABSTRACT

Renewable energies have an important role in providing energy demands and reducing environmental damages due to the fossil fuel consumption all over the world. Among the commercialized sources of renewable energies, the importance of geothermal resources is rising worldwide. Among direct utilizations of geothermal energy, Ground Source Heat Pumps (GSHPs) are a rapidly growing usage of geothermal energy, accounting for 70% of the installed capacity and 50% of the total direct geothermal energy use in 2015 worldwide. However, despite being one of the most common applications of geothermal energy, this technology is not as popular as other renewable energies in Japan due to the high drilling costs. New technologies are focused on possible opportunities to increase the GSHP system performance and make it competitive with conventional heating and cooling systems. The objective of this study is to investigate the effect of water pumping and injection on convective heat transfer in Ground Heat Exchangers (GHEs).

At the first step of this study, the effect of water pumping and injection in Thermal Response Tests (TRTs) was investigated. In this step, nine sets of TRTs were performed with different rates of water injection or pumping and different injecting water temperature on a GHE drilled in the campus of Akita University, Japan. Results of TRTs showed that with increasing water injection and pumping rate, average temperature of heat medium decreased. For example, the average of heat medium temperature for TRT without injection or pumping was 3.8°C higher than TRT with L/min water injection after 48 hours of heating. The GHE was modeled using a numerical simulator and outlet water temperature and ground temperature recovery were history-matched based on the TRT data. Then, sensitivity analyses were carried out to investigate the effects of injecting or pumping with different water rates and different inlet water temperatures and also different natural groundwater velocities. Results of experiments and simulations showed that heat exchange rate between ground and GHE increased significantly by applying water injection or pumping inside the GHE.

In the next step of this study, a new semi-open loop GSHP system was introduced that consists of two ungrouted GHEs. In order to increase the heat transfer rate of GHEs, groundwater is pumped from one GHE and is injected to the other one using a water pump. The GHE length is 60 m each and this system could meet the heating and cooling demands of 3 rooms in Akita University campus with total area of 100 m^2. Before starting the heating and cooling tests, two sets of TRTs were performed and effective thermal conductivity was calculated for each GHE. High effective thermal conductivity and fast temperature recovery after the TRTs showed the possibility of fast groundwater flow in the formation.

The effect of water-pumping and injection on the system performance was evaluated in heating and cooling field tests on the GSHP system. A numerical model was constructed and was validated by the experimental data. The system performance under different groundwater velocities and operating conditions was then evaluated in a sensitivity analyses. The results of

field tests and sensitivity analysis showed that water pumping and injection, especially in formations with slow groundwater flow, has significant effect in enhancing the system performance enhancement and also in increasing GHE heat transfer capacity. In the formations with fast natural groundwater flow, the effect of water pumping and injection on COP enhancement was limited to 12%. But in the absence of groundwater flow, this parameter could increase up to 40%-100%, for heating and cooling operations. The numerical model was modified to evaluate the effect of GHE spacing on thermal performance of semi-open loop GSHP system. Results of the numerical simulations showed that 5 m distance between GHEs is enough to ensure limited thermal interference between the GHEs in the semi-open loop GSHP system.

The economic study of semi-open loop GSHP system is the last step of the research. A sample building, which was built on a ground having a similar condition to the experimental condition, was considered and the hourly heating and cooling loads based on the Akita city's climate were calculated and applied in the simulation. The validated numerical model was used to calculate the necessary GHE length in the absence of natural groundwater flow, with and without water pumping and injection. This process was repeated for the formation with slow groundwater flow. According to the economic parameters in Japan such as annual inflation rate and interest rate, the final saving of semi-open loop GSHP system was calculated considering the parameters including drilling costs, heat pump and distribution system costs, water pumping and injection system costs, labor and piping costs. Results of economic analysis showed that semi-open loop GSHP system is more economical in comparison with normal GSHP systems, though the merit depends on groundwater velocities. The results of economic analysis showed the important effect of water pumping and injection on drilling cost reduction, especially in slow groundwater flow condition. Drilling cost could be reduced averagely around 65%, which is very important in the countries with high drilling cost like Japan. Considering the costs of water pumping and injection in GSHP system, semi-open loop technology was estimated to reduce system cost around 22%-36% in different scenarios.

As the conclusion, the introduction of the semi-open loop system is considered to be the promising solution in improving the performance of GSHP systems and its economic feasibility as a renewable and efficient heating and cooling technology.

Chapter 1: INTRODUCTION AND STUDY MOTIVATION

1.1 Trends of energy demand

Energy is an essential need for societies and energy security is one of the most important concerns for governments and decision-makers worldwide. The energy demand in different countries is increasing every year. According to U. S. Energy Information Administration (EIA) report (2016) there will be a significant growth in worldwide energy demand over the 28-year period from 2012 to 2040. Total world consumption of marketed energy expands from 160.1 PWh in 2012 to 184.3 PWh in 2020 and to 238.8 PWh in 2040 (Fig. 1-1).
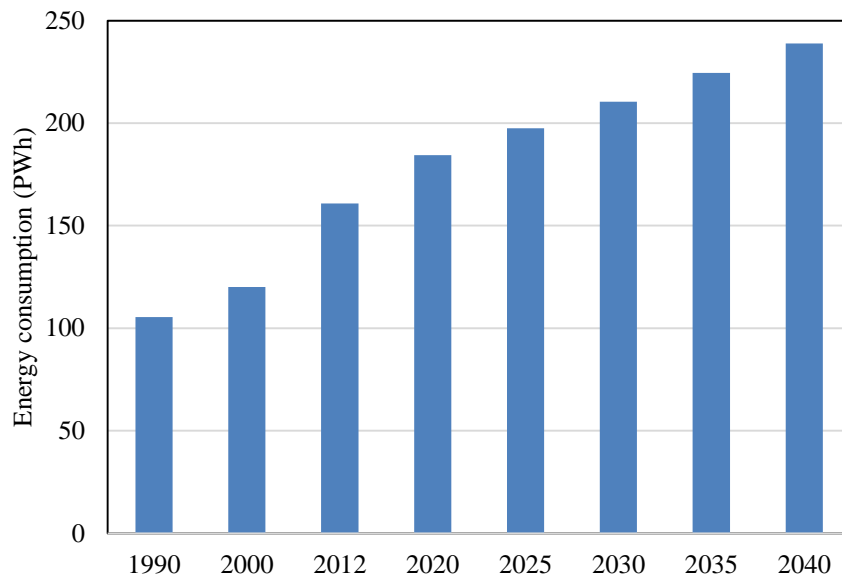
Fig. 1-1 World energy consumption, 1990-2040 (10^{15} Wh).

A 48% increase from 2012 to 2040 Economic growth, as measured in gross domestic product (GDP), is a key determinant in the growth of energy demand. The world's GDP (expressed in purchasing power parity terms) rises by 3.3% per year from 2012 to 2040.

Economic growth, along with accompanying structural changes, strongly influences world energy consumption. As countries develop and living standards improve, energy demand grows rapidly. For instance, in nations experiencing fast-paced economic growth, the share of the populace demanding improved housing, which requires more energy to construct and maintain, often increases. Increased demand for appliances and transportation equipment, and growing capacity to produce goods and services for both domestic and foreign markets, also lead to higher energy consumption.

Fossil fuel consumption is causing different hazards to the environment. One of the main damages is CO_2 emission to the atmosphere. World energy-related CO_2 emissions rise from 32.2 billion metric tons in 2012 to 35.6 billion metric tons in 2020 and to 43.2 billion metric tons in 2040, an increase of 34% over the 2012-2040 period (U. S. EIA, 2016) (see Fig. 1-2).
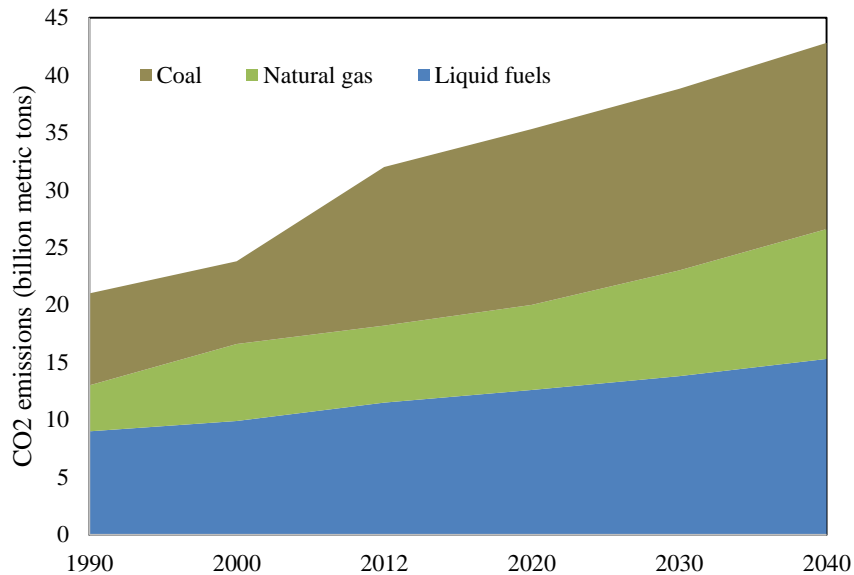
Fig. 1-2 World energy-related CO_2 emissions by fuel type, 1990-2040 (billion metric tons).

Concerns about energy security, effects of fossil fuel emissions on the environment, and sustained high world oil prices in the long term support expanded use of nonfossil renewable energy sources.

1.2 Importance of renewable energies

1.2.1 Renewables in last years

Today, renewable energy technologies are viewed not only as tools for improving energy security and mitigating and adapting to climate change, but are also increasingly recognized as investments that can provide direct and indirect economic advantages by reducing dependence on imported fuels; improving local air quality and safety; advancing energy access and security; propelling economic development; and creating jobs.

The global policy landscape has largely driven the expansion of renewable energy technologies by attracting investment and creating markets that have brought about economies of scale and supported technology advances, in turn, resulting in decreasing costs and fueling sustained growth in the sector. According to the report of Renewable Energy Policy Network for 21st century (REN21, 2014), handful of countries, particularly Germany, Denmark, the US and

10

Spain—have led the way, developing innovative policies that have driven much of the change witnessed over the past decade. Today, Germany's commitment to the "Energiewende", the transition to a sustainable economy based on renewable energy and energy efficiency, as well as Denmark's commitment to 100% renewable energy by 2050, are inspiring other countries around the globe to aim for a renewable energy future. Since 2004, the number of countries promoting renewable energy with direct policy support has nearly tripled, from 48 to over 140, and an ever-increasing number of developing and emerging countries are setting renewable energy targets and enacting support policies. Policy targets have become increasingly ambitious, and their focus is expanding beyond electricity to include heating, cooling, and transport.

Table 1-1 Annual market by renewable power technology (MW/year)

	2004	2005	2006	2007	2008	2009	2010	2011	2012	2013
Solar Photovoltaic	1,052	1,320	1,467	2,392	6,090	7,203	16,817	29,665	29,400	39,000
Concentration Solar Power	0	13	0	75	55	119	595	500	1,034	885
Wind Power	8,207	11,531	15,245	19,866	26,721	38,708	38,850	40,629	44,711	35,467
Bio Power	1,244	1,557	1,974	2,527	806	4,861	7,850	1,069	245	5,000
Geothermal power	13	165	408	340	280	200	200	200	301	500
Hydro Power	19,490	16,057	17,367	25,925	17,082	9,473	23,359	25,000	27,070	40,000
Total	30,006	30,643	36,461	51,125	51,033	60,369	87,471	96,863	102,760	120,852

Table 1-2 Total installed renewable power capacity (GW).

	2004	2005	2006	2007	2008	2009	2010	2011	2012	2013
Solar Photovoltaic	2.6	3.1	4.6	7.6	13.5	21	40	71	100	139
Concentration Solar Power	0.4	0.4	0.4	0.4	0.5	0.7	1.1	1.6	2.5	3.4
Wind Power	48	59	74	94	121	159	198	238	283	318
Bio Power	39	41	43	45	46	51	70	74	78	88
Geothermal power	8.9	9.8	10	10.4	10.7	11	10.2	11.4	11.7	12
Hydro Power	715	-	-	920	950	980	935	960	990	1,000
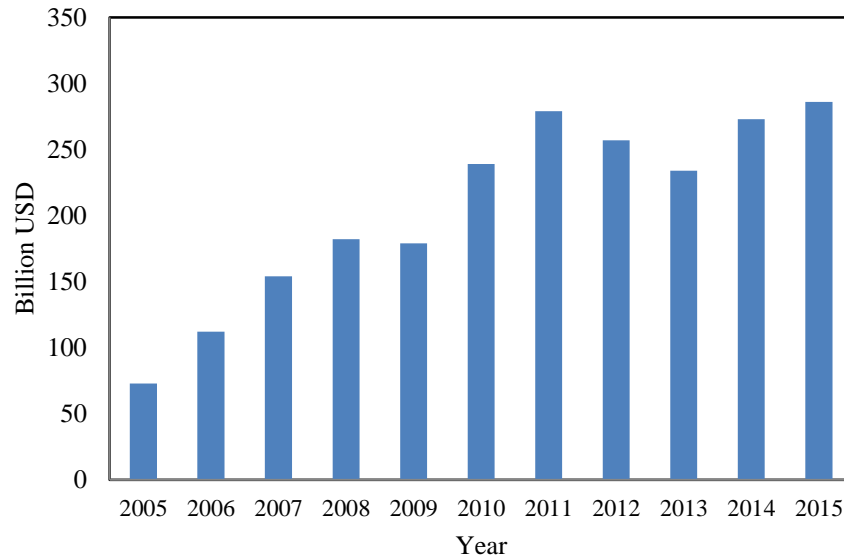
Fig. 1-3 Global new investment in renewable power and fuels, 2005-2015, billion USD

The recent years saw a steady increase in the global demand for renewable energy. While overall primary energy supply from renewables in 2004 was 57.7×10^{18} Joules per year, by 2013 the total supply had grown to 76 EJ annually, an overall increase of 30%. By 2013, renewables supplied approximately 19% of the world's final energy consumption. The new investments on renewable energies are shown in Fig. 1-3. In Table 1-1 and 1-2 it is necessary to note that "-"means that no trustable data are available (REN21, 2014).

According to U. S. Short-term Energy Outlook (EIA, 2016), U. S. has a big share in energy consumption worldwide. In recent years, American government tried to increase the energy production from renewable sources. The amount of energy production from renewable sources for 2006-2017 is shown if Fig. 1-4. Some explanation is necessary about this graph:

- The data for 2016 and 2017 are projections.
- Hydropower excludes pump storage generation.
- Liquid biofuels include ethanol and biodiesel.
- Other biomass includes municipal waste from biogenic sources, landfill gas, and other non-wood waste.

1.2.2 Renewable energies in future

With government policies and incentives promoting the use of nonfossil energy sources in many countries, renewable energy is the world's fastest-growing source of energy, at an average rate of 2.6% per year. The world energy consumption by energy source for 1990-2040 is shown in Fig. 1-5 (EIA, 2016). In this graph, the energy sources categorized as:

- Nuclear
- Renewables
- Natural gas
- Coal
- Liquids

There are different scenarios to predict the share of renewable energy for the next years. Some of the results of these studies are summarized in Table 1-3 (REN 21, 2016). In Table 1-3 it is necessary to note that "-" means that no data are available.
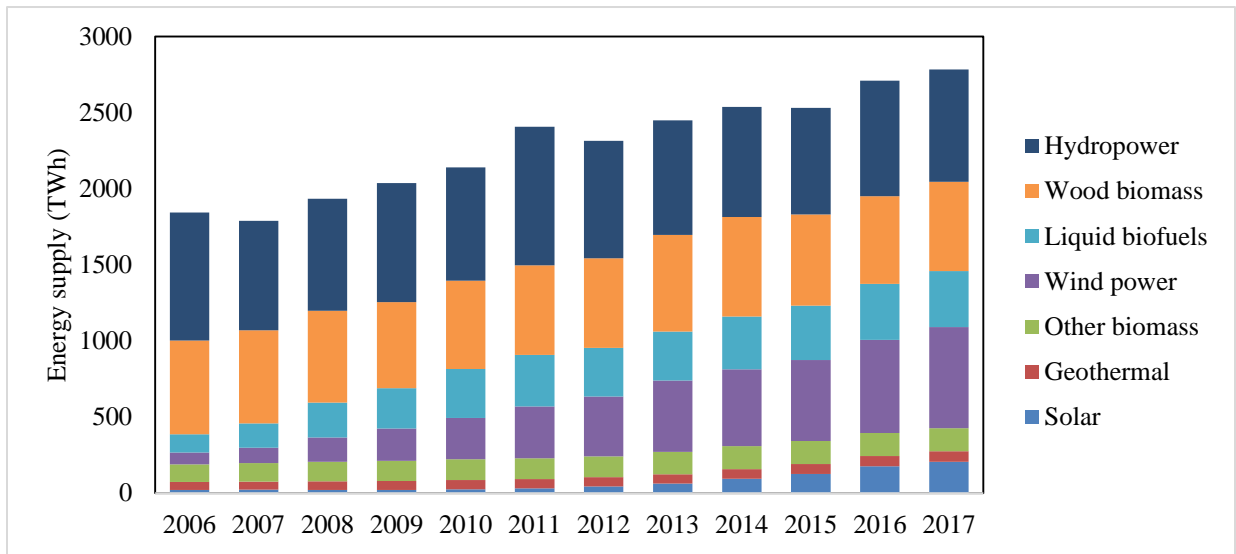
Fig. 1-4 U. S. renewable energy supply (TWh)
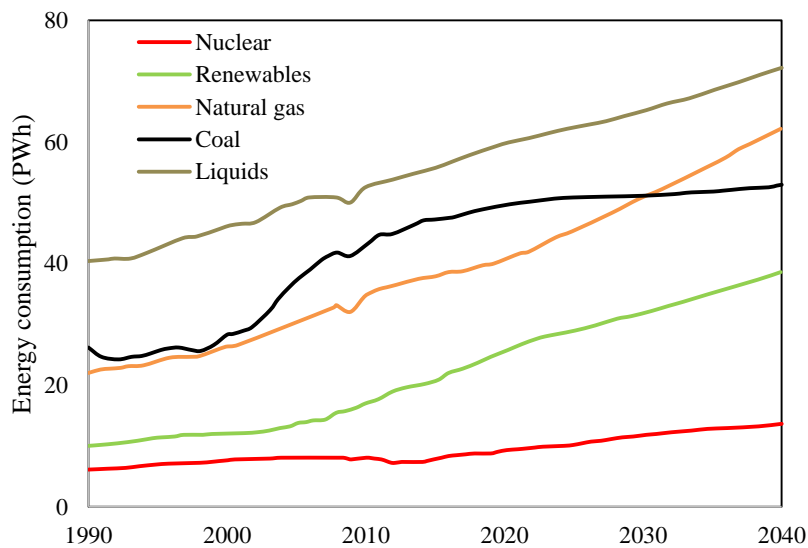
Fig. 1-5 World energy consumption by energy source, 1990-2040 (PWh).

13

Table 1-3 Sectorial shares of renewable energy in recent global scenarios.

	by year	Electricity	Heat	Transport
by 2030-2040				
Exxon Mobil Outlook for Energy: a View to 2040	2040	16%	-	-
BP Energy Outlook (2012)	2030	25%	-	7%
IEA World Energy Outlook (2013) *New Policies*	2035	31%[i]	12%[ii]	6%[iii]
IEA World Energy Outlook (2013) *450*	2035	48%	16%	15%
Greenpeace (2012) Energy Evolution	2030	61%	51%	17%
by 2050				
IEA Energy Technology Prospective (2014) *2DS*	2050	65%[vii]	-	29%[viii]
GEA Global Energy Assessment (2012)	2050	62%	-	30%
Greenpeace (2012) Energy Evolution	2050	94%	91%	72%
WWF (2011) Ecofys Scenario	2050	100%	85%	100%

i. As share of total generation.
ii. As share of total final heat demand, excludes traditional biomass.
iii. Biofuels as share of total transport.
iv. As share of total generation.
v. As share of total final heat demand, excludes traditional biomass.
vi. Biofuels as share of total transport.
vii. As a percentage of gross electricity generation, NB, under the 2DS High Renewable scenarios, renewables as a percentage of gross electricity generation are 80%
viii. Biomass as a share of final energy demand in the transport sector.

1.3 Energy situation and renewable energy policies in Japan

Driven by the urgency of energy security and the energy crisis that followed the Fukushima disaster, renewable energy has become a top priority among Japanese policymakers. While the future of nuclear power is subject to debate, it is certain that renewable and clean energy sources will continue to be focus in Japan. Clean technology is not a new area for Japan, as companies in Japan have been developed solutions since the 1970s.

According to Japan External Trade Organization report (JETRO, 2015), the Japanese market related to global warming mitigation, such as energy saving and renewable energy is estimated to experience a substantial increase of 53% from 32 trillion JPY in 2005 to 49 trillion JPY in 2015 according to statistics from the Ministry of Economy, Trade and Industry (METI). As the Japanese energy market will further liberalize, the Feed-In Tariff (FIT) and additional support from the government for green energies will enable the creation of attractive business models and further growth.

The most dynamism and growth in clean energy in Japan is currently to be found in the renewable energy market. As Japan lags behind in renewable energy generation as compared to other developed countries, high growth can be expected. According to Bloomberg New Energy Finance (2013), in the near future, the FIT is set to continue and diversify to include a separate tariff for offshore wind. Moreover, in the midterm Japan's

support for renewable energy is set to continue as the Japanese government said in a biennial report to the UN in December 2013. While 136.4 billion JPY is put forward for maximizing the installation of renewable energy (an increase of 62% as compared to 2013), just 24.9 billion JPY is attributed to acceleration of research and practical use of high efficiency thermal power generation (an increase of 5%). This latter budget also includes carbon capture and storage research and implementation (Lambrecht, 2014).

From 1973, the time of the first oil shock, energy saving has become an important topic in Japan. While the real GDP in Japan increased 2.4 times from 1973 to 2012, energy consumption only rose by 1.3 times. Therefore, the energy efficiency has been substantially improved and Japan has, as a result, one of the most efficient economies in the world as measured by energy intensity. However, while energy consumption has become more efficient in the industry sector, energy consumption in the consumer sector has gone up 2.4 times (Fig. 1-6) (Lambrecht, 2014). In particular, the building sector shows room for improvement.
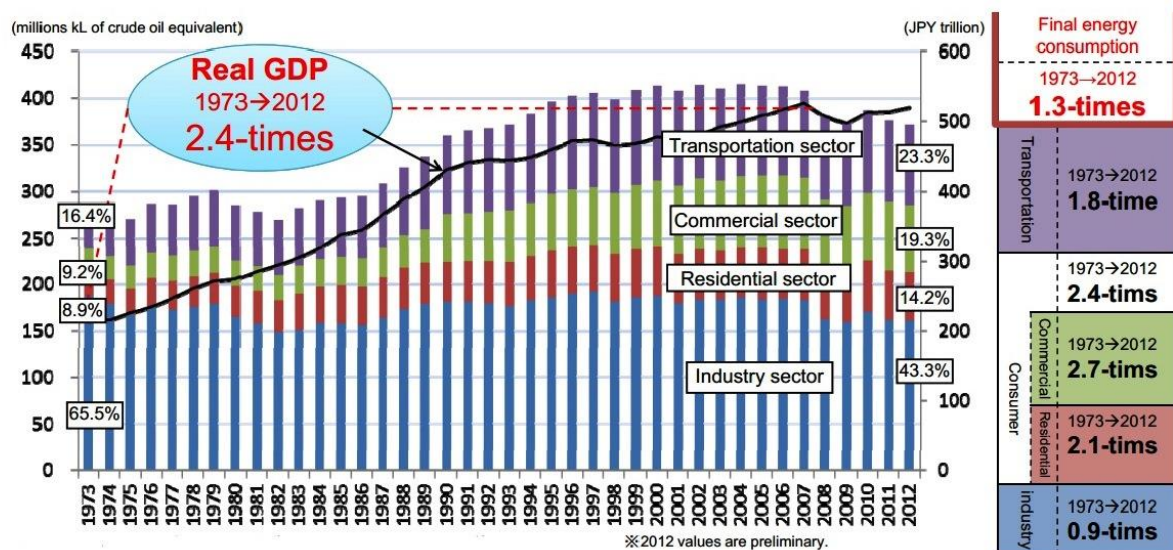
Fig. 1-6 Energy Usage by Sector in Japan 1973-2012.

According to Japan Ministry of Environment report (2013), the "Basic Act on Global Warming Countermeasures" is currently governing Japan's CO_2 reduction measures. It has a long term target of 80% emission reduction cut by 2050. A range of measures are included, from an emission trading scheme, over promoting lifestyle changes and local development (Ministry of Environment, 2010). However, Japan has weakened its greenhouse gas reduction target in November 2013 from a 25% cut from 1990, to 3.8% from fiscal 2005 levels by 2020 (Iwata, 2013). Still, this act provides stimulus for a transition to cleaner technologies.

Renewable energies are the most eye-catching element with the FIT that started in July 2012. It is important to look at the policies of local government. The national government supports the

15

initiatives of local governments that often go much farther in their targets for renewable energy and CO_2 emission reductions. They are often giving tax reductions and subsidies to domestic and foreign companies that wish to develop activities in their region (Lambrecht, 2014). The Japanese budget on a national level to support clean energy is quite substantial. For example, for 2014, the total Japanese budget amounts to 95.88 trillion JPY. Out of this, 872.7 billion JPY is reserved for the "Energy Resources Special Account", which is an extra budget for Ministry of Economy, Trade and Industry (METI). Half of this budget can be directly related to clean energy projects (see Table 1-4), an increase of 16% compared with the previous fiscal year (Lambrecht, 2014).

Table 1-4 Clean energy headings in the METI Energy Resources Special Account budget 2014 (billion JPY)

For the maximum installation of renewable energy	136.4
Acceleration of research and practical use of high efficiency thermal power generation	24.9
Acceleration of energy conservation investments related to energy costs reduction	156.5
Expansion of fuel sells utilization	14.9
Establishment of new energy management model	11.6
Promotion of innovative technological development	117.6
Total	461.9

Related to clean energy, smaller budgets for clean energy can also be found at other ministries such as the Ministry of Environment (e.g. low-carbon society development) and the Ministry of Agriculture, Forestry and Fisheries (e.g. biomass development). Furthermore, the "Special Account for Reconstruction from the Great East Japan Earthquake" provides on its part support for clean energy related reconstruction (e.g. renewable energy support). The distribution of these public funds improves the growth of the clean energy sector in Japan as it often targets bottlenecks in the system such as power grid development (Lambrecht, 2014).

1.4 Energy consumption for heating and cooling in buildings

1.4.1 Heating and cooling energy trends and drivers in buildings

Energy consumed in the buildings sector, divided between residential and commercial end users, accounts for one-fifth of the total delivered energy consumed worldwide. In the IEO2016 Reference case, total world energy consumption in buildings increases by an average of 1.5% per year from 2012 to 2040 (EIA, 2016). Energy use in the residential sector is defined as the energy consumed by households, excluding transportation uses. Energy is used in the residential sector for heating, cooling, lighting, and water heating and for many other appliances and equipment.

Income levels and energy prices influence the ways in which energy is consumed in the residential sector, as do various other factors, such as location, building and household

characteristics, weather, equipment types and efficiencies, access to delivered energy, availability of energy sources, and energy-related policies. As a result, the types and amounts of energy use by households can vary widely within and across regions and countries.

Buildings and activities in buildings contribute to a major share of global environmental concerns (Ürge-Vorsatz et al., 2013). Environmental pressures influenced by the quantity and quality of the energy in buildings are indoor and outdoor air pollution, related and additional health risks and damages, and energy dependence and insecurity. Buildings energy use is a major contributor to energy-related challenges to sustainable development such as deaths attributable to indoor cooking, insufficient energy resources to fuel economic development, lack of access to modern energy services for everyone, and climate change. Much of these environmental problems are due to the energy that fuel buildings and activities within them (Ürge-Vorsatz et al., 2013; Grumber et al., 2012; Ürge-Vorsatz et al., 2012). More concretely, in 2010 the building sector used approximately 115 EJ globally, accounting for 32% of global final energy demand (24% for residential and 8% for commercial) (Ürge-Vorsatz et al., 2015) and 30% of energy-related CO_2 emissions (IEA, 2012). The building sector is also responsible for approximately two-thirds of halocarbon and approximately 25–33% of black carbon emissions. Moreover, the building sector used 23% of the global primary energy and 30% of the global electricity. In Fig. 1-7, the final building energy consumption in the world by end-use in 2010 for residential and commercial buildings is shown (Ürge-Vorsatz et al., 2015). The same data for U. S homes in 1993 and 2009 is shown Fig. 1-8 (EIA online data services).

Energy use in homes will increase every year and accounts for about 13% of world delivered energy consumption in 2040 in the IEO2016 Reference case, as a result of strong economic growth and expanding populations. In 2040, the combined total residential energy use of China and India is double their 2012 total and accounts for 27% of total world residential energy consumption. According to U. S. Energy Information Administration (EIA) report (2016), the world's total commercial sector delivered energy consumption increases by an average of 1.6%/year, and the commercial sector share of total world delivered energy use rises from about 7% in 2012 to about 8% in 2040. Heating and cooling has a big share in energy consumption in the buildings and according using renewable sources to provide this energy and reduce the environmental issues and results a better energy mix in the building sector.

1.4.2　Renewables in building sector

The share of renewable energies in the residential buildings energy consumption is limited. For example, According to U. S. Energy Information Administration (EIA) report (2016), residential sector energy consumption for 1950-2015 in U. S. is shown in Fig. 1-9.
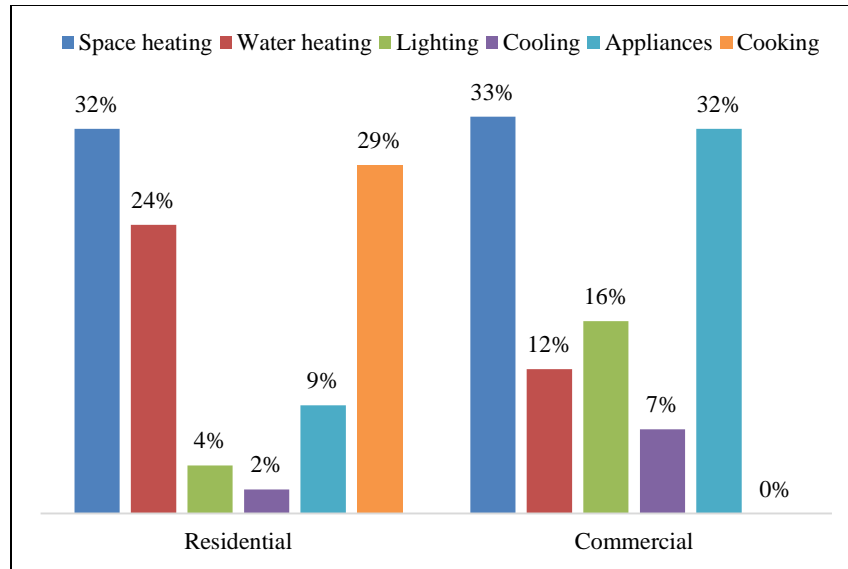
Fig. 1-7 Final building energy consumption in the world by end-use in 2010.
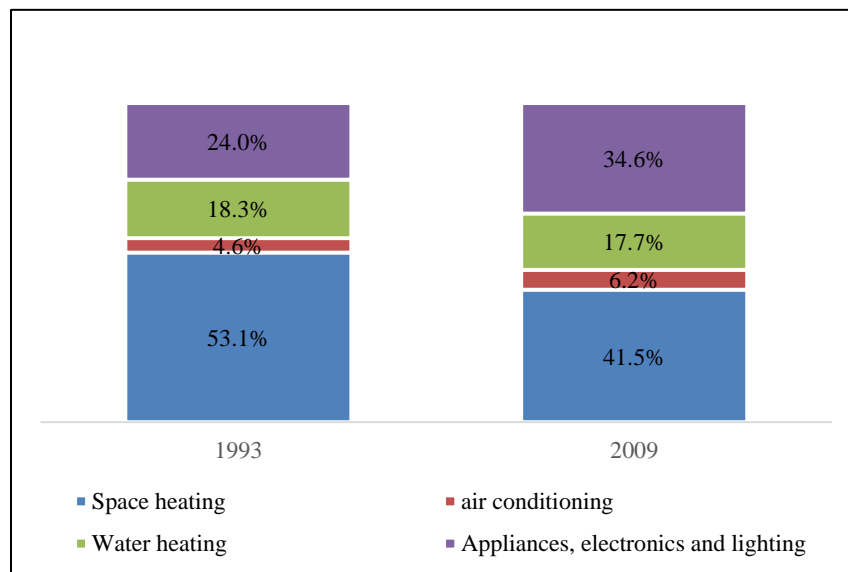
Fig. 1-8 Energy consumption in U. S. homes by end uses (eia, 2016).

Modern renewable energy supplies approximately 8% of final energy for heating and cooling services worldwide in buildings and industry, the vast majority of which is provided by biomass, with smaller contributions from solar thermal and geothermal energy. However, approximately three-quarters of global energy use for heat are fossil fuel-based. The supporting policies of renewable heating and cooling technologies are limited. Policies that have been adopted are directed mainly towards renewable heating technologies rather than renewable cooling, and they focus primarily on smaller-scale solar thermal heating options in residential and commercial buildings, such as solar water heaters. An estimated 47 countries worldwide had targets for

renewable heating or cooling in place by the end of 2015. Due to the slow progress in adopting regulatory support, fiscal incentives remain the primary mechanism that policy makers use to support the renewable heating and cooling sectors (REN21, 2016).
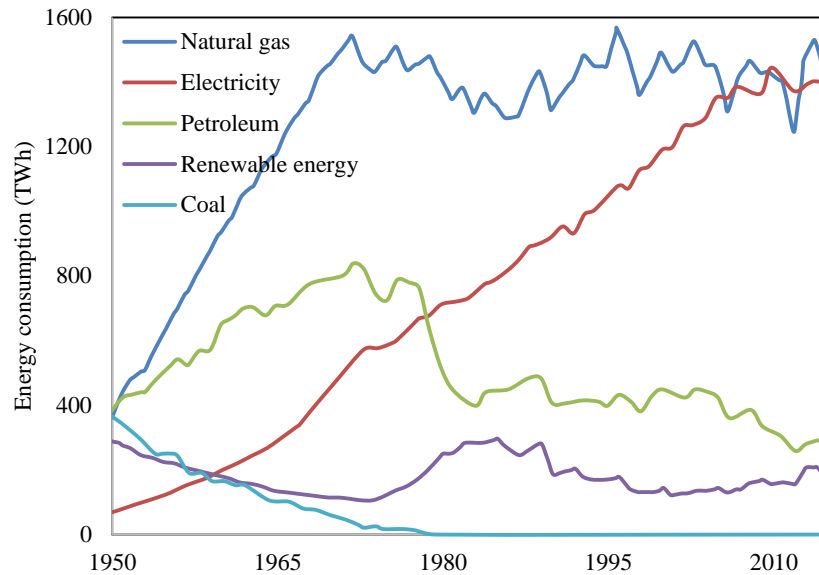
Fig. 1-9 U. S. residential sector energy consumption (TWh).

While renewable power generation continues to enjoy double-digit growth rates, renewable heating and cooling technologies have grown at a much slower rate. This is partly due to the small-scale nature of this sector as well as the multiple, decision-making processes primarily at the household level. More complex and therefore fewer renewable energy support policies have also hindered growth in this sector. Moreover, increases in high energy efficient buildings and passive solar architecture reduce heat demand (REN21, 2014) To achieve the transition towards renewable energy, more attention needs to be paid to the renewable sources for heating and cooling, as well as to integrated approaches that facilitate the use of renewables in these sectors. This sector continues to lag far behind the renewable power sector when it comes to policies that support technology development and deployment. Experience has shown that well-designed support policies have been highly effective in increasing the market expansion of renewable heating and cooling technologies.

Mandatory regulations in the building sector can help increase the penetration of renewable heating and cooling technologies. Improving the accuracy of national data collection on heating and cooling supply and demand is also important. The distributed nature of heat supply and local demand make it difficult to know what sources are available and what is needed; this information is crucial for good policy development. One of the most efficient and well-developed renewable technologies for heating and cooling of the buildings is Ground Source Heat Pump (GSHP) technology.

1.5 Ground source heat pump technology

A Ground Source Heat Pump (GSHP) system consists of 3 main parts: Ground Heat Exchangers (GHEs), heat pump unit and heat distribution system. Fig 1-10 shows the schematic view of the GSHP system. During the cold season (heating operation), the working fluid that consists of water and antifreeze liquid (usually ethylene glycol) circulates inside the GHE. It enters the GHE with low temperature and after transferring heat with the soil gives its heat to the refrigerant inside the heat pump unit in Evaporator part. The pressure and temperature of the refrigerant increases in Compressor after vaporizing in the Evaporator. The heat transfers to the room by heat exchange between refrigerant and working fluid of the heat distribution system in the condenser. The refrigerant expands in the Expansion Valve and its temperature drops and again enters the Evaporator. A GSHP system can work in both heating and cooling operations, using a reversing valve that reversing the refrigerant flow direction.
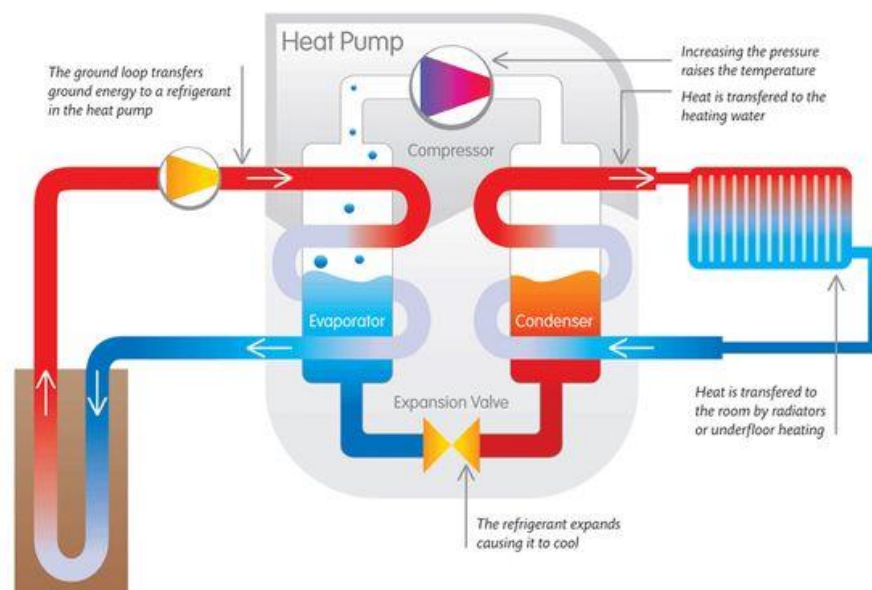
Fig. 1-10 Schematic view of the GSHP system.

Source:[http://www.energygroove.net/technologies/heat-pumps/]

The GHE part used in GSHP systems fall under 2 main categories: closed-loop and open-loop. The type of ground coupling employed will affect heat pump system performance (therefore the heat pump energy consumption), auxiliary pumping energy requirements, and installation costs. Choice of the most appropriate type of ground coupling for a site is usually a function of specific geography, available land area, and life-cycle cost economics.

Closed-loop systems consist of an underground network of sealed, high-strength plastic pipe acting as a heat exchanger. The loop is filled with a heat transfer fluid, typically water or a water

solution, although other heat transfer fluids may be used. When cooling requirements cause the closed-loop liquid temperature to rise, heat is transferred to the cooler earth. Conversely, when heating requirements cause the closed loop fluid temperature to drop, heat is absorbed from the warmer earth. Closed-loop systems use pumps to circulate the heat transfer fluid between the heat pump and the ground loop. Because the loops are closed and sealed, the heat pump heat exchanger is not subject to mineral buildup and there is no direct interaction (mixing) with groundwater. Fig. 1-11 shows the different types of closed-loop GSHP system, horizontal, spiral (slinky), vertical, and submerged systems.
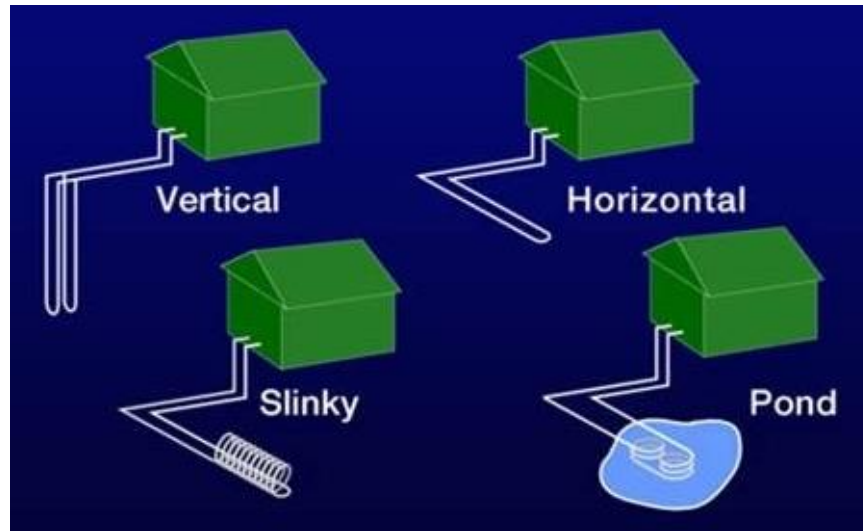
Fig. 1-11 Types of closed loop GSHP system.

Source: [http://www.health.state.mn.us/divs/eh/wells/geothermal.html]

Open loop systems use local groundwater or surface water (i.e., lakes) as a direct heat transfer medium instead of the heat transfer fluid described for the closed-loop systems. These systems are sometimes referred to specifically as "groundwater source heat pumps". Fig. 1-12 shows the schematic of open loop GSHP system.

There are several special factors to consider in open-loop systems. One major factor is water quality. In open loop systems, the primary heat exchanger between the refrigerant and the groundwater is subject to fouling, corrosion, and blockage. A second major factor is the adequacy of available water. The required flow rate through the primary heat exchanger between the refrigerant and the groundwater is typically between 1.6 and 3.2 liter per minute per system cooling kW. This can add up to a significant amount of water and can be affected by local water resource regulations.

A third major factor is what to do with the discharge stream. The groundwater must either be re-injected into the ground by separate wells or discharged to a surface system such as a river or lake. Local codes and regulations may affect the feasibility of open loop systems.

Depending on the well configuration, open-loop systems can have the highest pumping load requirements of any of the ground-coupled configurations. In ideal conditions, however, an open loop application can be the most economical type of GSHP system.
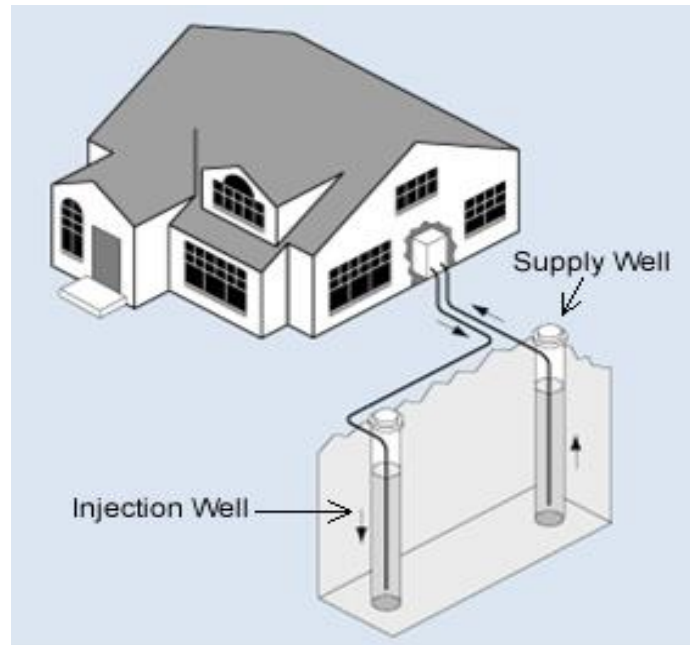
Fig. 1-12 Open loop GSHP system.

Source: [http://www.health.state.mn.us/divs/eh/wells/geothermal.html]

1.5.1 Benefits of GSHP systems

The importance of geothermal resources as a renewable and clean source of energy is rising worldwide. Among direct utilizations of geothermal energy, Ground Source Heat Pumps (GSHPs) are a rapidly growing usage of geothermal energy, accounting for 70% of the installed capacity and 55% of the total direct use of geothermal energy in 2015 (Lund and Boyd, 2015). GSHP systems are highly efficient technologies that meet the heating and cooling demands of houses and buildings while preserving fossil fuels and avoiding additional CO_2 emissions (Molina-Giraldo et al., 2011). As an alternative energy source, GSHP provides several advantages over other renewable energies:

1. The lowest environmental impact of any renewable energy source,
2. High availability under all weather conditions,
3. Decentralized and localized production,
4. Economic viability (Alcaraz et al., 2016).

The renewable energy production, carbon footprint of GSHP systems as well as geothermal potential of aquifers have been intensively studied (e.g. Arola et al., 2014; Arola and Korkka-

Niemi, 2014; Bayer et al., 2012; Laitinen et al., 2014; Mattinen et al., 2014). In closed loop GSHP systems, heat is extracted or discharged to the ground during cold and warm seasons, respectively, through Ground Heat Exchangers (GHEs). In open loop GSHP systems, groundwater is pumped to the surface and its heat is delivered for heating and cooling purposes.

In the cooling mode, the process is reversed and the heat is extracted from the cooler inside air and rejected to the warmer outdoor air or other heat sink. For space conditioning of buildings, heat pumps remove heat from indoor air and reject it to outdoor air in the cooling mode are common. These are normally called air-source or air-to-air heat pumps. Air source heat pumps have the disadvantage that the greatest requirement for building heating or cooling is necessarily coincident with the times when the outdoor air is least effective as a heat source or sink. Below about 3ºC, supplemental heating is required to meet the heating load. For this reason, air-source heat pumps are essentially unfeasible in cold climates with outdoor temperatures below 3ºC for extended periods of time (U.S. DOE, 2001)

The major barriers to rapid implementation of GSHP technology involve awareness and acceptance by users and HVAC designers (which is growing rapidly) and higher initial implementation costs than other options. In addition, there is a limited infrastructure and availability of skilled and experienced designers and installers of GSHP systems.

Closed-loop GSHP systems offer several advantages over conventional HVAC systems. For instance, they collect renewable ground heat or recuperate building heat rejection that accumulated in the ground during the cooling season. Furthermore, because of their relatively high coefficient of performance (COP) in both heating and cooling they are, as noted by the U.S. Department of Energy and the U.S. Environmental Protection Agency, among the most energy-efficient and environment-friendly heating and cooling systems. Finally, they emit less greenhouse gas than conventional HVAC systems given the power generation mix found in most jurisdictions (Bernier, 2006).

The idea of GSHPs was first presented more than a century ago by a Swiss turbine engineer Heinrich Zoelly (Zogg, 2008). GSHPs are used to extract heat from ground loop heat exchangers, either vertical (borehole) or horizontal, and deliver it for heating the house and sanitary water (Finnish). During the 1970s the world experienced the oil crises that launched a great global interest in alternative energy sources, including GSHPs. Two decades later, the growing climate concern and increasing need for energy security prompted governments in different countries to design policies with consequences also for the GSHP industry (Ürge-Vorsatz et al., 2015).

Among all direct utilization of geothermal energy, GSHPs have the largest energy use and installed capacity worldwide, accounting for 70.95% of the installed capacity and 55.30% of the annual energy use. The installed capacity is 49,898 MWt and the annual energy use is 325,028 TJ per yr, with a capacity factor of 0.21 (in the heating mode). Although, most of the

installations occur in North American, Europe and China, the number of countries with installations increased from 26 in 2000, to 33 in 2005, to 43 in 2010, and to 48 in 2015. The equivalent number of installed 12 kW units (typical of USA and Western Europe homes) is approximately 4.16 million. This is a 51% increase over the number of installed units reported in 2010, and over three times the number of units reported in 2005. The size of individual units: however ranges from 5.5 kW for residential use to large units over 150 kW for commercial and institutional installations (Lund and Boyd, 2015). Table 1-5 shows the capacity of the various categories of direct-use of geothermal energy worldwide for the period 1995-2015. Fig. 1-13 and 1-14 show the geothermal direct applications worldwide in 2015, distributed by percentage of total installed capacity (MWt) and total energy used (TJ/year), respectively (Lund and Boyd, 2015).

Table 1-5 Capacity (WMt) of the various categories of direct-use worldwide for the period 1995-2015.

Year	2015	2010	2005	2000	1995
Geothermal heat pumps	49,898	33,134	15,384	5,275	1,854
Space heating	7,556	5,394	4,366	3,263	2,579
Greenhouse heating	1,830	1,544	1,404	1,246	1,085
Aquaculture pond heating	695	653	616	605	1,097
Agricultural drying	161	125	157	74	67
Industrial uses	610	533	484	474	544
Bathing and swimming	9,140	6,700	5,401	3,957	1,085
Cooling, snow melting	360	368	371	114	115
Others	79	42	86	137	238
Total	70,329	48,493	28,269	15,145	8,664
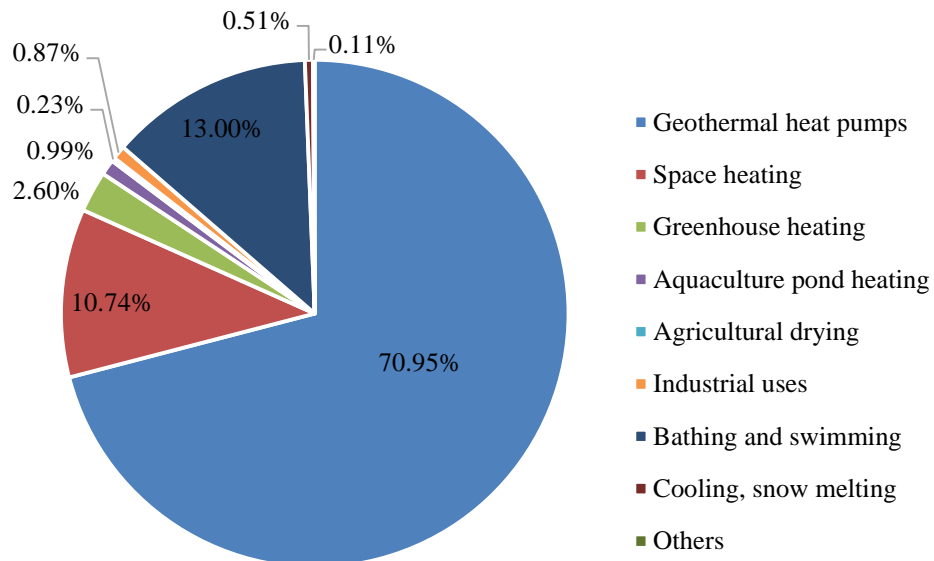
Fig. 1-13 Geothermal direct applications worldwide in 2015, distributed by percentage of total installed capacity (MWt).
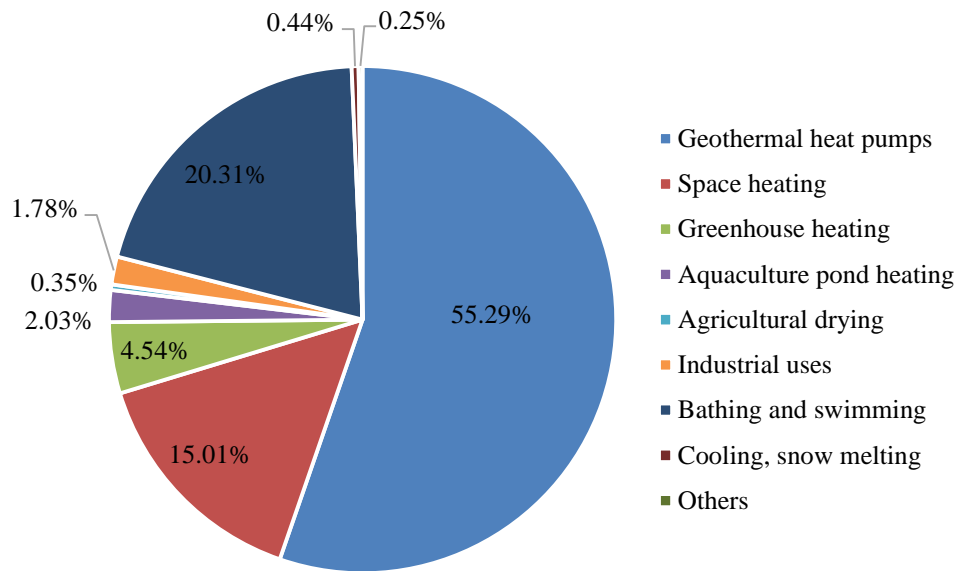
Fig. 1-14 Geothermal direct applications worldwide in 2015, distributed by percentage of total energy used (TJ/year).

In the United State, most GSHP units are sized for peak cooling load and are oversized for heating, except in the northern states; thus they are estimated to average only 2000 equivalent full-load hours per year (capacity factor of 0.23). In Europe, most units are sized for the heating load and are often designed to provide the base load with peaking by fossil fuel. As a result, these units may be in operation up to 6000 equivalent full-load hours per year (capacity factor of 0.68), such as in the Nordic countries (especially in Finland). The leaders in GSHP installation in 2015 are: United States, China, Sweden, Germany and France (Lund and Boyd, 2015).

1.5.2 Current distribution of GSHP in the world

As mentioned is section 1.5.1, GSHP technology has an important role in providing the heating and cooling demands of the buildings worldwide. For example in U. S. the largest application of direct utilization of geothermal energy is GSHP systems accounting for 88% of the annual energy use. In 2015, ground-source heat pumps are being installed at an 8% annual growth rate with 1.4 million units (12 kW size) in operation (Lund and Boyd, 2015). The installations of new GSHP systems are 60% in commercial and institutional buildings, and 40% in residential locations. Approximately 90% of the units are closed loop (ground-coupled) and the remaining open loop systems. Within the residential section, of the closed loops systems, approximately 30% are vertical and 70% horizontal. In the institutional and commercial section, 90% are vertical and only 10% horizontal (Boyd et al., 2015).
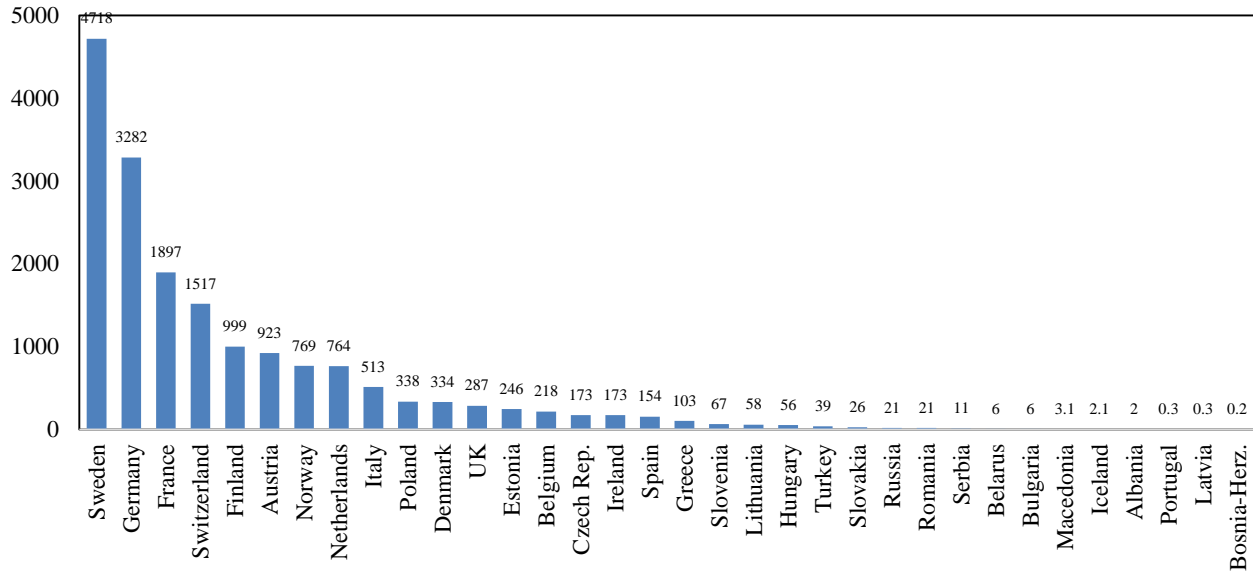
Fig. 1-15 Installed capacity in MWt of GSHP in European countries, 2012.
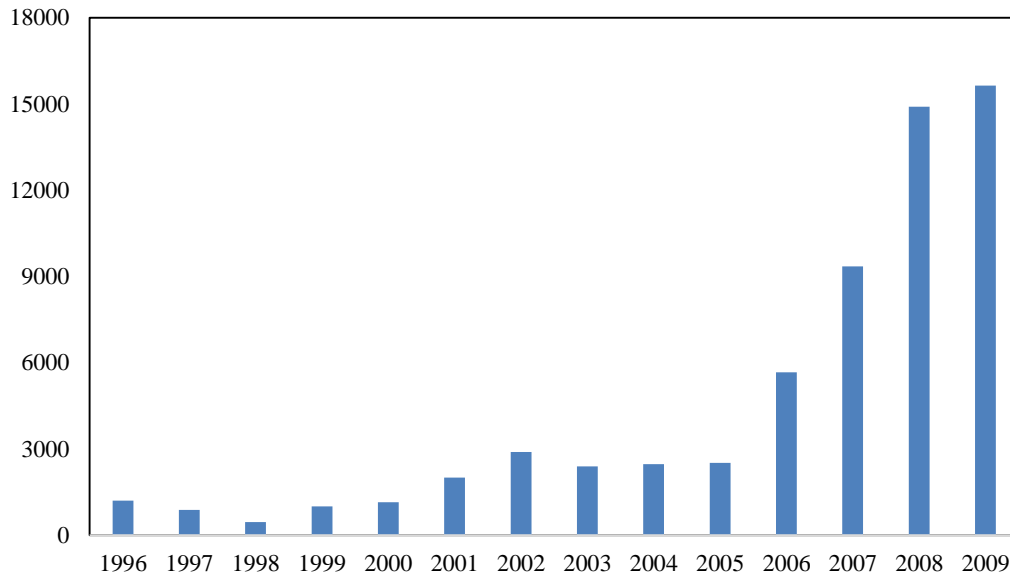
Fig. 1-16 Installed GSHP units in Canada for 1996-2009.

For the European countries it is estimated that at the end of 2013 the installed capacity was 17,700 MWt distributed over more than 1.3 million GSHP installations. The countries with the highest amount of geothermal heat pumps are Sweden, Germany, France and Switzerland (Fig. 1-15). These four countries alone account for 64% of all installed capacity for shallow geothermal energy in Europe. Looking at the time period 2010-2015, these four big players will have the greatest increase in terms of number of installations. In relative terms, Italy, Poland and

the Czech Republic are among the countries with the highest growth rate (European Geothermal Energy Council, 2015).

The Canadian GSHP industry has experienced phenomenal growth in the recent years. Early signs of such growth were observed in 2005 but a significant jump took place in 2007 and in 2008. The market for GSHP grew by more than 40% in 2005 over 2004 and by more than 60% annually in 2006, 2007 and 2008. Fig. 1-16 shows the Installed GSHP units in Canada for 1996-2009 (Canadian GeoExchange Coalition, 2010).

There are a number of reasons explaining the recent strong GSHP technology growth in Canada. Some would suggest that the recent growth in the GSHP industry is conjectural and is closely correlated with the rise of fossil fuel prices. This phenomenal growth also coincides with various grant and financial assistance programs deployed by utilities, provincial governments and the federal government. The "ecoENERGY Retrofit-Homes" program which started in April 2007 encouraged the demand for GSHPs in the residential retrofit market. Tax rebates in Ontario, a loan program offered by Manitoba Hydro as well as direct grants by Hydro-Québec and Saskatchewan contributed to increase demand in the new built market segment (Canadian GeoExchange Coalition, 2010).

The Republic of Korea adopted a law in 2004 that required new and reconstructed public buildings to have new and renewable energy systems installed, and consequently, in 2004-2007, 60% of new public buildings were equipped with a GSHP system (Lee, 2009). The rapid growth of the GSHP industry has raised questions about the environmental benefits and costs of GSHPs.

The use of shallow geothermal heat pump systems is available nationwide. Geothermal heat pumps are used for space heating and cooling, domestic hot water and snow melting. Many new systems have been installed in Hokkaido replacing old oil boilers. Approximately 84% of GSHPs are closed loop, 15% open loop, and 1% using both systems. The estimated installed capacity is 100 MWt and annual energy use of 500 TJ/yr, based on extrapolations from 2012 data (62 MWt at that time) (Yasukawa and Sasada, 2015).

1.6 Literature review and objectives of study

The wider use of GSHP systems is inhibited by their higher initial cost than conventional heating and cooling systems. The drilling cost of GHEs constitutes a large share of the GSHP initial cost and remains more expensive in Japan than in American and European countries. Another obstacle against the widespread usage of GSHP in Japan is the relatively limited land space for residences, which increases the difficulty of constructing GHEs, especially in horizontal systems (Niibori et al., 2005).

The coefficient of performance (COP) and capacity of heat pumps depend on several parameters such as fluid flow rate and temperatures on the source and load sides. The COP is defined as the ratio of useful energy (either in cooling or heating) to the power input to the unit (used to run the compressor and the fan). It is necessary to note that pumping power usually is not included in the COP values provided by manufacturers. It is also important to note the strong dependency of the COP on the inlet fluid temperature to the heat pump unit.

In cooling, the inlet fluid temperature to the heat pump should be as low as possible to reduce heat pump energy consumption. While in heating mode the inlet fluid temperature should be as high as possible. In other words, the temperature lift across the heat pump, i.e., the difference between the source and load temperatures should be minimized. One way to minimize the lift is to increase the length of the ground heat exchanger so that the inlet fluid temperature to the heat pump tends towards the undisturbed ground temperature, T_{ground}. However, oversized ground heat exchangers are not economically feasible. So, the design engineer must find the right compromise between the length of the ground heat exchanger that will give an acceptable inlet fluid temperature to the heat pump to reduce heat pump energy consumption as much as possible. In some cases, this may imply the use of a hybrid system to reduce peak ground loads and the length of the ground heat exchanger.

By increasing the heat transfer rate between the GHE and ground for a given building heat load, GHE length and as a result, system initial cost reduces to levels that are more competitive with conventional heating and cooling systems.

If the GHE is placed in a formation with highly thermally conductive soils, the heat conduction rate will be high. The heat transfer rate between the GHE and ground strongly depends on the groundwater flow around the GHE, and is mediated by a heat advection mechanism. The heat transfer rate (and consequently the system performance) increases in areas with high hydraulic conductivity and high hydraulic head difference around the GHE (Angelotti et al., 2014; Fujii et al., 2005; Molina-Giraldo et al., 2011; Wang et al., 2014). The proportion of convective heat transfer in the total heat transport significantly depends on the Darcy velocity; consequently, groundwater velocities exceeding 10 cm/day also increase the heat transport rate (Katsura et al., 2009; Witte and van Gelder, 2006).

Zanchini et al. (2012) demonstrated that even low groundwater velocities significantly improve the long-term performance of the GHEs, by reducing the maximum annual dimensionless temperature at the GHE–ground interface.

Fujii et al. (2005) numerically modeled a single U-pipe using a finite element simulator. Assuming no groundwater flow, they compared their model to a cylindrical source function, and then calibrated it with thermal response test (TRT) data using the thermal conductivity of the medium as the matching parameter. The heat transfer rate after 5 days was then modeled as a function of groundwater velocity. The increase due to groundwater flow was negligible for

Peclet numbers (Pe) <0.1, and approached 100% as Pe approached 1. Here the characteristic length was the U-pipe diameter.

Niibori et al. (2005) developed a two-dimensional numerical model to evaluate the heat transfer from groundwater to the GHE at different groundwater temperatures and velocities. Velocities exceeding 10^{-5} m/s permitted a shorter heat exchanger than in cases of heat conduction only.

Huber and Arslan (2015) performed experimental investigations with a conduction and convection laboratory device, and compiled an extensive database of groundwater-influenced geothermal systems. They reported that weakly aquiferous water-saturated sand (Darcy velocities up to 0.3 m/day) and clearly aquiferous sand (Darcy velocity 0.3–0.6 m/day) increase the effective thermal conductivity by up to 25% and 50%, respectively. In strongly aquiferous water-saturated sand (0.6–1.0 m/day), 100% increase of the effective thermal conductivity can be expected.

Wang et al. (2009) quantified the heat transfer enhancement provided by groundwater flow in an in situ GHE field experiment. Compared to the numerical results of a conductive scenario, the heat transfer rate improved the energy extraction and injection by 12.9% and 9.8%, respectively.

Using a 3D simulation model and a simplified analytical model, Wang et al. (2014) investigated the influence of groundwater flow on the thermal performance of a Pile Ground Heat Exchanger (PGHE) with cast-in spiral coils. The groundwater flow enhanced the heat transfer performance of the spiral-coiled PGHE and accelerated the stabilization time of the heat transfer process. At a seepage velocity of 10^{-4} m/s, the average enhancing rate was 22.98%

Lim et al. (2007) investigated the variations in thermal conductivity and thermal resistance of a GHE. They concluded that groundwater flow through the rock probably improves the thermal capacity of the borehole.

Molina-Giraldo et al. (2011) considered the effects of groundwater flow and axial effects in GHEs by a new analytical approach. Assuming the GHE length as the characteristic length, they showed that groundwater flow exerts negligible effect at Pe < 1.2, but increases the heat transfer rate at higher Peclet numbers.

Farabi Asl et al. (2015) studied the effect of water injection and pumping on the heat transfer rate in an ungrouted GHE. The TRT results showed that increasing the water injection/pumping rate decreases the average temperature of the heat medium. After 48 hr' TRT with 15 L/min of water injected into the well, the outlet temperature of the heat medium was approximately 4 °C lower than when no water was injected or pumped.

In summary, the present available results indicate that even relatively low-velocity groundwater flows can strongly affect the heat transfer rate in GSHP systems. However, groundwater flow is a natural characteristic of GHE sites and cannot be artificially changed. Groundwater flow can be improved only by injecting or pumping water into ungrouted vertical GHEs. Injection requires a cheap water source, whereas pumping may cause long-term damage to the groundwater source or violate the local regulations.

In the second chapter of this study, the effect of water pumping and injection on the results of Thermal Response Tests (TRTs) was investigated. 9 sets of TRTs were performed with different water pumping/injection rates in Akita University campus. A numerical model was developed using FEFLOW 6.2 and validated using experimental data. Sensitivity analysis was performed to evaluate the effect of different pumping/injection water flow rates and also natural groundwater flow on heat transfer rate of Ground Heat Exchanger (GHE).

In the third chapter of this study, semi-open loop GSHP system was introduced. This is a closed loop GSHP system, consisting of 2 ungrouted GHE wells that groundwater is pumping from one well and injecting to the other one when the heat pump is working. Heating and cooling tests were performed and the results were compared with the base case GSHP operation (without water pumping and injection). A numerical model was developed using FEFLOW 6.2 and validated using heating and cooling experimental data. Sensitivity analysis was performed to evaluate the performance of GSHP system in base case and semi-open loop operations, under different heat transfer rates and natural groundwater flow rates.

In the fourth chapter of this study, economic analysis of semi-open loop GSHP system was performed. The heating and cooling demands of a sample building in Akita city, similar to experimental condition, were calculated. Based on the calculated building heating and cooling loads, the heat transfer rate of GHEs was calculated. The validated numerical model was used to calculate the necessary GHE length to meet the expected heat transfer rate, in base case and semi-open loop operations. According to the economic parameters in Japan like annual inflation rate and interest rate, the final saving of semi-open loop GSHP system was calculated considering the parameters like: drilling cost, heat pump and distribution system costs, water pumping and injection system cost, labor and piping costs.

Chapter 2: THERMAL RESPONSE TESTS

2.1 Introduction

In this chapter, Thermal Response Test (TRT) will be introduced. The importance and process of TRT in Ground Source Heat Pump (GSHP) system design will be discussed. As mentioned in the previous chapter, water pumping and injection is expected to enhance heat transfer rate of GHEs. In order to evaluate the effect of water pumping and injection on the TRT results, 9 sets of TRTs were performed on a 102 m long Ground Heat Exchanger (GHE) in Akita University campus. The TRTs were performed with different water pumping and injection flow rates. The effect of injection water temperature on TRT results was investigated by performing TRTs with different injection water temperatures. A numerical model was developed using FEFLOW 6.2 and validated using experimental data. The sensitivity analysis was performed in order to evaluate the effect of higher flow rates of water injection/pumping on the heat exchange rate of GHEs. The sensitivity analysis also investigated the effect of natural groundwater flow on the TRT results.

2.2 Why TRT is necessary in GSHP system design?

To design GHEs for GSHP systems or Underground Thermal Energy Storage (UTES), the knowledge of underground thermal properties is paramount. The decision about how many meters of GHE has to be drilled to meet the heating or cooling load of a building is crucial for the successful and long-lived operation of the ground-coupled heat pump. The needed borehole length can be calculated if the thermal ground and well thermal properties are known. Important parameters are soil temperature, volumetric heat capacity, thermal borehole resistance and effective thermal conductivity at a site.

The knowledge of them will help to find a good compromise between costs (drilling and operation costs to run the GSHP system) and efficiency (supplying expected heating and cooling loads). Thermal borehole resistance and effective thermal conductivity are measured with the help of a TRT (Austin, 1998 and Gehlin, 1998). TRTs are applied as a standard procedure before a large well field is dimensioned and the results are considered to be essential for the proper dimensioning.

The knowledge of underground thermal properties is a prerequisite for the correct design of GHE. The most important parameter is the thermal conductivity of the ground. This parameter is site-specific and cannot be influenced by engineering. The thermal contact from the borehole wall to the fluid inside the pipes, however, is controlled by borehole diameter, pipe size and configuration, pipe material, and the filling materials inside the annulus. These items are subject

to efforts in order to reduce the thermal resistance between borehole wall and fluid, usually summarized in the parameter "borehole thermal resistance" (Liebel et al., 2011).

Since the mid-90s a method has been developed and refined to measure the underground thermal properties on site, and mobile equipment for these measurements has been built in several countries. The Thermal Response Test (TRT, also sometimes called "Geothermal Response Test", GRT) is a suitable method to determine the effective thermal conductivity of the underground and the borehole thermal resistance (or the thermal conductivity of the borehole filling, respectively). A temperature curve is obtained which can be evaluated by different methods. The thermal conductivity resulting is a value for the total heat transport in the underground, noted as a thermal conductivity. Other effects like convective heat transport (in permeable layers with groundwater) and further disturbances are automatically included, so it may be more correct to speak of an "effective" thermal conductivity λ_{eff}. The test equipment can be made in such a way that it can be transported to the site easily, e.g. on a light trailer (Fig. 2-1) (Sanner et al., 2005).
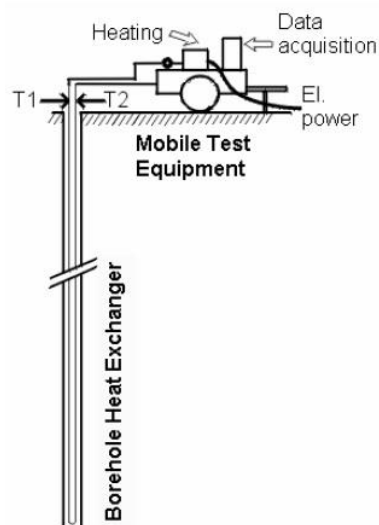
Fig. 2-1 Test setup for TRT.

The borehole thermal resistance may have a significant effect on the system performance and should be kept as small as possible. Filling materials (e.g. bentonite, concrete etc.) in grouted boreholes usually provide better heat transfer than pure stagnant water. However, in water-filled boreholes, the heat transfer induces natural convection of the borehole water and in surrounding permeable ground. This phenomenon, which is more pronounced at large heat transfer rates, leads to a reduction of the overall borehole thermal resistance (Kjellsson and Hellstrom, 1997; Kjellsson and Hellstrom, 1999).

The overall thermal performance of the borehole field that is subject to a certain heat load variation depends not only on the borehole thermal resistance, but also on the transient thermal resistance of the surrounding ground and the thermal influence from other boreholes. Remund (1999) discusses thermal resistance in GHE, relating the borehole thermal resistance to a grout thermal conductivity and a borehole shape factor and presents laboratory and field test of the borehole thermal resistance.

2.3 History of TRT

There are several ways to estimate the ground thermal properties for a GHE design. The simplest way is to use standard values for the type of rock at the location of the GSHP system. There are also several laboratory methods to determine the thermal conductivity of solid materials (Sundberg, 1988), however these methods require expensive samples, and will not give the entire picture of the ground profile at the site.

Mogensen (1983) first presented the thermal response test as a method to determine the in situ values of ground thermal conductivity and thermal resistance in GHE systems. He suggested a system with a chilled heat carrier fluid being circulated through a GHE system at constant heat extraction (or cooling) rate, while the outlet fluid temperature from the GHE was continuously recorded. The temperature data over time (i.e. the thermal response) is compared with a mathematical model of the heat transfer processes occurring in the borehole and surrounding ground. The model depends primarily on the ground thermal conductivity and borehole thermal resistance. Mogensen's method was used to evaluate existing GSHE systems at several occasions, e.g., Eskilson (1987), Nordell (1994), Hellstrom (1994).

The theoretical basis for the TRT was laid over several decades (e.g. by Choudary, 1976; Mogensen, 1983; Claesson and Eskilson, 1988; Hellström, 1991). In the 90s the first practical applications were made, e.g. for the investigation of borehole heat storage in Linköping (Hellström, 1997).

In 1995 a mobile test equipment was developed at Luleå Technical University to measure the ground thermal properties for GHE between some 10 m to over 100 m depth (Eklöf and Gehlin, 1996; Gehlin and Nordell, 1997). A similar development was going on independently since 1996 at Oklahoma State University in the USA (Austin, 1998). The first TRT in Germany were performed in summer 1999 (Sanner et al., 2005).

2.4 Interpretation of TRT

The easiest way to evaluate TRT data makes use of the line source theory. This theory already was used in the 1940s to calculate the temperature development in the ground over time for

GSHP plants (Ingersoll and Plass, 1948). An approximation is possible with Eq. 2-1, given in Eklöf and Gehlin (1996):

$$k = \frac{Q}{4\pi H \lambda_{eff}}$$ (2-1)

In Eq. 2-1:

- k Inclination of the curve of temperature versus logarithmic time
- Q heat injection/extraction rate
- H length of borehole heat exchanger
- λ_{eff} effective thermal conductivity (including influence of groundwater flow, borehole grouting, etc.)

To calculate thermal conductivity, the formula has to be transformed to Eq. 2-2:

$$\lambda_{eff} = \frac{Q}{4\pi H k}$$ (2-2)

A more complicated method to evaluate a thermal response test is parameter estimation using numerical modelling, as done for instance at a duct store in Linköping (Hellström, 1997). Further work on parameter estimation was done, among others, at Oklahoma State University by Spitler et al. (1999), Spitler et al. (2000), and at Oak Ridge National Laboratory (Shonder and Beck, 1999). The calculation of λ_{eff} follows the suggestions of Gehlin (2002) and Signorelli et al. (2007), which are based on the infinite line-source theory (Ingersoll 1948). The line-source model is based on a linear relationship between the average heat-carrier fluid in the collector and the natural logarithm of the time t, if the heat exchange rate per length unit, q, is constant (q is constant if the electric power supply to the heating elements is constant):

$$T_f(t) = k \ln(t) + m$$ (2-3)

In Eq. 1-3:

$$k = \frac{q}{4\pi\lambda}$$ (2-4)

$$m = q\left[R_b + \frac{1}{4\pi\lambda}\left(\ln\left(\frac{4\lambda}{r_b^2 S_{VC}}\right) - 0.5722\right)\right] + T_0$$ (2-5)

In Eq. 2-5, r_b is the borehole radius, S_{VC} is the volumetric heat capacity of the rock/sediment, and T_0 is the undisturbed ground temperature. The average heat carrier-fluid temperature, T_f, is calculated from the inlet and outlet temperatures, T_{in} and T_{out}:

$$T_f = \frac{T_{out} + T_{in}}{2}$$ (2-6)

The thermal conductivity λ is found by plotting T_f against the natural logarithm of the time in seconds and by reading off the slope where the conditions have stabilized (e.g., Signorelli et al. 2007; normally between 20 (t_1) and 70 hours (t_2)):

$$\lambda = \frac{q}{4\pi} \times \frac{ln(t_2) - ln(t_1)}{T_f(t_2) - T_f(t_1)} \tag{2-7}$$

2.4.1 Analytical models

Analytical models, such as the line source and cylinder source adopt the analytical solution of the heat transfer problem between the borehole and the nearby infinite region. They require several simplifying assumptions regarding the geometry of the borehole and heat exchanger pipes. For the purpose of the thermal response test evaluation, the heat flow to or from the borehole may be represented as an infinitely long heat source or sink in the ground with negligible influence of heat flows in a direction along the borehole axis. In the ground outside the borehole it is common practice to assume that the thermal process depends only on the radial distance from the borehole axis. The one- or two-dimensional heat flow process from the circulating fluid to the borehole wall is assumed to be represented by a thermal resistance that characterizes the temperature loss between heat carrier fluid and borehole wall. Some models also include the thermal mass of the materials in the borehole.

Ingersoll and H. J. (1948) applied the line source model to design of ground loop heat exchangers. Mogensen (1983) proposed to use the borehole similar to the probe to estimate the ground thermal conductivity from an experimental field test. This method is now commonly used for thermal response test evaluation in Europe. In practice, researchers have made use of this approach in somewhat different ways although they essentially follow Mogensen (1983).

The equation for the temperature field (Eq. 2-8) as a function of time (t) and radius (r) around a line source with constant heat injection rate (q) (Carslaw and Jaeger, 1959) may be used as an approximation of the heat injection from a GHE:

$$T(r,t) = \frac{q}{4\pi\lambda} \int_{\frac{r^2}{4at}}^{\infty} \frac{e^{-u}}{u} du = \frac{q}{4\pi\lambda} E_1\left(\frac{r^2}{4at}\right) \tag{2-8}$$

In Eq. 2-8, E_1 is the exponential integral. For large values of the parameter at/r^2, E_1 can be approximated with the following simple relation, for at/r^2 higher than 5:

$$E_1\left(\frac{r^2}{4at}\right) = \ln\left(\frac{4at}{r^2}\right) - \gamma \tag{2-9}$$

Where the term γ is Euler's constant (approximately 0.577). The maximum error is 2.5% for at/r^2 higher than 20, and 10% for at/r^2 higher than 5. Ground thermal conductivity is denoted λ and a is λ/C_p, where C_p is the ground specific heat capacity. The condition means that the accuracy increases as the thermal front increases as the thermal front reaches further beyond the

borehole, and the velocity of the thermal front is dependent on the ratio between thermal conductivity and heat capacity of ground i. e. ground thermal diffusivity.

The fluid temperature is evaluated by taking the line source temperature at the borehole radius ($r=r_b$) and adding the effect of the borehole thermal resistance (R_b) between the fluid and the borehole wall. Thus the fluid temperature as a function of time can be written as Eq. 2-10, where T_0 is the undisturbed ground temperature.

$$T_f(t) = \frac{q}{4\pi\lambda}\left(\ln\left(\frac{4at}{r^2}\right) - \gamma\right) + (q \times R_b) + T_0 \tag{2-10}$$

The cylinder source model, of which the line source model is a simplified variation, may be used for approximating the GHE as an infinite cylinder with a constant heat flux. The heat exchanger pipes are normally represented by an "equal diameter" cylinder. The cylindrical source solution for a constant heat flux is as follows (Eq. 2-11):

$$T(r, t) = \frac{q}{\lambda} \times G(z, p) \tag{2-11}$$

Where z is at/r^2, p is r/r_0 and G(z,p) is the cylindrical source function as described by INGERSOLL et al. (1954), where J_0, J_1, Y_0 and Y_1 are Bessel functions of the first and second kind.

$$G(z, p) = \frac{1}{\pi^2}\int_0^\infty f(\beta)d\beta \tag{2-12}$$

$$f(\beta) = \left(e^{-\beta^2 z} - 1\right) \times \frac{[J_0(p\beta)Y_1(\beta) - Y_0(p\beta)J_1(\beta)]}{\beta^2[J_1^2(\beta) + Y_1^2(\beta)]} \tag{2-13}$$

Carslaw and Jaeger (1959) developed analytical solutions with varying boundary conditions for regions bounded by cylinder geometry. Deerman and Kavanaugh (1991) and Kavanaugh S. P. and K. Rafferty (1997) describe the use of the cylinder source model in designing ground loop heat exchangers. The effective thermal conductivity (and diffusivity) of the ground formation is computed by reversing the process used to calculate the length of the ground loop heat exchanger. Based on a short-term in situ test, the measured effective thermal resistance of the ground of a daily heat pulse is fitted to a value computed from a dimensionless cylinder source function by varying the thermal conductivity and diffusivity of the ground.

2.4.2 Numerical models

Numerical models can be designed to handle detailed representations of the borehole geometry and thermal properties of the fluid, pipe, borehole filling and ground, as well as varying heat transfer rates. The more extensive set of required input data often make these models more difficult and time-consuming to use than the analytical methods, which sometimes may be implemented as simple spreadsheet applications.

Berberich et al. (1994) describe a response test type of measurement in groundwater filled ducts in water saturated clay stone where temperature sensors were placed along the borehole wall. The measured data were analyzed with both an analytical line source model and a numerical two-dimensional finite difference model using parameter estimation with ground thermal conductivity and volumetric heat capacity as variables.

Shonder and Beck (1999) developed a parameter estimation based method, which is used in combination with a one-dimensional numerical model. This model is similar to a cylinder-source representation, in that it represents the two pipes of the U-pipe as a single cylinder. However, it adds two more features:

1. a thin film that adds a resistance without heat capacity
2. a layer of grout, which may have a thermal conductivity and heat capacity different from the surrounding soil.

This model accommodates time-varying heat input.

A transient two-dimensional numerical finite volume model in polar co-ordinates for response test evaluation is reported in Austin (1998) and Austin et al. (2000). The geometry of the circular U-pipes is approximated by "pie-sectors" over which a constant flux is assumed. The convection resistance due to the heat transfer fluid flow inside the U-pipes is accounted for using fluid properties through an adjustment on the conductivity of the pipe wall material. A thorough description of the numerical model is found in Yavuzturk et al., (1999). The model has since been improved by introducing a boundary-fitted grid system that is more flexible and better represents the U-pipe geometry (Spitler et al., 2000).

2.4.3 Possible errors in TRT results

Possible sources of error during a TRT are:

- heat loss and gain (affects working fluid temperature (T_f))
- variable electric power supply (affects the power rate (q))
- accuracy of the determination of the undisturbed ground temperature (affects T_0)
- free convection of water in ungrouted boreholes (affects thermal conductivity (λ); Gustafsson et al. 2010)
- gradient-driven horizontal groundwater flow (affects λ; e.g., Gehlin and Hellström 2003)
- density-driven vertical groundwater flow (affects λ; e.g., thermosiphon effect, Gehlin et al. 2003, Gustafsson 2006, Gustafsson and Westerlund 2010).

Typical levels of confidence of TRT results are about 9% for the thermal conductivity (Zervantonakis and Reuss 2006).

For good results, it is crucial to set up the system correctly and to minimize external influences. This is done easier with heating the ground (electric resistance heaters) than with cooling (heat pumps). However, even with resistance heating, the fluctuations of voltage in the grid may result in fluctuations of the thermal power injected into the ground.

Another source of deviation is climatic influences, affecting mainly the connecting pipes between test rig and GHE, the interior temperatures of the test rig, and sometimes the upper part of the GHE in the ground. Heavy insulation is required to protect the connecting pipes, and sometimes even air-conditioning for the test rig is necessary. With open or poorly grouted GHE, also rainwater intrusion may cause temperature changes. Longer test duration allows for statistical correction of power fluctuations and climatic influence, and results in more trustworthy evaluation (Liebel et al., 2011).

2.4.4 Groundwater influence on GHE performance

The influence of groundwater flow on the performance of borehole heat exchangers has long been a topic of discussion. Field observations indicate that groundwater movements result in convective heat transport which influences the effective borehole performance as reflected in the literature, e.g. Gehlin (1998), Sanner et al. (2000), Chiasson et al. (2000), Witte (2001). Some theoretical studies have been published on the subject. Eskilson (1987), Cleasson and Hellstrom (2000), Chiasson et al (2000) present models for the influence of regional groundwater flow based on the assumption that the natural groundwater movement is reasonably homogeneously spread over the ground volume. This applies well on a homogeneous and porous ground material. Eskilson and Cleasson & Hellstrom use the line source theory for modelling the groundwater effect on a single vertical borehole. They conclude that under normal conditions, the influence of regional groundwater flow is negligible.

Chiasson et al. (2000) use a two-dimensional finite element groundwater flow and mass/heat transport model. They come to the conclusion that it is only in geologic materials with high hydraulic conductivity (sand, gravel) and in rocks with secondary porosities (fractures and solution channels in e.g. karst limestone), that groundwater flow has a significant effect on the borehole performance. Simulations of the effect on thermal response tests showed high effective thermal conductivity values. Witte (2001) performed a thermal response test where groundwater flow was induced by pumping in an extraction well located 5 m from the thermal well. Clear indications of enhanced heat transfer due to the induced groundwater flow were observed.

2.5 Thermal Response Tests in Akita University campus

Drilling cost has a considerable share of the initial investment in GSHP systems. By applying methods to reduce the length of GHE, the initial cost of system reduces and GSHP system can compete with conventional heating and cooling systems. The heat transfer between ground and

GHE occurs through two mechanisms: conduction and convection. The key physical factor in conduction between the ground and GHE is soil thermal conductivity (λ). In the formations with high λ (for example 3 W/m/K) for a given thermal load, GHE length is shorter in comparison with low λ formations. But the λ of soil cannot be changed in a specific area that GHE is embedded.

Convection is caused by groundwater flow around the GHE. In formations with high (k) for a specific hydraulic head difference in location, the groundwater velocity is high and convection mechanism causes better heat transfer between soil and the GHE. Several research efforts have been carried out to evaluate the capacity enhancement of GHE by groundwater flow based on field tests (e.g., Okubo, et al., 2006, Fujii, et al., 2009) or numerical simulations (e.g., Gehlin and Hellström, 2003, Fujii, et al., 2005). The advantages of positioning the GHE in a formation with groundwater flow have been confirmed through these studies.

In this study, 9 sets of TRTs are performed in an ungrouted GHE of 102 m deep drilled in a low λ (1.44 W/m/K) and low hydraulic conductivity formation in Akita City, northern Japan. TRTs are carried out with different water injection and pumping rates (0, 1, 3 and 5 L/min). The heat load and circulation rate in all of the TRTs were kept constant and injecting water temperature was kept constant at 16 °C. In the case of water injection with 3 L/min, two other TRTs were done by changing injecting water temperature to 12 °C and 20 °C. More detailed TRT conditions are described in the next section. Outlet water temperature and ground temperature are recorded during the TRTs and up to 48 hours after finishing the heating periods.

In the next step, GHE is modeled using FEFLOW 6.2 software. Outlet water temperatures and ground temperatures are calculated by numerical simulation and are validated using data from TRTs. After validating the model, sensitivity analysis is done by changing injecting/pumping water rate (0-15 L/min) with 2 different inlet water temperature (0 and 5 °C) and 2 different groundwater velocity (0 and 0.1 m/day) both in the cases of injection and pumping. The simulation is performed for 10 days in each case and the outlet water temperature is calculated. The average heat exchange rate is calculated in each case and compared with other cases.

We carried out nine sets of TRTs at a GHE installed in Akita City, Japan, from June 2014 to February 2015. The borehole is 102.0 m deep with a diameter of 179 mm. The schematic drawing of the GHE, the geological column at the well site and the undisturbed ground temperature measured using a thermo-resistance thermometers (Pt100Ω) are shown in Fig. 2-2 (Fujii, et al., 2015). The upper part (surface to 60 m) of the formation is an alluvial deposit of the Quaternary System mainly consisted of silt, sand and gravel. The lower part (60 m to bottom) consists of siltstone of the Tertiary System. Water injection tests were carried out twice at the GHE, which yielded hydraulic conductivities of 2.1 - 4.4 (10^{-7} m/s). These values indicate that the formation mainly consists of fine sand or silt of low hydraulic conductivity. Below 15 m, a clear geothermal gradient of 4.0°C/100m was observed (Fujii, et al., 2015).

A steel casing was inserted in the GHE from the land surface to the bottom of the GHE to prevent the collapse of the formation. The ID and OD of the casing were 100 mm and 114 mm, respectively. The annular space between the well wall and the casing was filled with 20–65 mesh/in. silica sand to stabilize the casing. From 31.3 m to the bottom, slotted casings were used to allow the groundwater flow through the GHE. The GHE was completed with single U-tube of high-density polyethylene without grouting. The ID, OD and the thermal conductivity of the U-tube are 27 mm, 34 mm and 0.46 W/m/K, respectively. Groundwater level is located at 5.2 m below the land surface. The U-tubes between the land surface and the groundwater level were thermally-insulated to avoid the heat loss from the U-tube to the air. TRTs conditions are described in Table 2-1. In all TRTs, circulating water rate and heat load are maintained constant as 15 L/min and 5 KW by system control device. Average temperatures of heat medium (average of inlet and outlet temperatures) in all TRTs are shown in Figure 2-2. For the names of TRTs, N, P and I are standing for normal, pumping and injection, respectively and the digit after these letters shows the injecting/pumping water rate (L/min). In the case of injection with different temperatures, the last number in the name of TRT shows the temperature of injection water. For example TRT-I3-12 is the name of TRT that water with 12 °C temperature injects by 3 L/min rate.

Fig. 2-3 shows that with increasing water injection/pumping rate, average temperature of heat medium decreases. The average of heat medium temperature for TRT-N is 3.8 °C higher than TRT-I5 after 48 hours of heating. For the case of TRT-N, some fluctuations can be seen in the results and based on results of numerical modeling (that shown in Fig. 2-10-1), average of heat medium temperature must be slightly higher than these values. As TRT-N is the first experiment done among all TRTs, these fluctuations may be related to experimental errors that are corrected for the next TRTs. For the case with 5 L/min, the results of pumping are slightly higher than the injection case. It can be predicted that with increasing water rate, the difference between injection and pumping cases will be more obvious. After 48 hours of heating, average temperature of heat medium for TRT-I3-20 is 1.2 °C higher than TRT-I3. This temperature for TRT-I3-12 is 1.7 °C smaller than TRT-I3.

Table 2-1 TRTs conditions.

TRT name	Start date	Injecting/Pumping water rate (L/min)	Groundwater level (m)	Injecting water temperature (°C)	Test duration (hours)
TRT-N	2014/6/10	-	-5.2	-	48
TRT-P1	2014/9/29	1	-6.1	-	48
TRT-P3	2014/9/16	3	-6.3	-	72
TRT-P5	2014/9/2	5	-7.7	-	48
TRT-I1	2014/11/25	1	-4.4	16	48
TRT-I3	2014/11/14	3	-3.1	16	48
TRT-I3-20	2015/1/19	3	-3.1	20	48
TRT-I3-12	2015/2/2	3	-3.1	12	48
TRT-I5	2014/11/4	5	-2.6	16	48
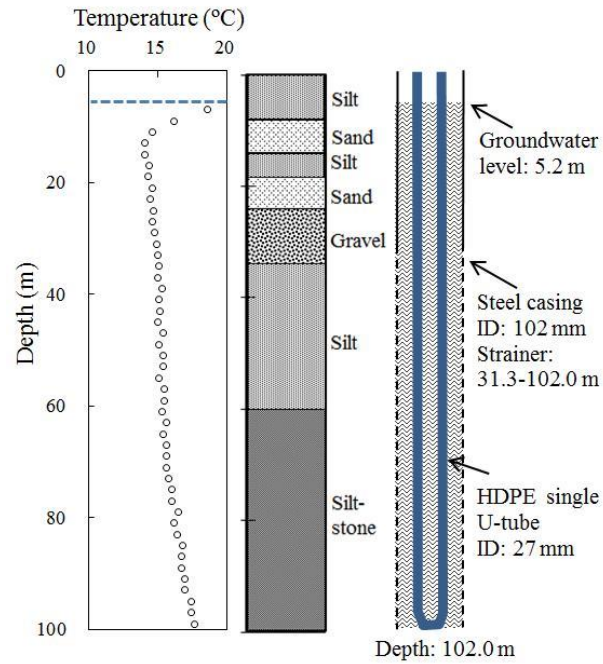
Fig. 2-2 Ground temperatures, geological column and well completion design of GHX (Fujii, et al., 2015).
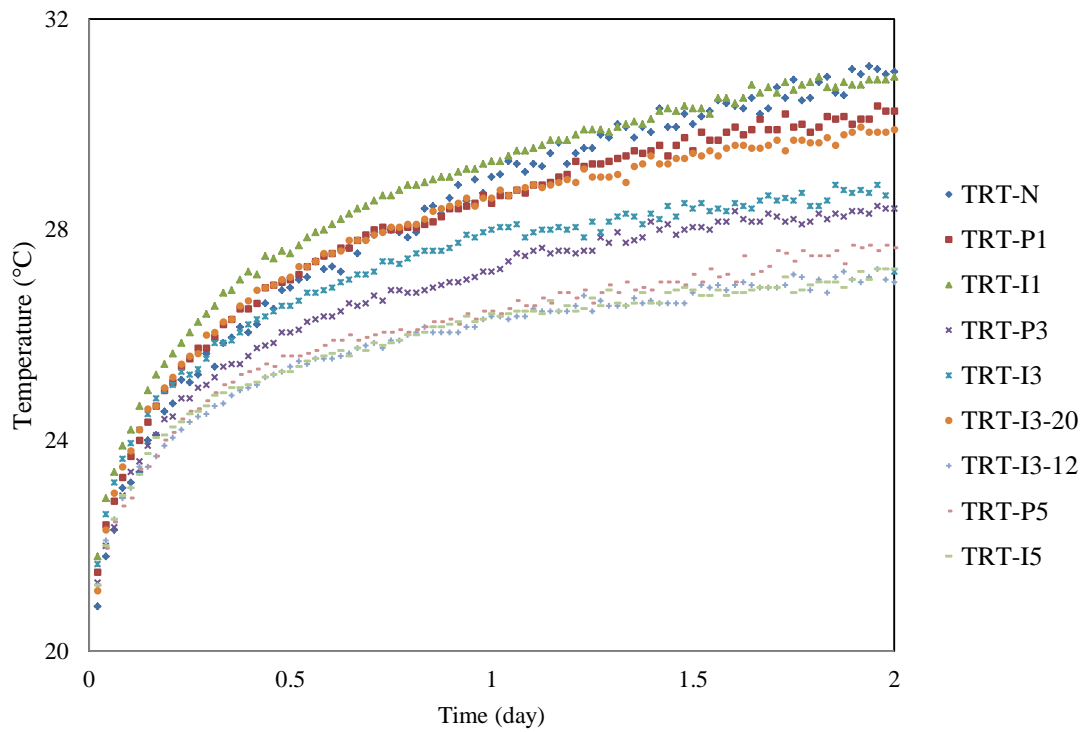
Fig. 2-3 Average temperature of heat medium in all TRTs.

2.6 Numerical simulation

2.6.1 Finite element equations for heat transfer

Solution of heat transfer problems in considered. Finite element equations are obtained using the Galerkin method. The conductivity matrix for a triangular finite element is calculated (Nikishkov, 2010).

2.6.1.1 Problem statement

Let us consider an isotropic body with temperature-dependent heat transfer. A basic equation of heat transfer has the following form:

$$-\left(\frac{\partial q_x}{\partial x} + \frac{\partial q_y}{\partial y} + \frac{\partial q_z}{\partial z}\right) + Q = \rho c \frac{\partial T}{\partial t}. \tag{2-14}$$

Here, q_x, q_y and q_z are components of heat flow through the unit area; $Q = Q(x,y,z,t)$ is the inner heat-generation rate per unit volume; ρ is material density; c is heat capacity; T is temperature and t is time. According to Fourier's law the components of heat flow can be expressed as follows:

$$q_x = -k\frac{\partial T}{\partial x},$$

$$q_y = -k\frac{\partial T}{\partial y}, \tag{2-15}$$

$$q_z = -k\frac{\partial T}{\partial z},$$

where k is the thermal conductivity coefficient of the media. Substitution of Fourier's relations gives the following basic heat transfer equation:

$$\frac{\partial}{\partial \mathrm{x}}\left(k\frac{\partial T}{\partial x}\right) + \frac{\partial}{\partial \mathrm{y}}\left(k\frac{\partial T}{\partial y}\right) + \frac{\partial}{\partial \mathrm{z}}\left(k\frac{\partial T}{\partial z}\right) + Q = \rho c \frac{\partial T}{\partial t}. \tag{2-16}$$

It is assumed that the *boundary conditions* can be of the following types:

1. Specified temperature

$T_s = T_1(x, y, z, t)$ *on* S_1,

2. Specified heat flow

$q_x n_x + q_y n_y + q_z n_z = -q_s$ *on* S_2,

3. Convection boundary conditions

$$q_x n_x + q_y n_y + q_z n_z = -h(T_s - T_e) \text{ on } S_3,$$

4. Radiation

$$q_x n_x + q_y n_y + q_z n_z = \sigma \varepsilon T_s^4 - \alpha q_r \text{ on } S_4,$$

where h is the convection coefficient; T_s is an unknown surface temperature; T_e is a convective exchange temperature; σ is the Stefan–Boltzmann constant; ε is the surface emission coefficient; α is the surface absorption coefficient, and q_r is the incident radiant heat flow per unit surface area. For transient problems it is necessary to specify an initial temperature field for a body at the time t = 0:

$$T(x, y, z, 0) = T_0(x, y, z). \tag{2-17}$$

2.6.1.2   Finite element discretization of heat transfer equations

A domain *V* is divided into finite elements connected at nodes. We shall write all the relations for a finite element. Global equations for the domain can be assembled from finite element equations using connectivity information.

Shape functions N_i are used for interpolation of temperature inside a finite element:

$$T = [N]\{T\},$$

$$[N] = [N_1 N_2 \dots], \tag{2-18}$$

$$\{T\} = \{T_1 T_2 \dots\}.$$

Differentiation of the temperature-interpolation equation gives the following interpolation relation for temperature gradients:

$$\begin{Bmatrix} \frac{\partial T}{\partial x} \\ \frac{\partial T}{\partial y} \\ \frac{\partial T}{\partial z} \end{Bmatrix} = \begin{bmatrix} \frac{\partial N_1}{\partial x} & \frac{\partial N_2}{\partial x} & \dots \\ \frac{\partial N_1}{\partial y} & \frac{\partial N_2}{\partial y} & \dots \\ \frac{\partial N_1}{\partial z} & \frac{\partial N_2}{\partial z} & \dots \end{bmatrix} \{T\} = [B]\{T\}. \tag{2-19}$$

Here, *{T}* is a vector of temperatures at nodes, *[N]* is a matrix of shape functions, and *[B]* is a matrix for temperature-gradient interpolation. Using the Galerkin method, we can rewrite the basic heat transfer equation in the following form:

$$\int_V \left(\frac{\partial q_x}{\partial x} + \frac{\partial q_y}{\partial y} + \frac{\partial q_z}{\partial z} - Q + \rho c \frac{\partial T}{\partial t} \right) N_i dV = 0. \tag{2-20}$$

Applying the divergence theorem to the first three terms, we arrive at the relations:

$$\int_V \rho c \frac{\partial T}{\partial t} N_i dV - \int_V \left[\frac{\partial N_i}{\partial x} \frac{\partial N_i}{\partial y} \frac{\partial N_i}{\partial z}\right]\{q\}dV = \int_V Q N_i dV - \int_S \{q\}^T\{n\} N_i dS, \qquad (2\text{-}21)$$

$$\{q\}^T = [q_x q_y q_z],$$

$$\{n\}^T = [n_x n_y n_z],$$

where *{n}* is an outer normal to the surface of the body. After insertion of boundary conditions into the above equation, the discretized equations are as follows:

$$\int_V \rho c \frac{\partial T}{\partial t} N_i dV - \int_V \left[\frac{\partial N_i}{\partial x} \frac{\partial N_i}{\partial y} \frac{\partial N_i}{\partial z}\right]\{q\}dV = \int_V Q N_i dV - \int_{S_1} \{q\}^T\{n\} N_i dS + \int_{S_2} q_s N_i dS -$$
$$\int_{S_3} h(T - T_e)N_i dS - \int_{S_4} (\sigma\varepsilon T^4 - \alpha q_r)N_i dS. \qquad (2\text{-}22)$$

It is worth noting that

$$\{q\} = -k[B]\{T\}. \qquad (2\text{-}23)$$

The discretized finite element equations for heat transfer problems have the following form:

$$[C]\{\dot{T}\} + ([K_c] + [K_h] + [K_r])\{T\} = \{R_T\} + \{R_Q\} + \{R_q\} + \{R_h\} + \{R_r\}, \qquad (2\text{-}24)$$

$$[C] = \int_V \rho c[N]^T[N]dV,$$

$$[K_c] = \int_V k[B]^T[B]dV,$$

$$[K_h] = \int_{S_3} h[N]^T[N]dS,$$

$$[K_r]\{T\} = \int_{S_4} \sigma\varepsilon T^4[N]^T dS,$$

$$\{R_T\} = -\int_{S_1} \{q\}^T\{n\}[N]^T dS, \qquad (2\text{-}25)$$

$$\{R_Q\} = \int_V Q[N]^T dV,$$

$$\{R_q\} = \int_{S_2} q_s[N]^T dS,$$

$$\{R_h\} = \int_{S_3} hT_e[N]^T dS,$$

$$\{R_r\} = \int_{S_4} \alpha q_r[N]^T dS.$$

Here, $\{\dot{T}\}$ is a nodal vector of temperature derivatives with respect to time.

2.6.1.3 Different type problems

Equations for different types of problems can be deducted from the above general equation:

Stationary linear problem

$$([K_c] + [K_h])\{T\} = \{R_Q\} + \{R_q\} + \{R_h\}. \tag{2-26}$$

Stationary nonlinear problem

$$([K_c] + [K_h] + [K_r])\{T\} = \{R_Q(T)\} + \{R_q(T)\} + \{R_h(T)\} + \{R_r(T)\}. \tag{2-27}$$

Transient linear problem

$$[C]\{\dot{T}\} + ([K_c] + [K_h(t)])\{T(t)\} = \{R_Q(t)\} + \{R_q(t)\} + \{R_h(t)\}. \tag{2-28}$$

Transient nonlinear problem

$$[C(T)]\{\dot{T}\} + ([K_c(T)] + [K_h(T,t)] + [K_r(T)])\{T\} = \{R_Q(T,t)\} + \{R_q(T,t)\} + \{R_h(T,t)\} +$$
$$\{R_r(T,t)\}. \tag{2-29}$$

2.6.1.4 Triangular elements

Calculation of element conductivity matrix *[kc]* and heat flow vector *{rq}* is illustrated for a two-dimensional triangular element with three nodes. A simple triangular finite element is shown in Fig. 2-4 . The temperature distribution *T(x,y)* inside the triangular element is described by linear interpolation of its nodal values:

$$T(x,y) = N_1(x,y)T_1 + N_2(x,y)T_2 + N_3(x,y)T_3,$$

$$N_i(x,y) = \alpha_i + \beta_i x + \gamma_i y. \tag{2-30}$$

Interpolation functions (usually called shape functions) $N_i(x,y)$ should satisfy the following conditions:

$$T(x_i, y_i) = T_i , i = 1, 2, 3. \tag{2-31}$$

Solution of the above equation system provides expressions for the shape functions:

$$N_i = \frac{1}{2\Delta}(a_i + b_i x + c_i y),$$

$$a_i = x_{i+1}y_{i+2} - x_{i+2}y_{i+1},$$

$$b_i = y_{i+1} - y_{i+2},$$

$$c_i = x_{i+2} - x_{i+1},$$

$$\Delta = \frac{1}{2}(x_2 y_3 + x_3 y_1 + x_1 y_2 - x_2 y_1 - x_3 y_2 - x_1 y_3), \qquad (2\text{-}32)$$

where Δ is the element area.
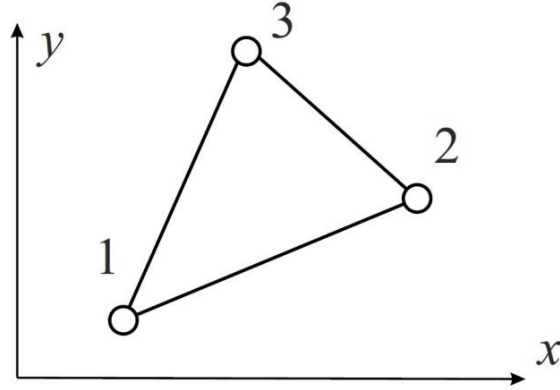
Fig. 2-4 Triangular finite element.

The conductivity matrix of the triangular element is determined by integration over element area A (assuming that the element has unit thickness),

$$[k_c] = \int_A k[B]^T[B]dxdy. \qquad (2\text{-}33)$$

The temperature differentiation matrix *[B]* has expression

$$[B] = \begin{bmatrix} \frac{\partial N_1}{\partial x} & \frac{\partial N_2}{\partial x} & \frac{\partial N_3}{\partial x} \\ \frac{\partial N_1}{\partial y} & \frac{\partial N_2}{\partial y} & \frac{\partial N_3}{\partial y} \end{bmatrix} = \frac{1}{2\Delta} \begin{bmatrix} b_1 & b_2 & b_3 \\ c_1 & c_2 & c_3 \end{bmatrix}. \qquad (2\text{-}34)$$

Since the temperature differentiation matrix does not depend on coordinates, integration of the conductivity matrix is simple;

$$[k_c] = \frac{k}{4\Delta} \begin{bmatrix} b_1^2 + c_1^2 & b_1 b_2 + c_1 c_2 & b_1 b_3 + c_1 c_3 \\ b_1 b_2 + c_1 c_2 & b_2^2 + c_2^2 & b_2 b_3 + c_2 c_3 \\ b_1 b_3 + c_1 c_3 & b_2 b_3 + c_2 c_3 & b_3^2 + c_3^2 \end{bmatrix}. \qquad (2\text{-}35)$$
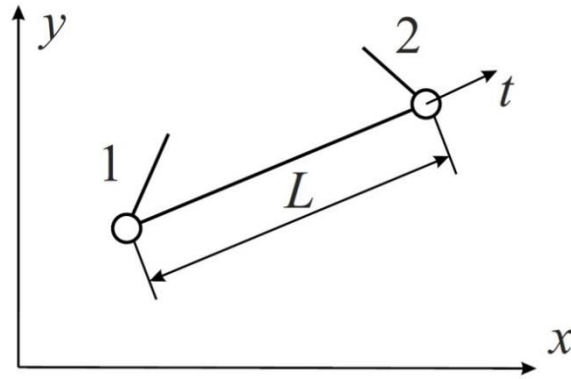
Fig. 2-5 Integration along an element side.

The heat-flow vector $\{r_q\}$ is evaluated by integration over the element side, as shown in Fig. 2-5:

$$\{r_q\} = -\int_L q_s [N]^T dL = -\int_0^1 q_s [N_1 N_2]^T L dt. \tag{2-36}$$

Here, integration over an element side L is replaced by integration using variable t ranging from 0 to 1. Shape functions N_1 and N_2 on element side 1–2 can be expressed through t:

$$N_1 = 1 - t, \ N_2 = t. \tag{2-37}$$

After integration with substituting integration limits, the heat-flow vector equals

$$\{r_q\} = -q_s \frac{L}{2} \begin{bmatrix} 1 \\ 1 \end{bmatrix}. \tag{2-38}$$

Element matrices and vectors are calculated for all elements in a mesh and assembled into the global equation system. After application of prescribed temperatures, solution of the global equation system produces temperatures at nodes.

2.6.2 GHE modeling in FEFLOW

In this section, different types of GHE with their individual pipe and grout components are described. They form highly slender cylindrical boreholes. The GHE systems are represented by 1D schematizations, where the pipe and grout components have a reduced spatial dimension. They imply that the variation of the temperature is along the vertical axis. The heat fluxes normal to the contact surfaces for the 1D pipe and grout components are modeled by heat transfer relations.

2.6.2.1 Double U-tubes (2U)

The double U-tubes (2U) exchange is a cylindrical borehole consisting of two inner pipes forming a U-tube and filled with a grout material. Basically, the grout can be considered as a homogenous impervious material and could be schematized by only one component so as proposed in Al-Khoury (2012), Al-Khoury and Bonnier (2006), Al-Khoury et al. (2005) (Diersch, 2014). However, to improve the approximation of the inner pipe-to-grout heat transfer FEFLOW introduces a larger number of grout components, which correlates with the number of the pipes of GHE (Bauer et al., 2011). In total, FEFLOW schematizes a 2U exchanger be eight components (Fig. 2-6):

- Two pipes-in (denoted as *i1* and *i2*)
- Two pipes-out (denoted as *o1* and *o2*)
- Grout material, which is subdivided into four zones (denoted as *g1*, *g2*, *g3*, *g4*)
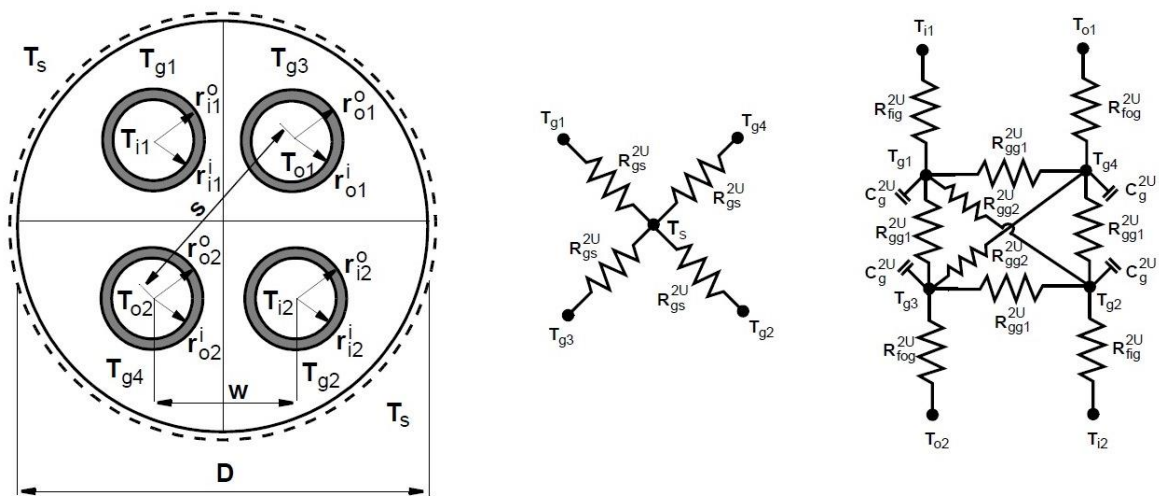
Fig. 2-6 Inner pipe-grout heat flux resistance relationship of a 2U GHE (Diersch, 2014).

The four pipe components *i1*, *i2*, *o1* and *o2* transfer heat across their cross-sectional areas and exchange fluxes across their surface areas. The radial heat transfer from the pipe is directed to the grout zones *gi (i=1, 2, 3 and 4)*. The grout zones *gi (i=1, 2, 3 and 4)* exchange heat directly to the surrounding soil (the porous matrix with the filled fluid in the void space) denoted as s and to other contacted grout zones too. It can be seen that, as physically occurring, the heat coupling only occurs via the grout zones *gi (i=1, 2, 3 and 4)*, which work as intermediate media that transfer heat from one pipe to another and vice versa. Only the grout zones exchange heat with the surrounding soil *s* because there is no direct thermal contact between the pipes *i1, i2, o1* and *o2* with the soil.

The 2U system involves several materials and geometric parameters, which are either given by the manufacturer of the heating system or determined experimentally. These relations are used to express the overall thermal resistance between the 2U borehole and the soil. The usual practice is to lump the effects of the 2U components into effective heat transfer coefficients representing the reciprocal of the sum of the thermal resistances between the different components. The inner pipe-grout heat flux resistance relationships are shown in Fig. 2-6.

2.6.2.2 Single U-tube (1U)

The single U-tube (1U) exchanger can be easily degenerated from a 2U configuration when dropping the second U-tube. A 1U configuration only consists of four components (Fig. 2-7):

- one pipe-in (denoted as *i1*)
- one pipes-out (denoted as *o1*)
- Grout material, which is subdivided into two zones (denoted as *g1*, *g2*)
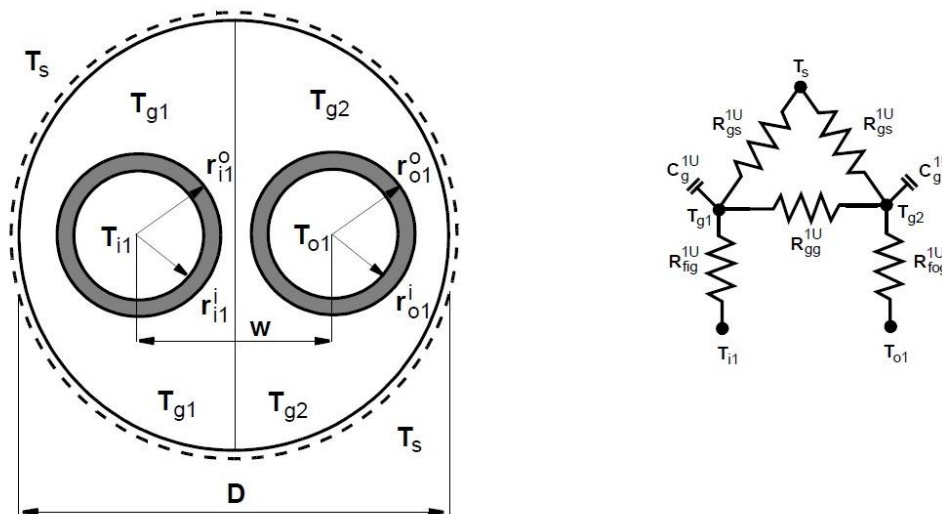
Fig. 2-7 Inner pipe-grout heat flux resistance relationship of a 1U GHE (Diersch, 2014).

Similar to the 2U exchanger the pipe of the 1U configuration transfers heat in radial directions to the grout zones *gi (i=1, 2, 3 and 4)*, while the grout material zones exchange heat directly to the surrounding soil s and to the adjacent grout zone. The corresponding inner pipe-grout heat flux resistance relationships are shown in Fig. 2.

2.6.2.3 Thermal resistances

Thermal resistance is a measure of material's ability to resist heat transfer through its surface and contact zone. Thermal resistances are determined from the physical, material and geometric engineering parameters of the different GHE configuration as shown in Fig. 1 for the 2U and in

49

Fig. 2 for 1U exchanger. As indicated the interaction between the different components of the pipe exists between the pipe-in and grout zone(s), the pipe-out and grout zone(s) as well as the pipe-in and pipe-out. The thermal resistances due to heat conduction in the grout material are derived by adding correction terms gained from numerical simulations to well-known 2D heat conduction shape factors. These resistances then are divided in such a manner, that the grout points are suitably located to obtain accurate transient computation results, see (Bauer et al., 2011). The following *specific* thermal resistances can be derived.

The thermal resistance between the pipes and grout zones in caused by the advection of the pipe flow and thermal conductivity of the pipe wall material specified separately for pipe-in and pipe-out.

$$R_{fig}^{2U} = R_{adv_k}^{2U} + R_{con_k^a}^{2U} + R_{con^b}^{2U} \quad (k = i1 \cap i2) \tag{2-39}$$

$$R_{fog}^{2U} = R_{adv_k}^{2U} + R_{con_k^a}^{2U} + R_{con^b}^{2U} \quad (k = o1 \cap o2) \tag{2-40}$$

Thermal resistance due to the advective flow of refrigerant in the pipes for 2U exchanger

$$R_{adv_k}^{2U} = \frac{1}{Nu_k \Lambda^r \pi} \quad (k = i1, o1, i2, o2) \tag{2-41}$$

where Λ^r is the thermal conductivity of the refrigerant. In Eq. 3 the Nusselt numbers, Nu_k ($k = i1, o1, i2, o2$), differ between laminar and turbulent flow,

$$Nu_k = \begin{cases} 4.364 \\ \quad for\ laminar\ flow\ if\ Re_k < 2,300 \\ \dfrac{(\xi_k/_8)Re_kPr}{1+12.7\sqrt{\xi_k/_8}(Pr^{2/3}-1)}\left[1+\left(\dfrac{d_k^i}{L}\right)^{2/3}\right] \\ \quad for\ turbulent\ flow\ if\ Re_k \geq 10^4 \\ (1-\gamma_k)4.364 + \gamma_k\left\{\dfrac{(0.0308/_8)10^4 Pr}{1+12.7\sqrt{0.0308/_8}(Pr^{2/3}-1)}\left[1+\left(\dfrac{d_k^i}{L}\right)^{2/3}\right]\right\} \\ \quad for\ flow\ in\ transition\ range\ if\ 2,300 \leq Re_k < 10^4 \end{cases} \tag{2-42}$$

in which Pr represents the Prandtl number and Re_k are the Reynolds numbers defined as

$$Pr = \frac{\mu^r c^r}{\Lambda^r}, \quad Re_k = \frac{|u_k|^{2U} d_k^i}{\left(\mu^r/_{\rho^r}\right)} \quad (k = i1, o1, i2, o2) \tag{2-43}$$

50

where d^i_k are the inner diameters of the pipes $d^i_k = 2\ r^i_k$ $(k = i1,\ o1,\ i2,\ o2)$. Furthermore, L corresponds to the length of the pipe and

$$\left.\begin{aligned}\xi_k &= (1.8 \log_{10} Re_k - 1.5)^{-2}\\ \gamma_k &= \frac{Re_k - 2{,}300}{10^4 - 2{,}300}\ \ (0 \le \gamma_k \le 1)\end{aligned}\right\}$$

(2-44)

$$|\boldsymbol{u}_k|^{2U} = \begin{cases} \dfrac{Q_r}{2\pi(r^i_k)^2}\ for\ parallel\ discharge \\ \dfrac{Q_r}{\pi(r^i_k)^2}\ for\ serial\ discharge \end{cases} \quad (k = i1, o1, i2, o2)$$

(2-45)

where Q_r is the total refrigerant flow discharge of the 2U exchanger.

Thermal resistances due to the pipes wall material and grout transition for 2U exchanger

$$R^{2U}_{con^a_k} = \frac{\ln\left(r^o_k / r^i_k\right)}{2\pi\Lambda^\pi_k} \quad (k = i1, o1, i2, o2)$$

(2-46)

where $\Lambda^\pi_{i1},\ \Lambda^\pi_{o1},\ \Lambda^\pi_{i2},\ \Lambda^\pi_{o2}$ correspond to thermal conductivities of the pipe wall material.

$$R^{2U}_{con^b} = x^{2U} R^{2U}_g$$

(2-47)

with

$$x^{2U} = \frac{\ln\left(\frac{\sqrt{D^2 + 4d^2_o}}{2\sqrt{2}d_o}\right)}{\ln\left(\frac{D}{2d_o}\right)}$$

(2-48)

and

$$R^{2U}_g = \frac{arcosh\left(\frac{D^2 + d^2_o - s^2}{2Dd_o}\right)}{2\pi\Lambda^g}\left(3.098 - 4.432\frac{s}{D} + 2.364\frac{s^2}{D^2}\right)$$

(2-49)

where D denotes the borehole diameter, $d_o = \frac{1}{4}\sum_k d^o_k$ is the average outer diameter of the pipes $d^o_k = 2\ r^o_k$ $(k = i1,\ o1,\ i2,\ o2)$ and $s = w\sqrt{2}$ corresponds to diagonal distances of pipes (see Fig. 2-6).

Thermal resistance due to inter-grout exchange for 2U exchanger

$$R^{2U}_{gg1} = \frac{2R^{2U}_{gs}\left(R^{2U}_{ar1} - 2x^{2U}R^{2U}_g\right)}{2R^{2U}_{gs} - R^{2U}_{ar1} + 2x^{2U}R^{2U}_g}$$

(2-50)

51

$$R_{gg2}^{2U} = \frac{2R_{gs}^{2U}\left(R_{ar2}^{2U} - 2x^{2U}R_g^{2U}\right)}{2R_{gs}^{2U} - R_{ar2}^{2U} + 2x^{2U}R_g^{2U}}$$

(2-51)

with

$$R_{ar1}^{2U} = \frac{\operatorname{arcosh}\left(\frac{s^2 - d_o^2}{d_o^2}\right)}{2\pi\Lambda^g}$$

(2-52)

$$R_{ar2}^{2U} = \frac{\operatorname{arcosh}\left(\frac{2s^2 - d_o^2}{d_o^2}\right)}{2\pi\Lambda^g}$$

(2-53)

Thermal resistance due to grout-soil exchange for 2U exchanger

$$R_{gs}^{2U} = (1 - x^{2U})R_g^{2U}$$

(2-54)

For 1U exchanger it is:

$$R_{fig}^{1U} = R_{adv_k}^{1U} + R_{con_k^a}^{1U} + R_{con^b}^{1U} \quad (k = i1)$$

(2-55)

$$R_{fog}^{1U} = R_{adv_k}^{1U} + R_{con_k^a}^{1U} + R_{con^b}^{1U} \quad (k = o1)$$

(2-56)

Thermal resistance due to the advective flow of refrigerant in the pipes for 1U exchanger:

$$R_{adv_k}^{1U} = \frac{1}{Nu_k\Lambda^r\pi} \quad (k = i1, o1)$$

(2-57)

where Nu_k is given by the expressions (2.42) - (2.44) in which the refrigerant fluid velocity for 1D pipe is

$$|\boldsymbol{u}_k|^{2U} = \frac{Q_r}{2\pi(r_k^i)^2} \quad (k = i1, o1)$$

(2-58)

Thermal resistances due to the pipes wall material and grout transition for 1U exchanger:

$$R_{con_k^a}^{1U} = \frac{\ln\left(r_k^o / r_k^i\right)}{2\pi\Lambda_k^\pi} \quad (k = i1, o1)$$

(2-59)

$$R_{con^b}^{1U} = x^{1U}R_g^{1U}$$

(2-60)

with

$$x^{1U} = \frac{\ln\left(\frac{\sqrt{D^2+2d_o^2}}{2d_o}\right)}{\ln\left(\frac{D}{\sqrt{2}d_o}\right)} \tag{2-61}$$

and

$$R_g^{1U} = \frac{arcosh\left(\frac{D^2+d_o^2-w^2}{2Dd_o}\right)}{2\pi\Lambda^g}\left(1.601 - 0.888\frac{w}{D}\right) \tag{2-62}$$

where *w* corresponds to distances between the pipes (see. Fig. 2-6).

Thermal resistance due to inter-grout exchange for 1U exchanger:

$$R_{gg}^{1U} = \frac{2R_{gs}^{1U}\left(R_{ar}^{1U}-2x^{1U}R_g^{1U}\right)}{2R_{gs}^{1U}-R_{ar}^{1U}+2x^{1U}R_g^{1U}} \tag{2-63}$$

with

$$R_{ar}^{1U} = \frac{arcosh\left(\frac{2w^2-d_o^2}{d_o^2}\right)}{2\pi\Lambda^g} \tag{2-64}$$

Thermal resistance due to grout-soil exchange for 1U exchanger:

$$R_{gs}^{1U} = (1 - x^{1U})R_g^{1U} \tag{2-65}$$

2.6.3 Numerical modeling of TRTs

In this study, FEFLOW 6.2 software is used to model the thermal behavior of the GHE and to calculate the outlet temperature during TRTs and the ground temperatures up to 2 days after finishing TRTs. As shown in Fig. 2-9, the model has 20 m length and width (in x and y directions) and 110 m depth (in z direction) and consists of 29 layers from top to bottom. The number of elements in each layer is 1711 elements and grids are finer close to the GHE. The GHE is placed in the middle of model from surface to -102 m, same as the experimental condition.

Ground thermal conductivity profile is estimated using the TRT with optical fiber thermometer as shown in Fig. 2-8 (Fujii, et al., 2015). GHE model and cross sectional views of U-tube are shown in Figs. 2-9 and 2-10. The simulation needs initial conditions (ground temperature, hydraulic head), boundary conditions and material properties. Measured data are used for ground initial temperature and hydraulic head. The physical properties of model and GHE are shown in Tables 2-2 and 2-3. TRT data was used as inlet temperatures and water circulation rates inside

the U-tube. The boundary condition for top surface of model was assigned as impermeable and without heat flux. For the side surfaces, hydraulic head and temperature were assigned as constant. The boundary condition for the bottom surface was assigned as impermeable and with a fixed temperature.
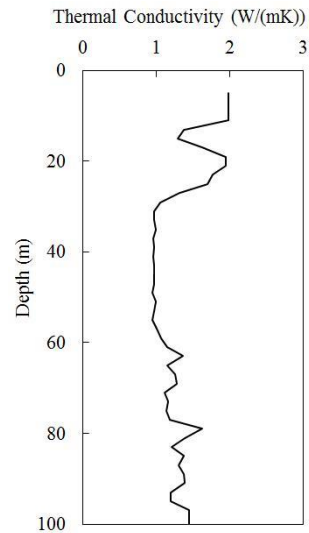
Fig. 2-8 Estimated thermal conductivity profile (Fujii, et al., 2015).
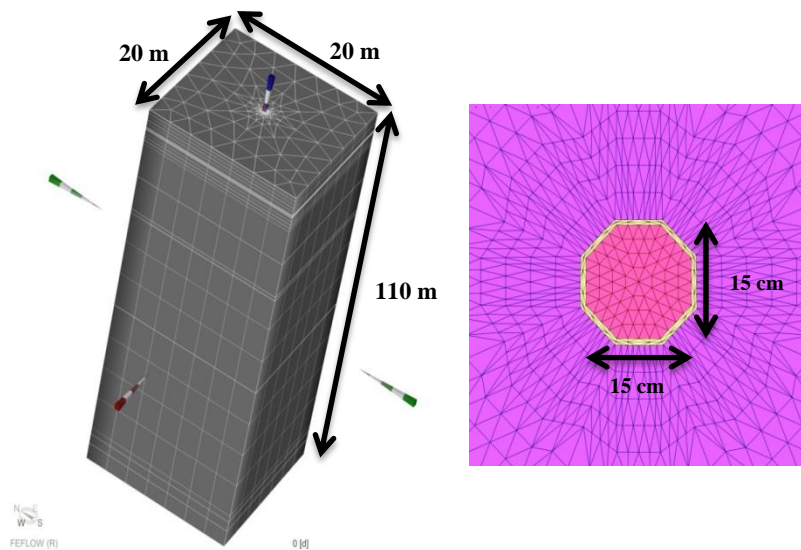
Fig. 2-9 Ground heat exchanger model.
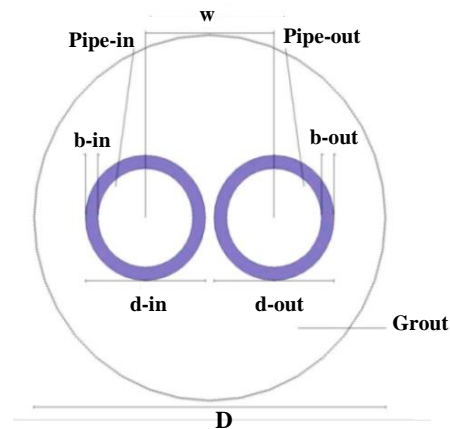
Fig. 2-10 Cross sectional view of GHE.

Table 2-2 Physical properties of the model.

Porosity (-)	0.2
Coefficient of permeability (10^{-6} m/s)	0.1
Thermal conductivity of solid (W/m/K)	from Figure 4
Thermal conductivity of fluid (W/m/K)	0.65
Heat capacity of solid (10^6 J/m^3/K)	2.5
Heat capacity of fluid (10^6 J/m^3/K)	4.2

Table 2-3 Properties of GHE.

Borehole diameter (D) (m)	0.1
Pipe distance (w) (m)	0.0365
Inlet pipe diameter (d-in) (m)	0.034
Inlet pipe wall thickness (b-in) (m)	0.0035
Outlet pipe diameter (d-out) (m)	0.034
Outlet pipe wall thickness (b-out) (m)	0.0035
Inlet pipe thermal conductivity (W/m/K)	0.46
Outlet pipe thermal conductivity (W/m/K)	0.46
Grout volume thermal conductivity (tc-grout) (W/m/K)	3
Refrigerant volumetric heat capacity (10^6 J/m^3/K)	4.168
Refrigerant thermal conductivity (W/m/K)	0.6064
Refrigerant dynamic viscosity (10^{-3} kg/m/s)	0.9
Refrigerant density (kg/m^3)	997.1

2.6.4 Model validation

TRT data and simulation result of FEFLOW model were history matched for all TRTs. The measured parameters are water outlet temperatures during TRT and ground temperatures one day and two days after finishing heating. The history matching for the above mentioned parameters for all of TRTs were done but some of them were selected as the samples to be shown in this section.

55

Histories matching for outlet temperature and ground temperature two days after TRT-N are shown in Figs. 2-11 and 2-12, respectively. Some fluctuations can be seen in the measured outlet water temperature, and also simulated temperatures are slightly higher than measured data. The reason for this issue described in section 2.5. In Fig. 2-12, it can be seen that there is a difference between simulated and experimental results of ground temperature recovery in shallow depths; the temperatures of ground near the land surface are affected by weather conditions. In the layers deeper than -5m, there is good matching between simulated and experimental results.

In Figs. 2-13 and 2-14, history matching results for TRT-P5 are shown. The calculated and measured outlet water temperatures showed a good match, while some difference was found in the shallow ground temperature. The average of difference between calculated and measured ground temperatures from -5 m to -100 m is 1.0 °C that is acceptable.

The history matching results of TRT-I5, are shown in Figs. 2-15 and 2-16. There is good agreement between calculated and measured results for both water outlet temperature and ground temperature recovery. By increasing the injecting water rate, groundwater level approaches to ground surface and the results become more accurate for shallow depths. History matching results for TRT-I3-20 is shown in Fig. 2-17 with good agreement. These results are validating the numerical model for different injecting/pumping water rates with different injecting water temperature.
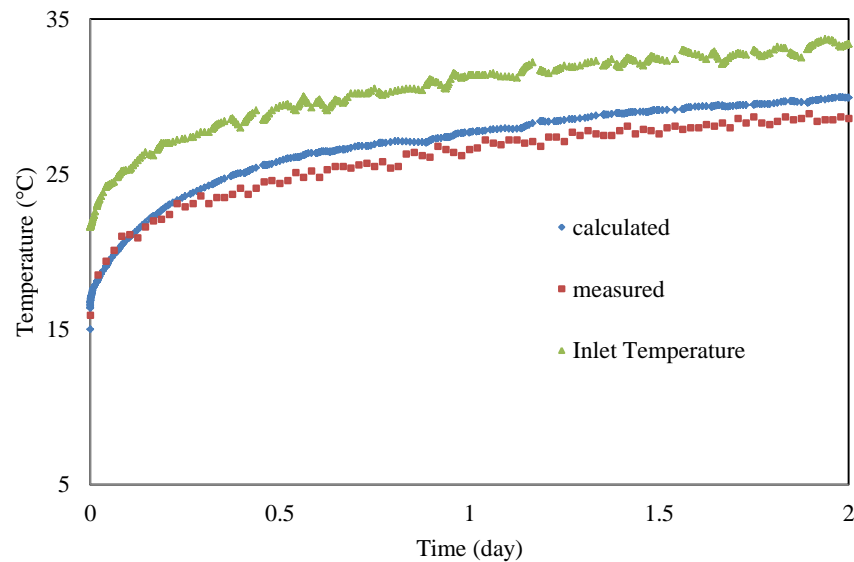
Fig. 2-11 Outlet Temperature history matching for TRT-N.
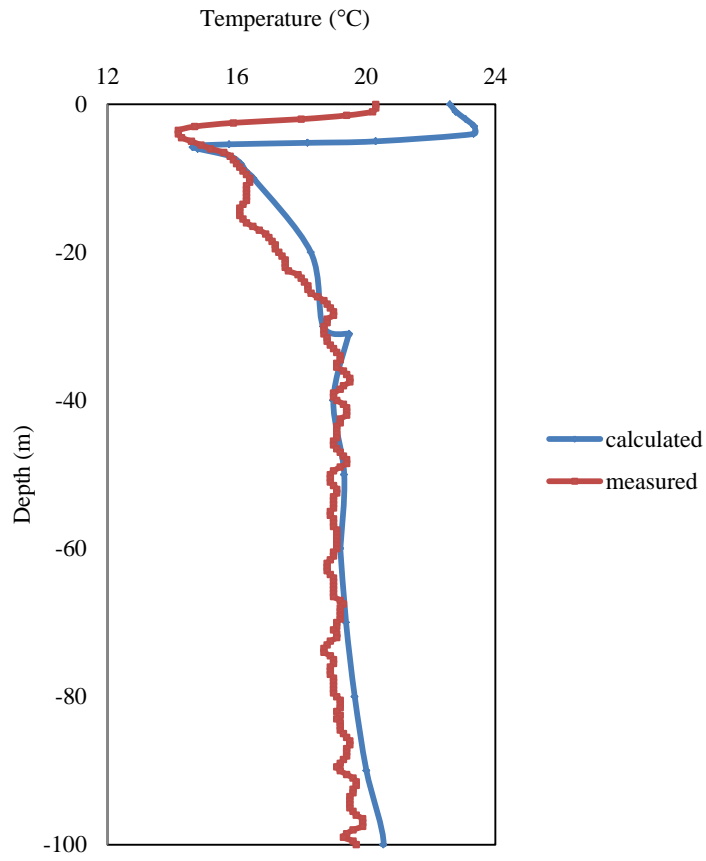
Fig. 2-12 History matching for ground Temperature 2 days after TRT-N.
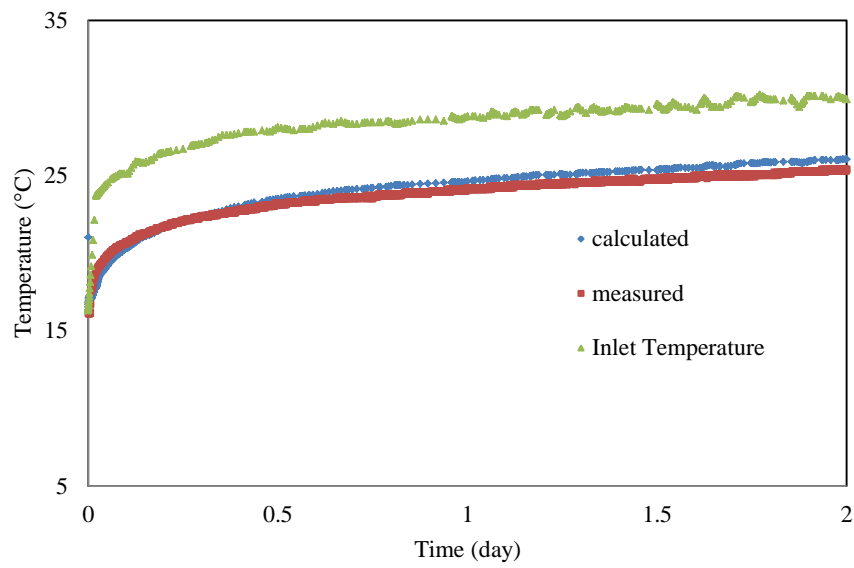
Fig. 2-13 Outlet Temperature history matching for TRT-P5.

57
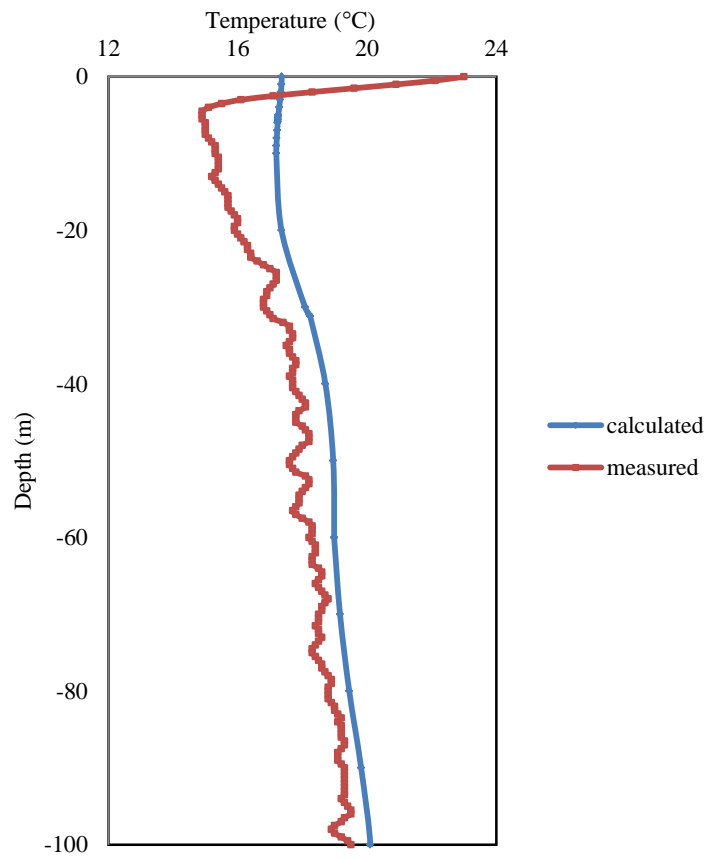
Fig. 2-14 History matching for ground Temperature 1.75 days after TRT-P5.
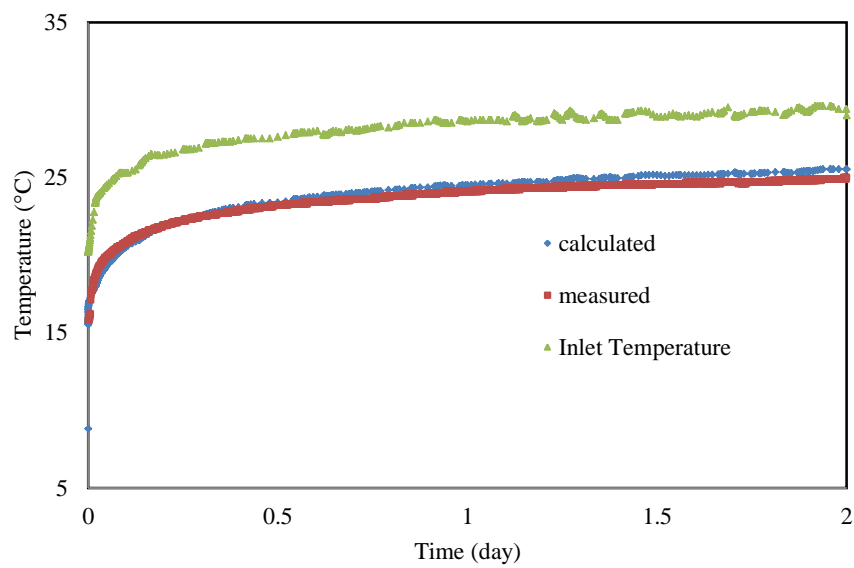
Fig. 2-15 Outlet Temperature history matching for TRT-I5.
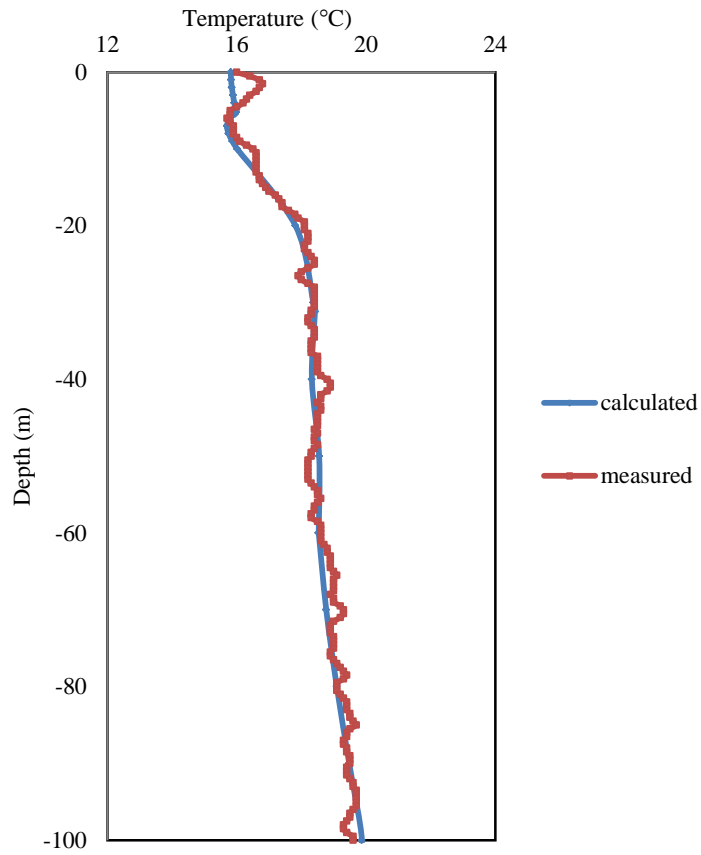
Fig. 2-16 History matching for ground Temperature 2 days after TRT-I5.
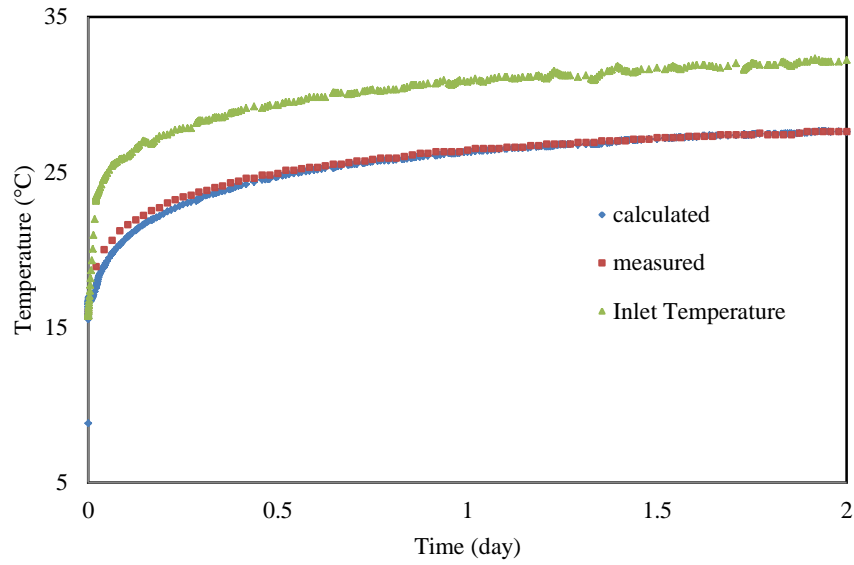
Fig. 2-17 Outlet Temperature history matching for TRT-I3-20.

2.7 Sensitivity analysis

Since the simulated temperatures showed good agreement with TRTs results, this model is used to study the effect of injection/pumping rate on heat transfer between the GHE and the ground. In this case study, the rates of injecting/pumping water are varied from 0 to 15 L/min, with different GHE inlet water temperatures (0 and 5 °C). The effect of groundwater velocity is also studied by setting the velocity as 0.1 m/day in comparison with no groundwater flow case, in both injection and pumping modes. In each case, the simulation was performed for 10 days (operation time 24 hours/day) and the average of heat transfer between the GHE and the ground per 1 meter of GHE was calculated. Physical conditions of the model and the simulation parameters are shown in Table 2-4.

In Figs. 2-18 and 2-19, the average heat exchange rate per unit GHE length versus injection/pumping rate with the 0 °C and 5 °C as inlet water temperatures are shown. By increasing injection/pumping rate, heat exchange rate between the GHE and the ground is increased but for the rates above 5 L/min, heat exchange rate is less affected by water flow rate. The heat exchange rate for 0 °C inlet water temperature is higher than the case with 5 °C inlet water temperature in both injecting and pumping modes, because in this case the difference between the initial temperature of ground and the inlet water temperature is larger. The heat exchange rate for injection is slightly higher than pumping mode for the same water rate and inlet water temperatures. By increasing water injection rate, the groundwater level approaches to the ground surface but with increasing water pumping rate, groundwater level gets deeper and effective length of GHE decreases. As a result, heat exchange rate in pumping mode is slightly less than injection mode under the same condition.

Table 2-4 Sensitivity analysis conditions.

Ground heat exchanger length (m)	102
Inlet water temperature (°C)	0 and 5
Circulating water rate (L/min)	15
Simulation period (day)	10 (24 hours/day)
Water injection/pumping rate (L/min)	0, 0.5, 1, 3, 5, 7, 10 and 15
Injecting water temperature (°C)	15
Injection depth (m)	0
Pumping depth (m)	-20
Initial ground temperature (°C)	15
Coefficient of permeability (m/s)	1.0×10^{-3}
Ground thermal conductivity (W/m/K)	1.2
Groundwater level (without injection or pumping) (m)	-5.2
Groundwater Velocity (m/day)	0 and 0.1

In Figures 2-20 and 2-21, the average heat exchange rate per unit length of GHE versus injection/pumping rate without groundwater flow and groundwater flow of 0.1 m/day are shown. In the case of no injection/pumping, heat exchange rate with 0.1 m/day groundwater velocity is three times larger than the case with no groundwater flow. With 15 L/min water injection, heat exchange rate in the case of 0.1 m/day groundwater velocity is 20% higher than the no groundwater flow mode and 10% higher in the case of pumping with 15 L/min. Heat exchange rate is less affected by water injection/pumping rate in the case of 0.1 m/day groundwater velocity in comparison with no groundwater flow case. In the cases with groundwater flow, the heat transfer between GHE and ground is dominated by forced convection with groundwater flow. As a result, heat exchange rate is less affected by injecting/pumping water rate, in comparison with no groundwater flow case. The temperature distribution around GHE after 0.4 days of simulation for groundwater flow case is shown in Fig. 2-22.
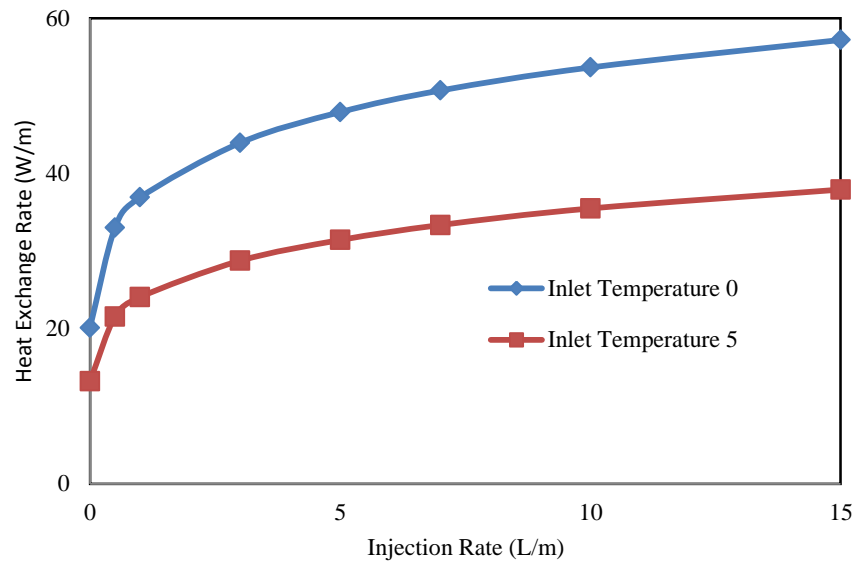
Fig. 2-18 Average heat exchange rate in the case of no groundwater flow for different inlet water temperatures, injection mode.
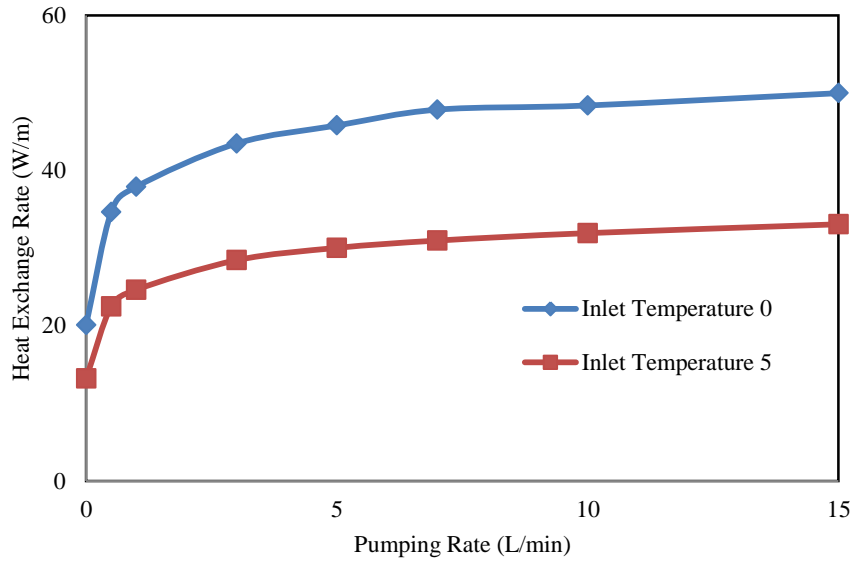
Fig. 2-19 Average heat exchange rate in the case of no groundwater flow for different inlet water temperatures, pumping mode.
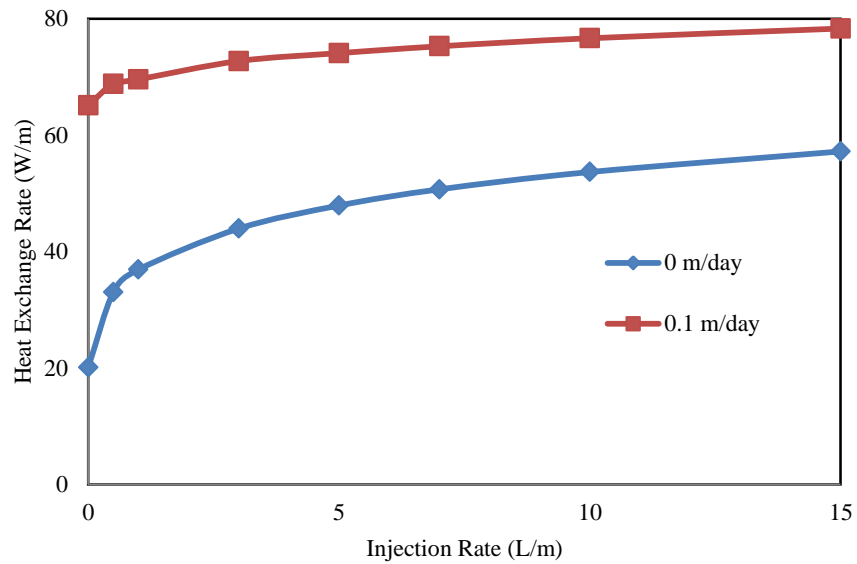
Fig. 2-20 Average heat exchange rate for different groundwater velocities, injection mode.
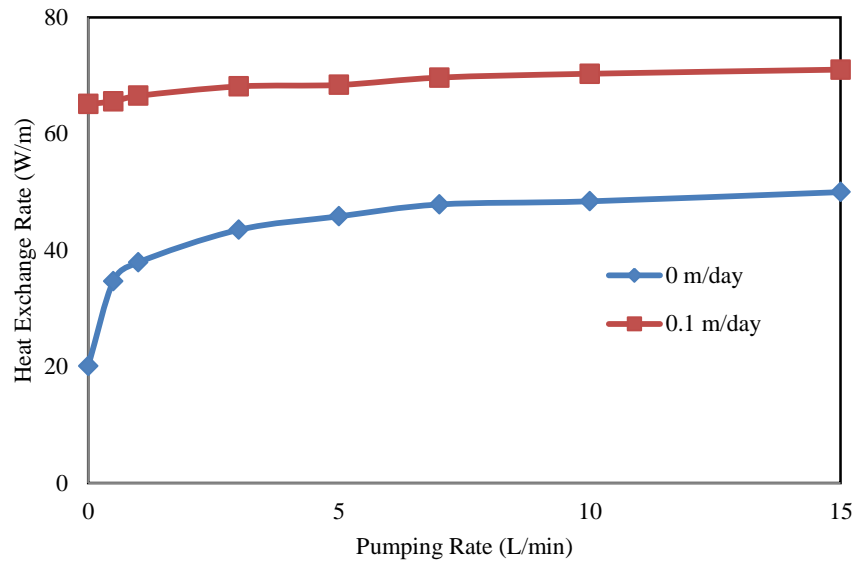
Fig. 2-21 Average heat exchange rate for different groundwater velocities, pumping mode.
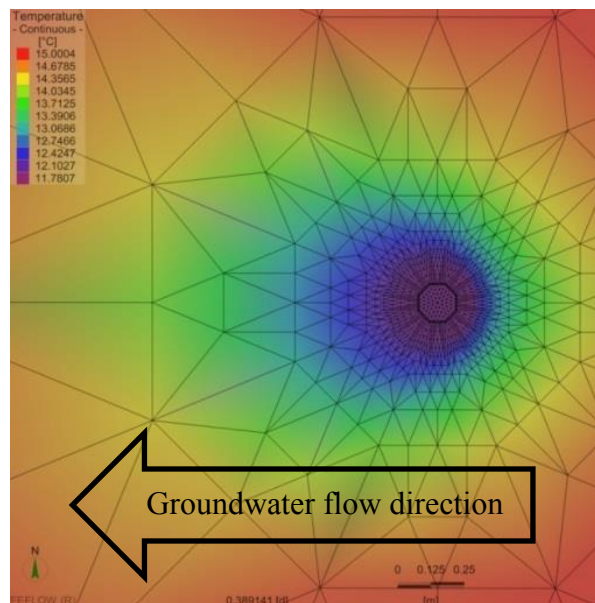
Fig. 2-22 Temperature distribution around GHE in the case of groundwater flow, 0.4 days after simulation.

2.8 Conclusions

In this chapter, the effect of water injection and pumping on heat exchange rate of a GHE were studied under different inlet temperatures and groundwater velocities by performing nine sets of TRTs. The TRT results showed that with increasing water injection/pumping rate, the average temperature of heat medium decreased. Numerical simulations were then carried out using FEFLOW 6.2 software and the model was validated by the TRT data. The results of simulation were in a good agreement with TRT results.

Sensitivity studies were then performed using validated model. Water injection/pumping rates were varied from 0 to 15 L/min with two different GHE inlet temperatures. Results of simulation showed that the average heat exchange rate increased by increasing water injection/pumping rate, but was less affected in the cases with water rates higher than 5 L/min. Under the same operating conditions, the average heat exchange rate for injection was slightly higher than the pumping mode. For the case with groundwater flow, the heat exchange rate was higher than the case without groundwater flow and it was 3 times higher in the case without injection or pumping. With increasing injecting/pumping water rate, the difference between two cases became smaller. In the case with groundwater velocity, heat exchange rate was less affected by water injection/pumping rate.

Chapter 3: SEMI-OPEN LOOP GSHP SYSTEM

3.1 Introduction

In this chapter, the results of field tests of semi-open loop GSHP system, numerical modeling of the system and also the sensitivity analysis will be presented. In order to evaluate the effect of water pumping and injection on the GSHP system performance, an experimental facility was prepared in Akita university campus. Before starting the field tests, TRTs were performed on each GHE individually to evaluate the effective thermal conductivity as well as temperature recovery after the TRT.

Heating and cooling tests under different operational conditions were performed, during the winter and summer of 2016, respectively. During each experiment, all of the system influential parameters including the working fluid temperatures, flow rates and power consumptions were measured. Based on the measured data, COP and SCOP for each test were calculated and compared with other tests.

In order to simulate the semi-open loop GSHP system behavior, numerical modeling was performed using FEFLOW 6.2. The numerical model was validated using the experimental data in heating and cooling operations. In the last step of this stage of semi-open loop GSHP study, a sensitivity analysis was performed using the validated FEFLOW model to evaluate the GSHP system performance and GHE heat transfer capacity for the base case (without water pumping and injection) and semi-open loop operations. In the sensitivity analysis, the effect of natural groundwater flow on the GSHP system performance was also investigated. In the last section of this chapter, the numerical model was modified to evaluate the effect of GHE spacing on system thermal performance. The heat pump COP and minimum working fluid temperature were calculated in each case, considering the effect of GHE spacing and natural groundwater flow in the formation.

3.2 Characteristics of the experimental facility

To evaluate whether water pumping and injection enhances the heat transfer rate in semi-open loop GSHP systems, two vertical GHEs (GHE1 and GHE2) were drilled at Akita University campus, Japan. The upper part (surface to 60 m) of the formation is an alluvial deposit of the Quaternary System, consisting mainly of silt, sand and gravel. The lower part consists of siltstone of the Tertiary System. The geological column and undisturbed ground temperature are shown in Fig. 3-1. Below 15 m, a clear geothermal gradient of 0.04 °C/m was observed.

Ground temperature (°C)
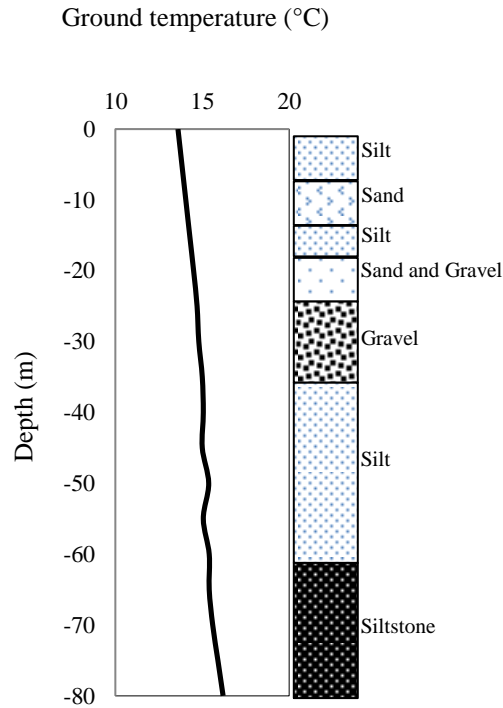
Fig. 3-1 Undisturbed ground temperature and geological column (Fujii et al., 2015)

The system specifications are shown in Fig. 3-2 and Table 3-1. The GHE part of GSHP system consists of two GHEs with 5 m distance in Akita University campus. Well length in GHE1 and GHE2 are 60 m and 70 m, respectively. The well length in GHE2 is 10 m longer than GHE1, although heat exchangers have same length as shown in Fig. 3-2. The additional 10 m interval of GHE2 was drilled to install an ESP (Electrical Submersible Pump) in case the surface water pump could not pump enough quantity of groundwater, which was proved unnecessary later. Fig. 3-3 shows the rotary drilling equipment.

Both GHEs are enclosed in a steel casing from the ground surface to the well bottom. Between -10 m and -60 m, the casing is slotted to allow groundwater flow across the GHEs. Fig. 3-4 shows the casings of GHE wells. Double U-tubes are installed in both GHEs from the surface to -60 m. Fig. 3-5 shows the installation process of the U-tubes.

Table 3-1 System specifications.

GHE type	Double U-tube
Borehole diameter	230 mm
Casing ID/OD	151 mm/165 mm
U-tube ID/OD	27 mm/34 mm
Primary loop Antifreeze	Ethylene glycol (20%)
Secondary loop Antifreeze	Propylene glycol (25%)
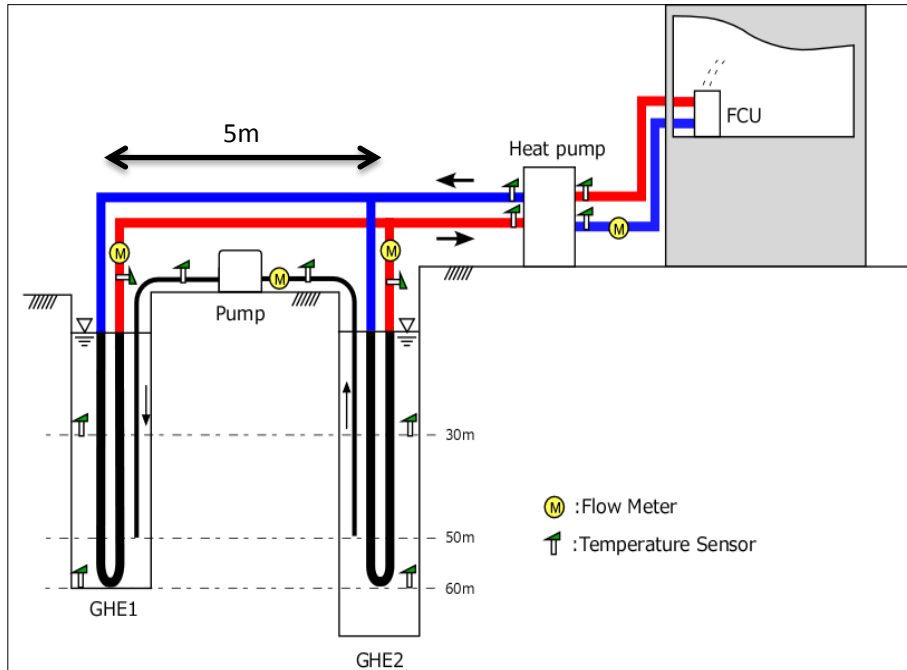
Fig. 3-2 Schematic of the semi-open loop system.

Fig. 3-3 Rotary drilling equipment.

Fig. 3-4 Casings for GHEs.

Fig. 3-5 U-tube installation process.

The two GHEs are placed 5 m apart and water is pumped between them by a water pump (Teral, 85 W output power, PG-87A-5) with a controlling unit placed on the ground surface. The water pumping and injection pipes in GHE2 and GHE1 are located at depth 50 m and installed with double U-tube GHEs at the same time. Fig. 3-6 shows the water pump and controlling unit. The heat pump unit has a heating and cooling capacity of 10 kW (Sunpot model GSHP-1001, produced in Japan). Fig. 3-7 shows the inside on the heat pump unit.

In order to evaluate the system performance during the heating and cooling operations, various data were measured at an interval of 1 minutes:

- Inlet and outlet temperatures of GHEs
- Heat pump primary and secondary loops inlet and outlet temperatures
- Ground temperature at -30 m and -60 m for both GHEs
- Pumping and injecting water temperatures
- Working fluid flow rate for each GHE and for heat pump secondary loop
- Water pumping and injection flow rate
- Heat pump power consumption
- Water pump power consumption

The water pumping and injection was monitored by a Keyence FD-Q20C flow meter (measuring range: 2.5-100 L/min, accuracy: 0.01 L/min) , and the flow rates of the heat medium in the primary and secondary loops of the heat pump were measured by a Keyence FD-M50AY flow meter (measuring range: 2.5-50 L/min, accuracy: 0.01 L/min). The temperatures of the heat medium, ground and groundwater pumping were measured by thermoresistance thermometers (Pt100, accuracy $\pm$ 0.15 ℃).

Fig. 3-6 Water pump and controlling unit.

Fig. 3-7 Heat pump unit.

The heat medium in the primary and secondary sides of the GHEs was circulated by the built-in pumps of the heat pumps. The total power consumption of the two circulation pumps was measured as 190 W. A measurement and control panel was placed close to heat pump unit to gather and record the necessary data (Fig. 3-8). In order to have a visual access to the experimental parameters during the field tests, a monitoring system was designed and placed in the room to be heated and cooled (Fig. 3-9).

Fig. 3-8 Measurement and control unit.
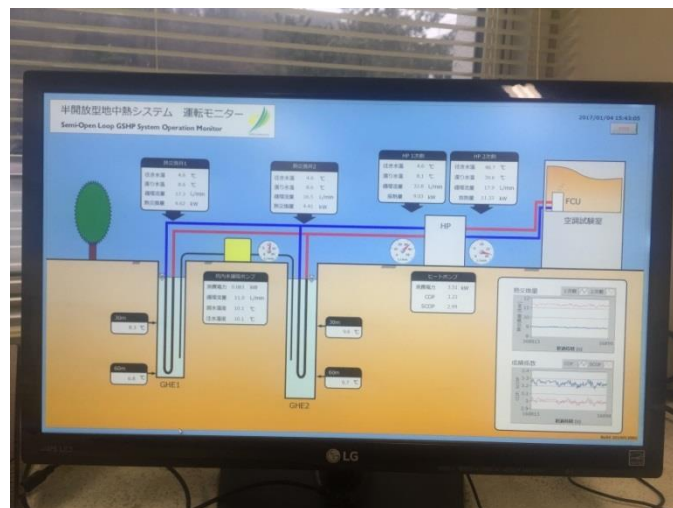
Fig. 3-9 Monitoring device.

Fig. 3-10 Fan coil unit.
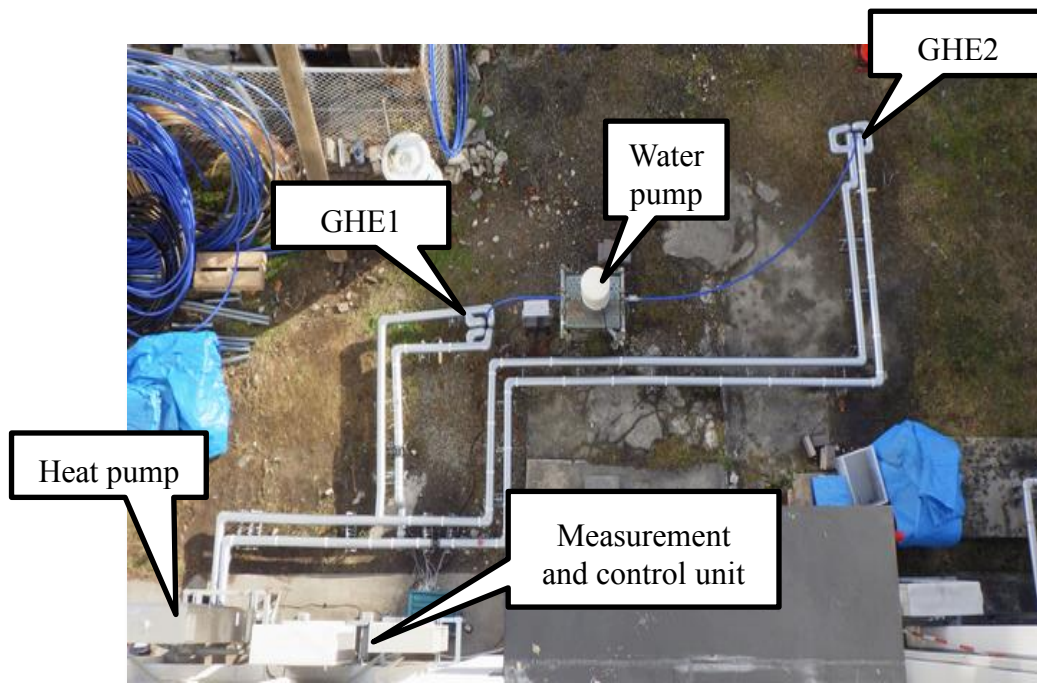
Fig. 3-11 Up-view of the installed semi-open loop GSHP system.

During the heating tests, the heat pump system was heating 2 rooms, each with 25 m^2 area, in the Akita University campus. During the cooling tests, a seminar room with 50 m^2 area was added to the conditioned rooms, which gives the total area of 100 m^2. One fan coil unit in each room was used as the heat distribution system (Fig. 3-10). The fan coils in small rooms are Mitsubishi LV-400WFE-C2 with total cooling and heating capacity of 3.48 and 6.57 kW, respectively. The fan coils in the large room is Mitsubishi LV-1200WFE-C3 with total cooling and heating capacity of 9.08 and 17.48 kW, respectively. Fig. 3-11 shows the up-view of the installed semi-open loop GSHP system.

3.3 TRTs of the semi-open loop system

TRTs were performed on the GHEs of the semi-open loop GSHP system in order to evaluate the effective thermal conductivity of the GHEs. Each TRT was performed for 48 hour and the necessary data (including GHE inlet and outlet temperature, GHE flow rate and heat transfer rate) were measured and recorded. The fluid temperature along the GHE (from ground surface to -60 m depth) was measured during the TRTs and until 24 hours after the TRT to observe the temperature recovery. The Heat transfer rate and flow rate were set as 3 kW and 15 L/min, respectively. Fig. 3-12 shows the TRT equipment.
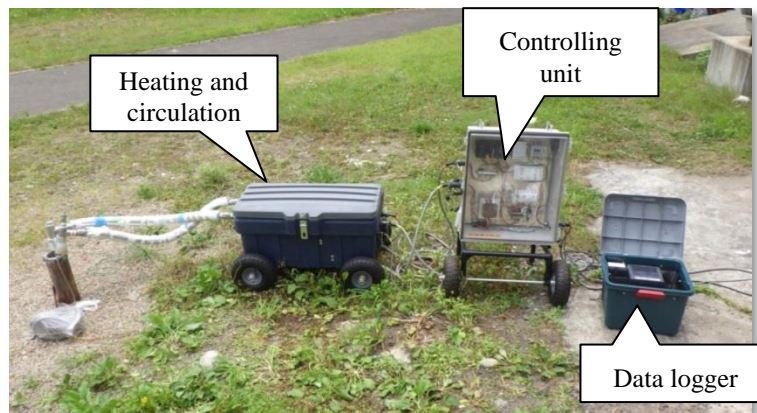
Fig. 3-12 TRT equipment of semi-open loop GHEs.

The TRT for GHE1 started at 24/Sep/2015 and continued for 48 hours. Fig. 3-13 shows the heat medium temperature (average of GHE inlet and outlet temperature) during the TRT. It is necessary to note that the time axis is in logarithmic scale. Results of the calculations (using equation 2-2 and considering the effective GHE length as 55 m) showed that the effective thermal conductivity of the GHE1 is 5.49 W/m/K. This is a high value and shows the possibility of strong groundwater flow in the formation. The temperature recovery diagram for GHE1 is shown in Fig. 3-14. The temperature along the GHE was recovered to the initial value 24 hours after TRT. The recovery process was faster at around -10 m depth.

The TRT for GHE2 started at 14/Sep/2015 and continued for 48 hours. Fig. 3-15 shows the temperature of the heat medium during the TRT. The effective thermal conductivity for GHE2 was calculated as 6.23 W/m/K. The effective thermal conductivity is higher than GHE1 and also showed the possibility of strong groundwater flow in the formation. Fig. 3-16 shows the temperature recovery of the GHE2. The temperature recovery was achieved 24 hours after the TRT and it is very fast above -20 m, which indicates the existence of fast groundwater flow in the shallow formation. The direction of groundwater pumping/injection direction in semi-open loop GSHP system was decided to be from GHE2 to GHE1 based on the better thermal and hydraulic performance of GHE2.
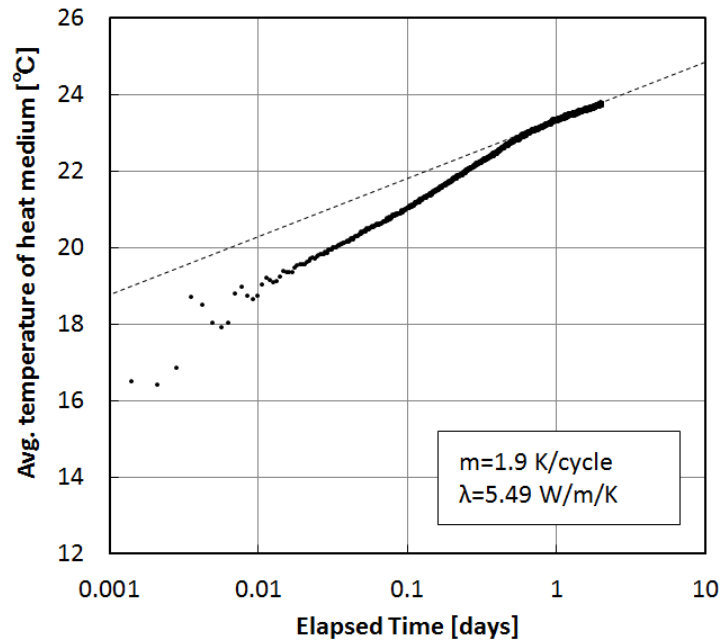
Fig. 3-13 The heat medium temperature during TRT on GHE1.
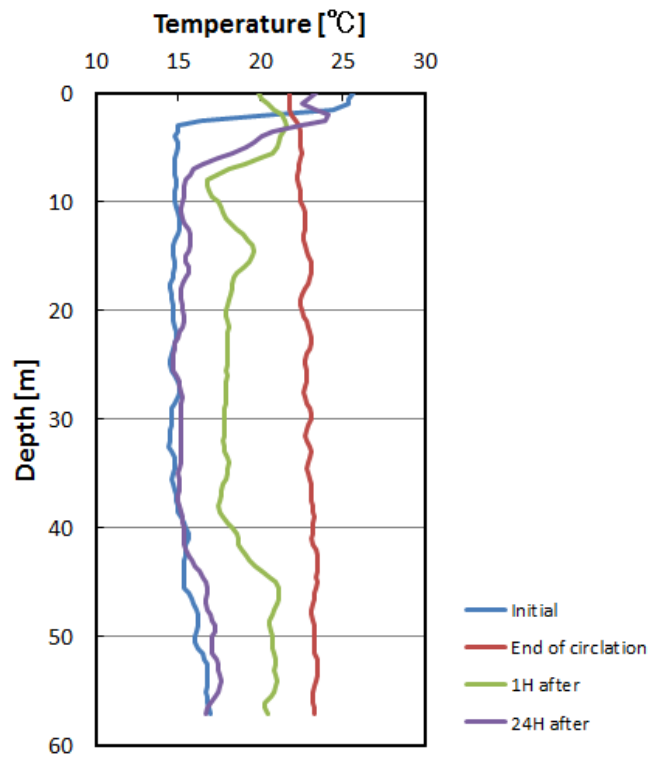
Fig. 3-14 Temperature recovery of GHE1.

73
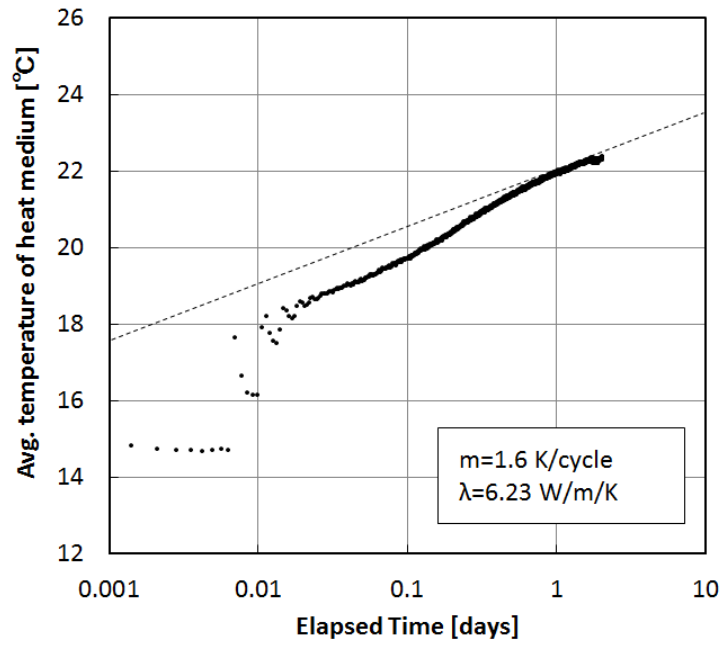
Fig. 3-15 The heat medium temperature during TRT on GHE2.
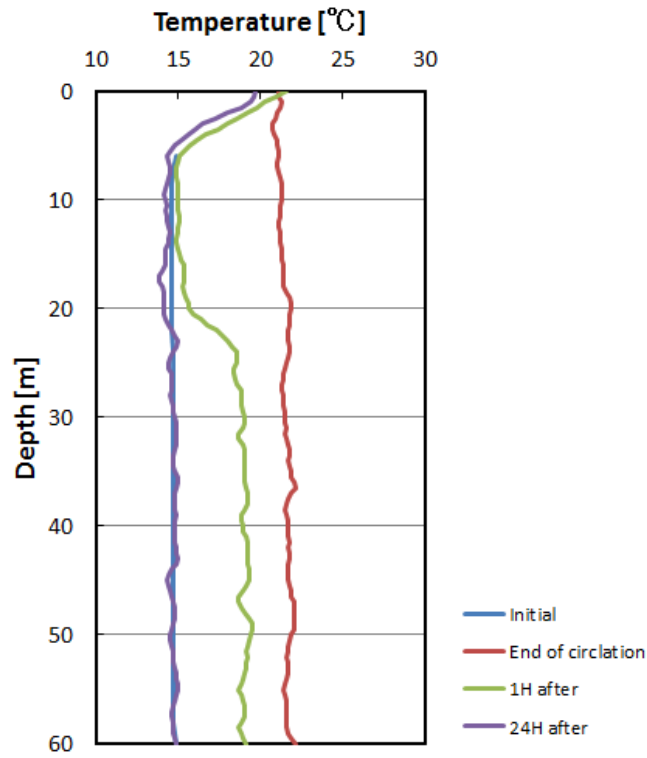
Fig. 3-16 Temperature recovery of GHE2.

3.4 Heating tests, conditions and results

The effect of water pumping and injection on the semi-open loop system performance was evaluated in four sets of heating tests. The experiments are identified by their water pumping and injection rates (Table 3-2). In the base case, the system operated as a conventional GSHP system with no water injection or pumping. In the "15 L/min" and "10 L/min" tests, groundwater was pumped from GHE2 and continuously injected into GHE1 at flow rates of 15 and 10 L/min, respectively. In the "15 L/min cyclic" test, the water pump was operated in cyclic mode with 1-hour intervals. After each heating test, the thermal recovery time was estimated to be at least as long as the operation time of the GSHP system (Rybach and Eugster, 2010). The recovery period is important in GSHP field tests, especially when operating multiple neighboring installations (Chen et al., 2015).

During the cold seasons, heat is extracted from the ground through the GHEs (Q_{GHE}) and delivered to the targeted rooms (Q_{room}). This process consumes electricity (W). The total power consumption of the system (W_{tot}) is the sum of the power consumptions of the heat pump compressor (W_{hp}), circulation pump (W_{cp}) and water pump (W_{wp}). During the heating tests, W_{cp} was almost constant at 0.19 kW. The coefficient of performance (COP) and SCOP were calculated by Eqs. 3-1 and 3-2, respectively.

$$\text{COP} = \frac{Q_{room}}{W_{hp}} \tag{3-1}$$

$$\text{SCOP} = \frac{Q_{room}}{W_{tot}} \tag{3-2}$$

The results of the heating tests are shown in Table 3-2 and Figs. 3-17 and 3-18. During the heating tests, the average flow rates in the primary and secondary loops were approximately 34 L/min and 16 L/min, respectively. In Table 3-2, the parameters marked with stars refer to a 15-L/min cyclic test conducted during the working hours of the water pump. In this test, the average pumping and injection rate was 7.5 L/min over two days, and the average power consumption of the water pump was 0.05 kW.

The most influential parameter on the system performance of a heat pump is the GHE array outlet temperature (T_{out}), which is usually linearly related to the COP. As shown in Fig. 3-19, increasing the water pumping and injection rates increased the T_{out} and improved the stability of the system over longer-period operation, relative to the base case. In Fig. 3-19, it is shown that in the base case there is a sudden decrease in T_{out} after around 1 day of operation, but T_{out} is more stable in the cases with water pumping and injection. The average T_{out} in the base case was 7.8 °C, 1.8 °C lower than in the 15 L/min case. Water pumping and injection at semi-open loop tests improved the COP by only 5%, but SCOP negligibly improved in 15 L/min cyclic test. Due to the high power consumption of water pump, SCOP slightly decreased in 10 and 15 L/min tests (Table 3-2). The limited COP enhancement might be attributable to fast groundwater flow in the

75

testing area. The effect of groundwater flow on the performance of the semi-open loop GSHP system will be discussed in the sensitivity analysis sections.
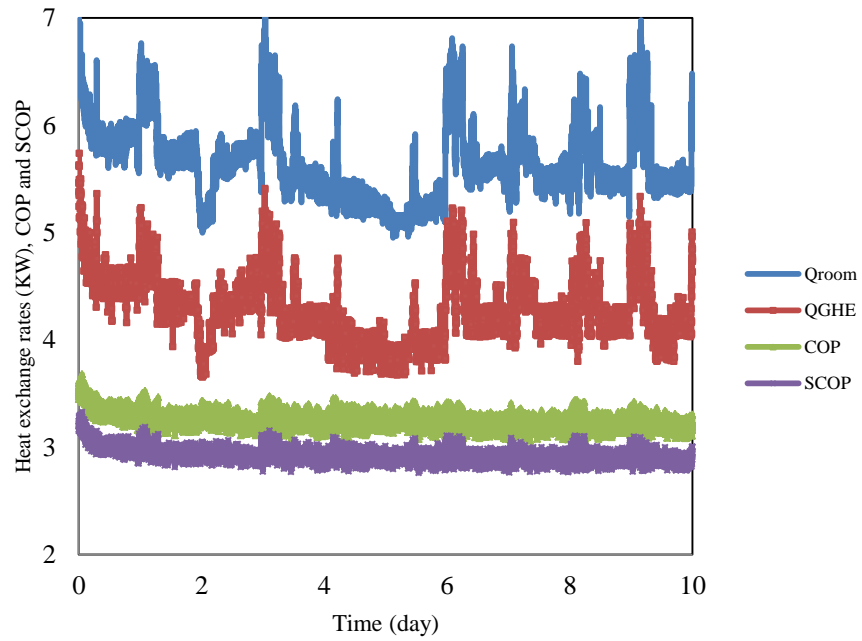
Fig. 3-17 Test results in the base case.
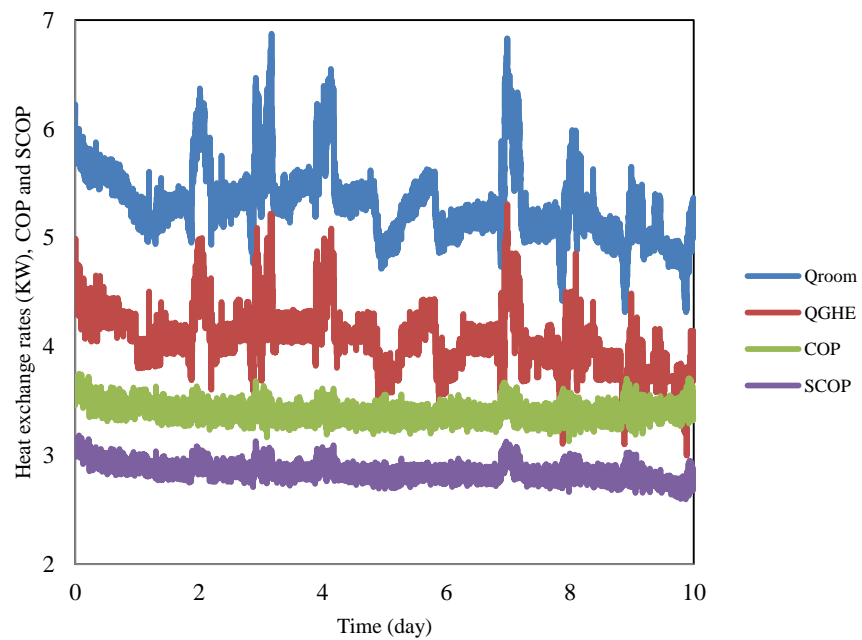
Fig. 3-18 Results of the 15 L/min test.

Table 3-2 Results of space-heating tests.

parameter	Unit	Base case	10 L/min	15 L/min cyclic	15 L/min
Period	hours	240 2016-Feb-09 2016-Feb-19	48 2016-Jan-26 2016-Jan-28	48 2016-Feb-03 2016-Feb-05	240 2016-Mar-07 2016-Mar-17
Water injection and pumping rate	L/min	0	10.00	15.00*	15.00
T_{out}	°C	7.82	9.80	9.70	9.60
Q_{GHE}	kW	4.28	4.53	4.55	4.05
Q_{room}	kW	5.64	5.82	5.81	5.31
W_{hp}	kW	1.74	1.70	1.70	1.56
W_{wp}	kW	0	0.136	0.099*	0.109
W_{tot}	kW	1.93	2.03	1.95	1.86
SCOP	-	2.93	2.87	2.98	2.85
COP	-	3.25	3.414	3.42	3.40
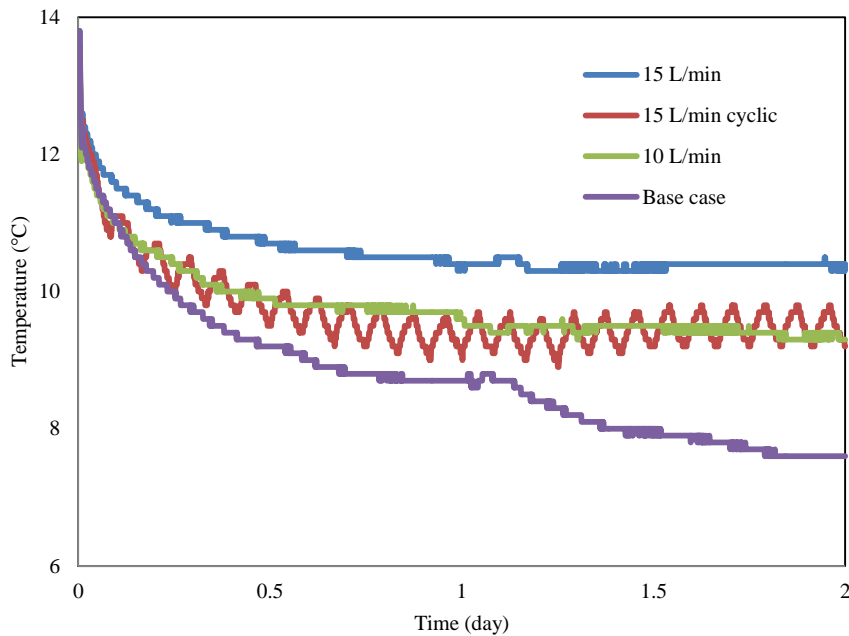
Fig. 3-19 GHE array outlet temperature.

One of the most important factors is GSHP system sizing is the minimum working fluid temperature inside the GHE during the heating operation. If this minimum temperature falls below a certain value, there will be a possibility of freezing inside the GHEs. In Table 3-3 the minimum working fluid temperature during 2 days of heating operation for each test is shown. Comparison between base case and other heating tests shows that water pumping and injection increased the minimum working fluid temperature. Difference between the base case and 15 L/min case is 1.6 °C for the first 2 days of operation. This value is 2.0 °C for the 10 days of heating tests and shows that water pumping and injection has more effect on long-term GSHP operations.

Table 3-3 Min. working fluid temperature (°C).

Period	Base case	10 L/min	15 L/min cyclic	15 L/min
48 hours	5.7	7.2	6.8	7.3
240 hours	4.8	-	-	6.8

Table 3-4 shows the average ground temperature after 48 and 240 hours of heating tests. This parameter was calculated by averaging the measured temperature by the 4 thermometers that placed in -30 m and -60 m depths in each GHE. The results show that water pumping and injection could have a positive effect on the ground temperature during the heating field tests.

Table 3-4 Average ground temperature (°C).

Period	Base case	10 L/min	15 L/min cyclic	15 L/min
After 48 hours	7.9	9.4	9.1	9.6
After 240 hours	6.8	-	-	9.8

3.5 Cooling tests, conditions and results

The cooling tests of GSHP system in base case (without water pumping and injection) and semi-open operation (with different water pumping and injection rates) were performed in July and August 2016, Akita University campus. All of the cooling tests were performed for 48 hours, with 5-8 days of recovery time between the tests. Table 3-5 and 3-6 show the conditions and the results of the cooling tests. The field tests for cooling operation were started at July 1, 2016, with base case GSHP operation (no water pumping and injection). Because of the fresh formation and also the heating tests on the last winter period, results of this experiment showed very high COP in comparison with all other cooling tests, regardless of water pumping and injection condition. The system performance in the next 6 cooling tests will be compared to see the effect of water pumping and injection on the COP and SCOP.

Because of the ambient temperature and room heat load fluctuation during cooling period, the tests with 10 and 15 L/min of water pumping and injection, were repeated 2 times. Same as the heating test, a cooling test with cyclic 15 L/min of water pumping and injection was performed. During this test, the water pump was operated in cyclic mode with 1-hour intervals. In Table 3-6, the parameters marked with stars refer to a 15-L/min cyclic test conducted during the working hours of the water pump. In this test, the average pumping and injection rate was 7.5 L/min over two days, and the average power consumption of the water pump was 0.05 kW. Similarly to the GSHP performance in heating operation, there is a linear relationship between the heat pump COP and outlet temperature of GHEs (T_{out}). The heat pump COP increases by decreasing T_{out}. The average of T_{out} is 21.0, 18.9, and 18.5 for the base case, first 10 L/min and first 15 L/min cooling tests, respectively. This trend shows the positive effect of water pumping and injection on the outlet temperature of GHEs (T_{out}). Fig. 3-20 shows the T_{out} for the base case, first 10 L/min and first 15 L/min cooling tests. These experiments were performed on July 2016.

Table 3-5 Cooling tests during July 2016.

parameter	Unit	Base Case#1	10 L/min#1	15 L/min#1	Base Case#2
Period	Hours	48 2016-July-01 2016-July-03	48 2016-July-11 2016-July-13	48 2016-July-19 2016-July-21	48 2016-July-26 2016-July-28
GHE1 flow rate	L/min	15.89	15.04	15.55	15.73
GHE2 Flow rate	L/min	16.21	14.65	15.18	15.91
Array Flow rate	L/min	32.1	29.69	30.73	31.64
Pumping-injection flow rate	L/min	0	9.85	14.99	0
Array inlet T	°C	21.5	21.5	21.1	23.83
Array outlet T	°C	19.1	18.9	18.5	21.0
GHE1 ΔT	°C	2.2	2.1	2.0	2.43
GHE2 ΔT	°C	2.7	3.2	3.4	3.31
Array ΔT	°C	2.4	2.6	2.6	2.81
GHE1 heat exchange rate	kW	2.38	2.16	2.09	2.61
GHE2 heat exchange rate	kW	3.00	3.17	3.51	3.59
Array heat exchange rate	kW	5.38	5.33	5.60	6.20
Room heat exchange rate	kW	4.47	4.68	4.73	5.18
System power consumption	kW	1.06	1.19	1.25	1.31
Water pump power consumption	kW	0	0.06	0.10	0
Heat Pump power consumption	kW	0.87	0.94	0.96	1.12
SCOP	-	4.22	3.94	3.80	3.97
COP	-	5.15	5.04	4.98	4.67

Table 3-6 Cooling tests during August 2016.

parameter	Unit	15 L/min cyclic	15 L/min#2	10 L/min #2
Period	Hours	48 2016-Aug-03 2016-Aug-05	48 2016-Aug-10 2016-Aug-12	48 2016-Aug-17 2016-Aug-19
GHE1 flow rate	L/min	15.94	17.11	16.87
GHE2 Flow rate	L/min	15.97	16.13	16.62
Array Flow rate	L/min	31.91	33.24	33.49
Pumping-injection flow rate	L/min	14.99*	14.99	10.1
Array inlet T	°C	24.17	22.9	23.6
Array outlet T	°C	21.0	19.9	20.5
GHE1 ΔT	°C	2.47	2.4	2.5
GHE2 ΔT	°C	3.94	3.7	3.8
Array ΔT	°C	3.12	3	3.1
GHE1 heat exchange rate	kW	2.69	2.82	2.86
GHE2 heat exchange rate	kW	4.30	4.13	4.28
Array heat exchange rate	kW	6.99	6.95	7.17
Room heat exchange rate	kW	5.71	5.51	5.60
System power consumption	kW	1.53	1.50	1.49
Water pump power consumption	kW	0.10*	0.10	0.065
Heat Pump power consumption	kW	1.30	1.21	1.23
SCOP	-	3.73	3.68	3.78
COP	-	4.45	4.60	4.57
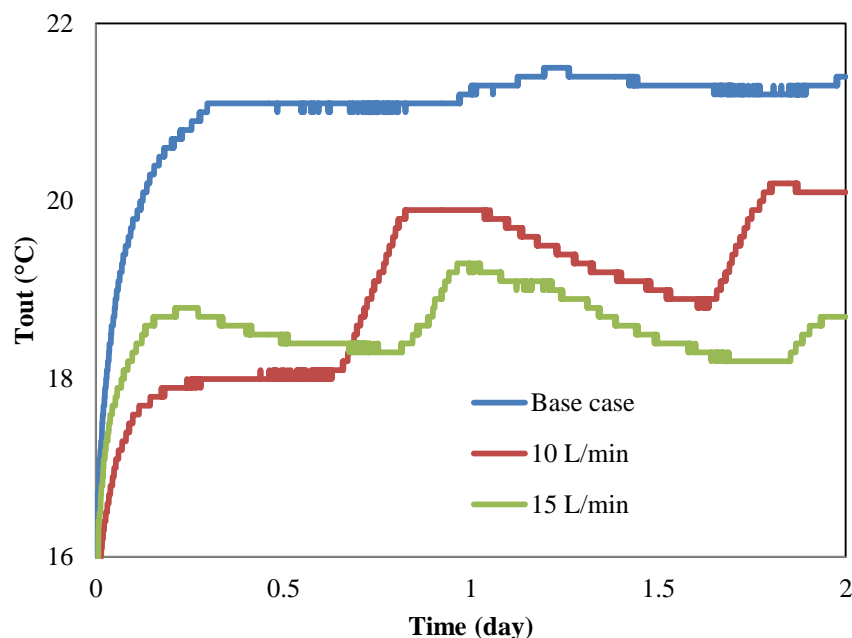
Fig. 3-20 Tout for the cooling tests of July 2016.

In the same concept as GSHP heating operations, maximum GHE outlet temperature (T_{out}) during the cooling period is the key factor in GSHP system sizing. If it is higher than specific value (based on the heat pump unit characteristics), the heat pump unit will show inferior performance to air-source heat pumps. Table 3-7 shows the maximum T_{out} for the July 2016 cooling tests (base case, first 10 L/min and first 15 L/min cooling tests). The calculated results show the positive effect of water pumping and injection on the maximum T_{out}. This parameter for base case cooling test is 2.2 °C higher than semi-open loop operation with 15 L/min water pumping and injection.

Table 3-7 also shows the average ground temperature (T_{ground}) after 48 hours of cooling tests. This parameter was calculated by averaging the measured temperature by the 4 thermometers that placed in -30 m and -60 m depths in each GHE. This parameter for base case cooling test is 3.1 °C higher than semi-open loop operation with 15 L/min water pumping and injection. The results show that water pumping and injection could have a positive effect on the T_{ground} during the GSHP cooling field tests.

Table 3-7 Max. Tout during cooling tests and average Tground after July 2016 cooling tests.

Parameter	Base case	10 L/min	15 L/min
Max. T_{out} during tests	21.5	20.2	19.3
Avg. T_{ground} after tests	21.5	19.7	18.4

In order to make comparison between the COP and SCOP of the cooling tests, the cooling tests were categorized in 2 groups. In the first group, base case operation performance was compared with the average of two 10-L/min and also two 15-L/min cooling tests. In this case, room heat transfer rate (Q_{room}) for these experiments will be close. The Q_{room} for the group 1 of the cooling tests is 5.18, 5.14 and 5.12 for the base case, average of 10 L/min cases and average of 15 L/min cases. As mentioned already, these values are very close to each other; in comparison with the Q_{room} values for the original cooling tests in Table 3-5 and 3-6.

Fig. 3-21 shows the COP and SCOP for group 1 of cooling tests. This figure shows that water pumping and injection could increase the COP by 3%, in average point of view. But due to the water pump power consumption effect, SCOP averagely decreases by around 4%. Same as the GSHP heating tests, the limited COP enhancement might be attributable to fast groundwater flow in the testing area. The effect of groundwater flow on the performance of the semi-open loop GSHP system will be discussed in the sensitivity analysis section.

This Group 2 of cooling tests contains the second 10 L/min, second 15 L/min and 15 L/min cyclic semi-open loop cooling tests. The Q_{room} for the Group 2 of the cooling tests is 5.60, 5.71 and 5.51 for the Second 10 L/min, 15 L/min cyclic and Second 10 L/min, respectively. The calculated values for Q_{room} are close to each other. Fig. 3-22 shows the COP and SCOP for group 2 of cooling tests. The COP in 15 L/min test is higher in comparison with other semi-open loop cases, although water pump power consumption effect caused a decrement in SCOP.
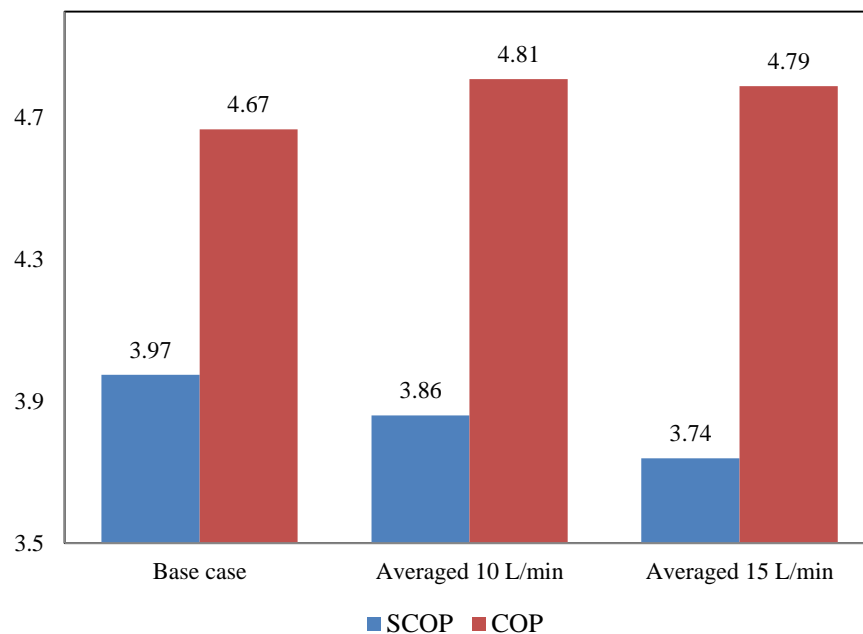
Fig. 3-21 COP and SCOP for Group 1 of cooling tests.
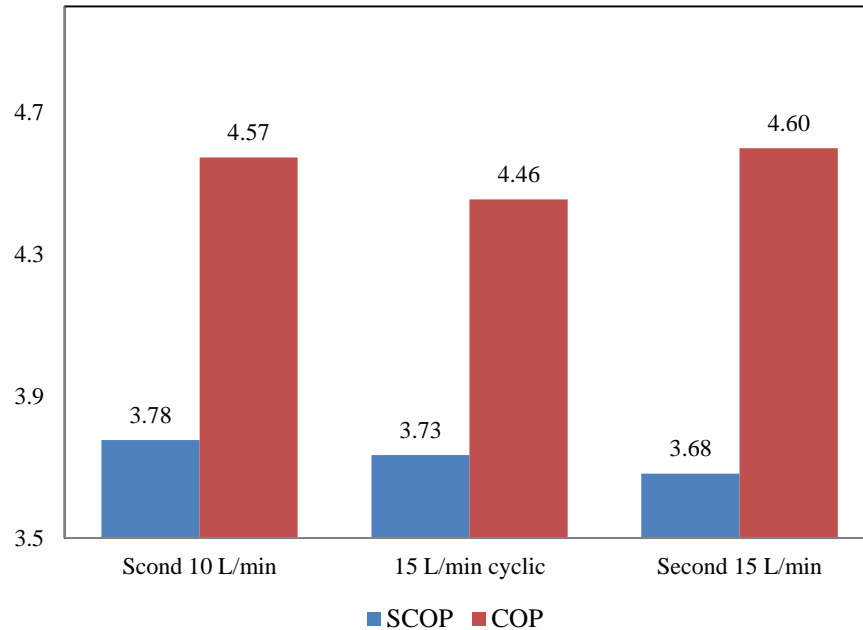
Fig. 3-22 COP and SCOP for Group 2 of cooling tests.

3.6 Numerical modeling and validation using experimental data

In order to evaluate the performance of the semi-open loop system, we developed a numerical model in FEFLOW 6.2 (DHI-WASY, 2015). The dimensions and cross sectional views of the model are shown in Figs. 3-23 and 3-24. Fig. 3-25 shows the View of the GHE well.

The meshing was refined around the GHEs to increase the accuracy of the model. Each layer of the model contains 5,562 elements. The undisturbed water table at the test site was measured as −5 m. The model layers were 1 m thick from the ground surface to −5 m, and 5 m thick from −5 m to −80 m (a total of 21 layers).

The pumping and injection depth is set as 50 m in GHE2 and GHE1, respectively. In this layer "Well boundary condition" is assigned for 2 nodes inside GHE1 and GHE2, representing the water injection and pumping points, respectively. In Fig. 3-26, "Borehole heat exchanger boundary condition" assigned in the central node inside the casing. In order to prevent the conflict between the BCs, the Well BC was set in a different node from central node inside the casing as shown in Fig. 3-26.
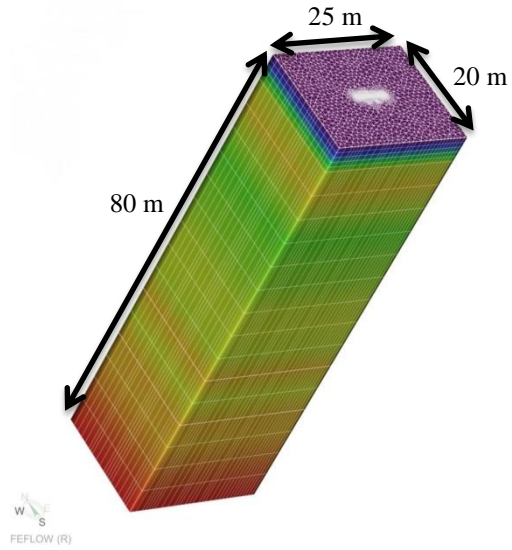
Fig. 3-23 3D view of model.
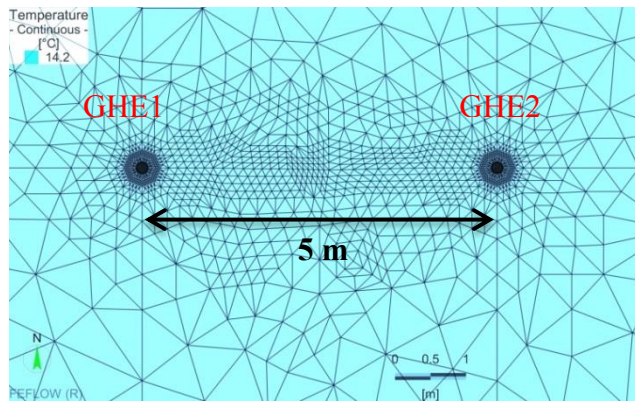
Fig. 3-24 2D view of model.
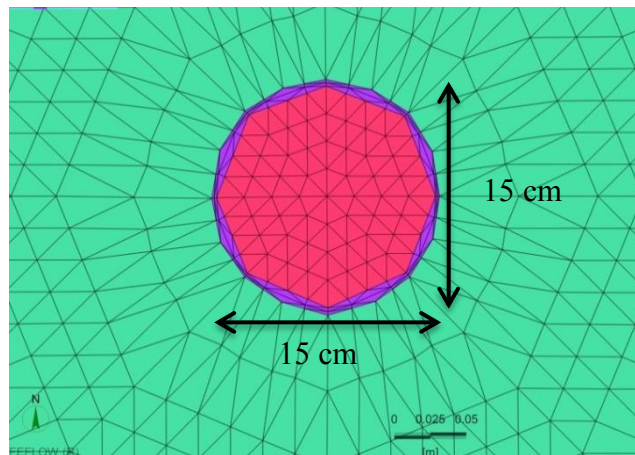
Fig. 3-25 View of the GHE well.
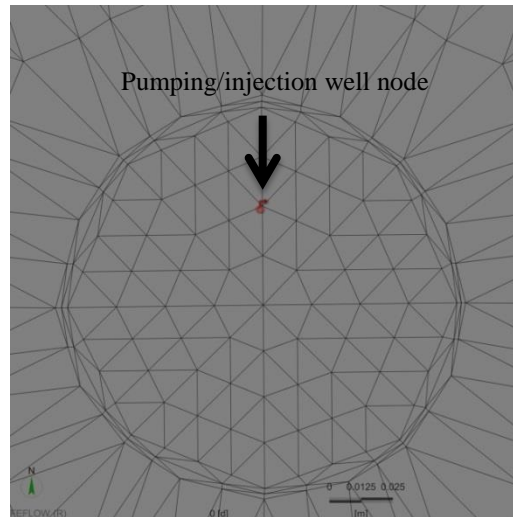
Fig. 3-26 Pumping/injection well node.

The initial ground temperature was determined from field measurements as shown in Fig. 3-1. The boundary conditions were set as follows:

- Constant temperature at the bottom and peripheral boundaries
- Constant hydraulic head at the eastern boundary: −5.0 m
- Constant hydraulic head at the western boundary: −5.2 m

Note that the boundary conditions impose a hydraulic head difference between the eastern and western lateral boundaries, generating a natural groundwater flow from the eastern to the western boundaries. The history-matching parameter in the model is the head difference, which is restricted to maintain reasonable values of the maximum groundwater velocity in the domain. According to the literature, the hydraulic gradient and groundwater velocity depend on the site conditions. The United States Environmental Protection Agency (1996) reported that typical hydraulic gradients range from 0.0001 to 0.05. Some specific examples of natural groundwater velocities are as follows: 1.5–6.0 m/day under a hydraulic gradient of 0.002 to 0.012 in the Snake River Group basalt, Idaho, USA (Lindholm and Vaccaro, 1988); 0.3 m/day in a High Plains sand and gravel aquifer, western central USA (Weeks and Gutentag, 1988); and 10^{-6}–10^{-5} m/day in glacial clay soils in Southern Ontario, Canada (Stephenson et al., 1988). Local pumping activities may further increase the groundwater flow rates in aquifers (Chiasson et al., 2000). The head difference in our model, 0.2 m, was determined by history matching of the outlet temperatures to the space-heating test results. As the boundaries are separated by 20 m, the hydraulic gradient was calculated as 0.01. In the history matching, the groundwater velocity in the main groundwater flowing interval (−10 m to −30 m) was determined as 15 cm/day.

Table 3-8 lists the material properties of the modeled system based on Fig. 3-1, and the typical values of the porosity and thermal and hydraulic conductivities (K and λ, respectively). The typical values for the soil porosity, K and λ are derived from the literature (Chiasson et al., 2000; Diao et al., 2004). The material properties in Table 3-8 are the history matching parameters in the numerical model.

Table 3-8Model material properties.

Depth (m)	0–10	10–30	30–60	60–80
Porosity (-)	0.15	0.15	0.15	0.05
K_{xx} and K_{yy} (10^{-5} m/s)	4	17	7	0.1
K_{zz} (10^{-5} m/s)	0.4	1.7	0.7	0.01
Soil thermal conductivity (W/(mK))	1.2	1.5	1.2	1.15
thermal conductivity inside the casing (W/(mK))	0.025 for 0-5 m 1.2 for 5-10 m	1.2	1.2	1.2

Because the test site contains sedimentary formations, the coefficient of permeability in the vertical direction (K_{zz}) was set to one-tenth the coefficient of permeability over the horizontal surfaces (K_{xx} and K_{yy}). Also recall that the water table in both GHEs locates at −5 m and the GHE uses a slotted casing without grouting. Therefore, from −5 m to the bottom of the GHEs, the annular space between the U-tube and the GHE casing is filled with groundwater. From the surface to −5 m, it is filled with air. Accordingly, the thermal conductivity inside the casing was set to 0.025 W/(mK) (thermal conductivity of air at $T = 20$ °C) from 0 to −5 m, and to 1.2 W/(mK) from −5 m to bottom of the GHEs. The deeper value accounts for the effect of advective heat transfer by the water flow inside the casing.

3.6.1 Validating the numerical model using heating tests results

Figs. 3-27–3-30 present the history matching results of the outlet temperature from the GHE array to the space-heating tests of the semi-open loop GSHP system. Fig 3-27 shows the results of the history matching for the base case heating test (without pumping and injection). This experiment was performed for 10 days. The results of the calculated GHE outlet temperature (red line) are in the good agreement with the measured data of T_{out} (blue line). Same as base case heating test, the semi-open loop GSHP system test with 15 L/min of water pumping and injection was performed for 10 days and results of the history matching are shown in Fig. 3-28. The numerical model could successfully simulate the values for T_{out} for the beginning of the experiment as well as the local minimum and maximum temperatures.

Fig. 3-29 shows the results of the numerical modeling for the semi-open loop GSHP system heating test with 15 L/min of water pumping and injection in cyclic mood. As it was mentioned in section 3.3, in this experiment the water pump was working with 1-hour intervals. When the water pump is off, T_{out} decreases and when it is on, T_{out} increases (higher expected COP).
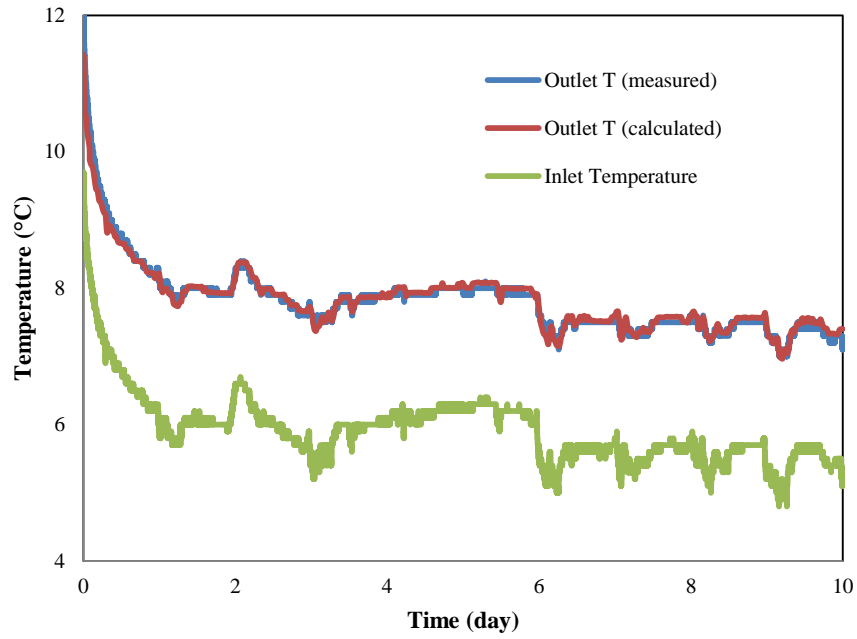
Fig. 3-27 Result of history matching to the base case heating test.
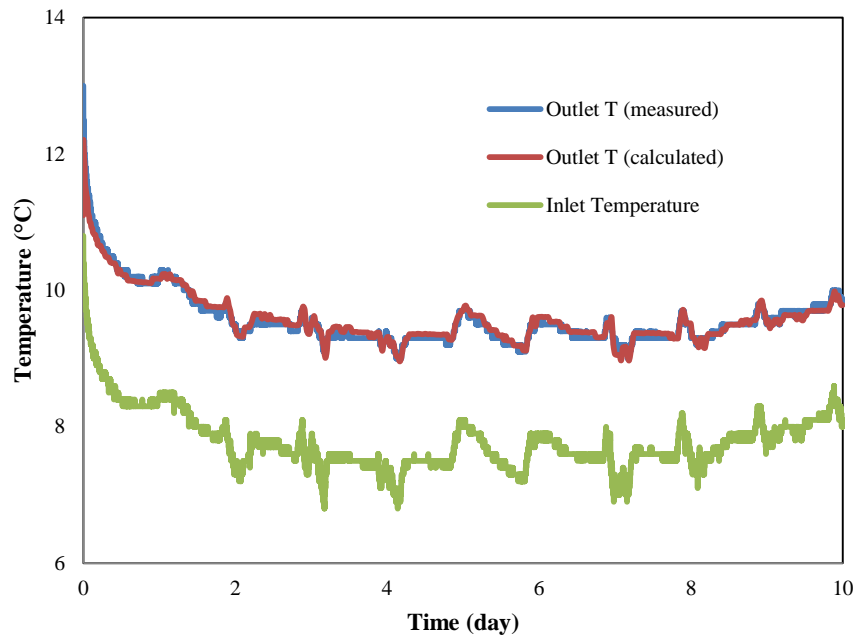
Fig. 3-28 Result of history matching to the 15 L/min heating test.
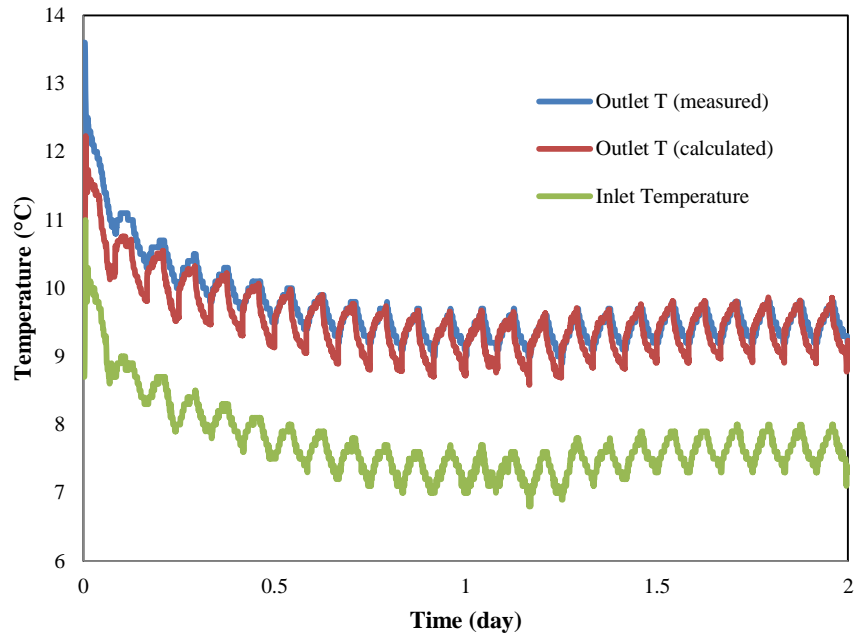
Fig. 3-29 Result of history matching to the 15 L/min cyclic heating test.
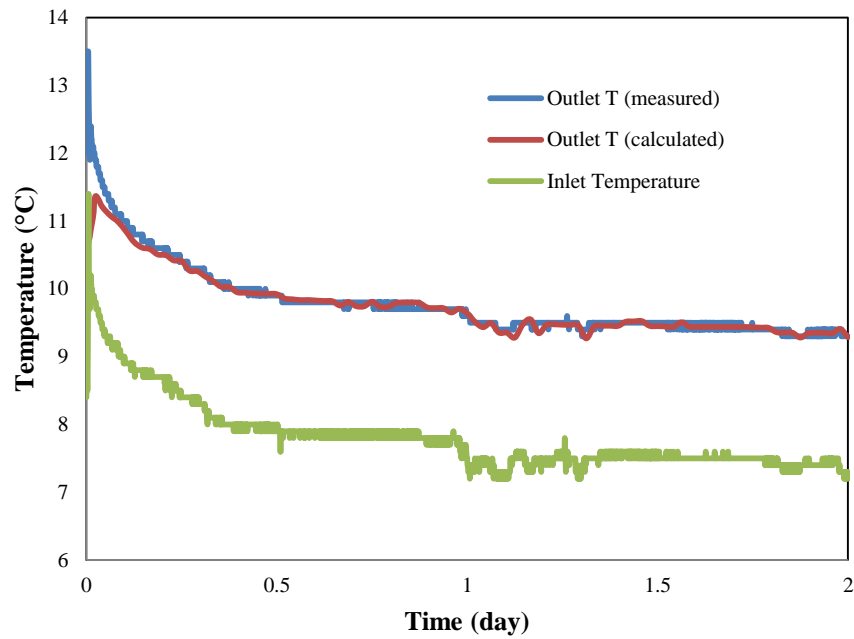
Fig. 3-30 Result of history matching to the 10 L/min heating test.

The numerical model could successfully simulate the fluctuating behavior of the T_{out} and results were in good agreement with the measured data. The semi-open loop GSHP system cooling test with 10 L/min of water pumping and injection was performed for 2 days (same as 15 L/min cyclic test) and the results of numerical modeling are shown in Fig. 3-30. During this experiment, the T_{out} showed more steady behavior (mainly because of fewer fluctuations and the results of numerical modeling are in good agreement with the measured data. In general, for all of the heating tests, the calculated outlet temperatures well agree with the field test results, demonstrating the validity of the model for sensitivity analysis.

3.6.2 Validating the numerical model using cooling tests results

Figs. 3-31–3-34 present the history matching results for the T_{out} in 4 of the cooling tests. Fig. 3-31 shows the results of the base case GSHP system cooling test (without water pumping and injection). This experiment started at 2016-July-26, for 2 days. Results of the calculated GHE outlet temperature (red line) are in good agreement with the measured data (green line). The second semi-open loop GSHP system cooling test was started in 2016-Aug-10 (duration: 2 days). The results of numerical modeling for this experiment are shown in Fig. 3-32. The calculated and measured data for T_{out} are in good agreement and numerical model could successfully simulate the sudden increase in T_{out} before finishing the first day of the experiment.

Fig. 3-33 shows the results of numerical modeling for semi-open loop GSHP system cooling test with 15 L/min cyclic water pumping and injection. During this experiment, the water pump was working with 1-hour interval. When water pump is off, T_{out} increases and when it is on, the T_{out} decreases (higher expected COP). Same as the cyclic heating test, the numerical model could successfully simulate the fluctuating behavior of the T_{out} and results were in good agreement with the measured data.

Fig. 3-34 shows the results of numerical modeling for the second semi-open loop GSHP system with 10 L/min water pumping and injection. This experiment started on 2016-Aug-17 and it was continued for 2 days. Same as the cooling test with 15 L/min water pumping and injection, the calculated and measured data for T_{out} are in good agreement and numerical model could successfully simulate the sudden increase in T_{out} before finishing the first day of the experiment. For all of the cooling tests, the calculated outlet temperatures well agree with the field test results, demonstrating the validity of the model for sensitivity analysis.
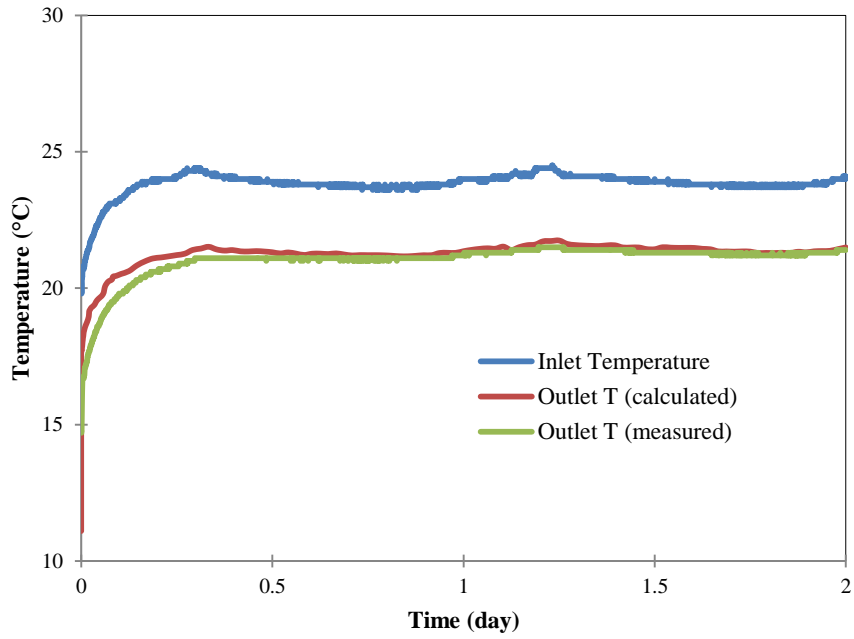
Fig. 3-31 Result of history matching to the base case cooling test.
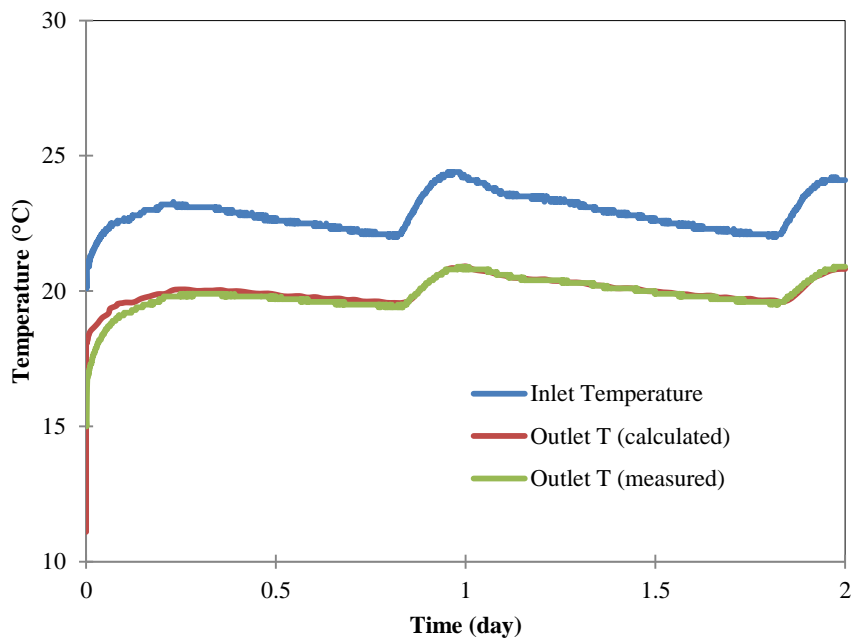
Fig. 3-32 Result of history matching to the second 15 L/min cooling test.
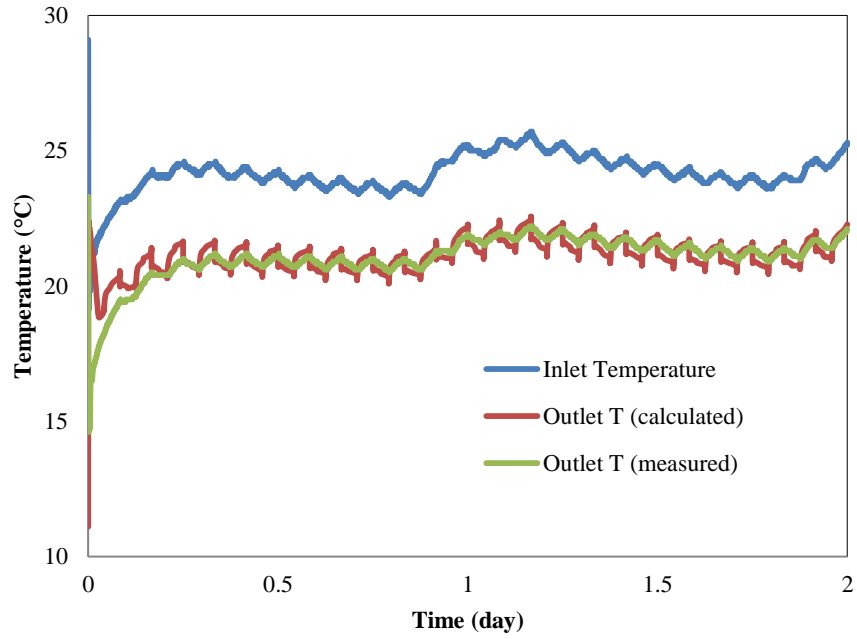
Fig. 3-33 Result of history matching to the cyclic 15 L/min cooling test.
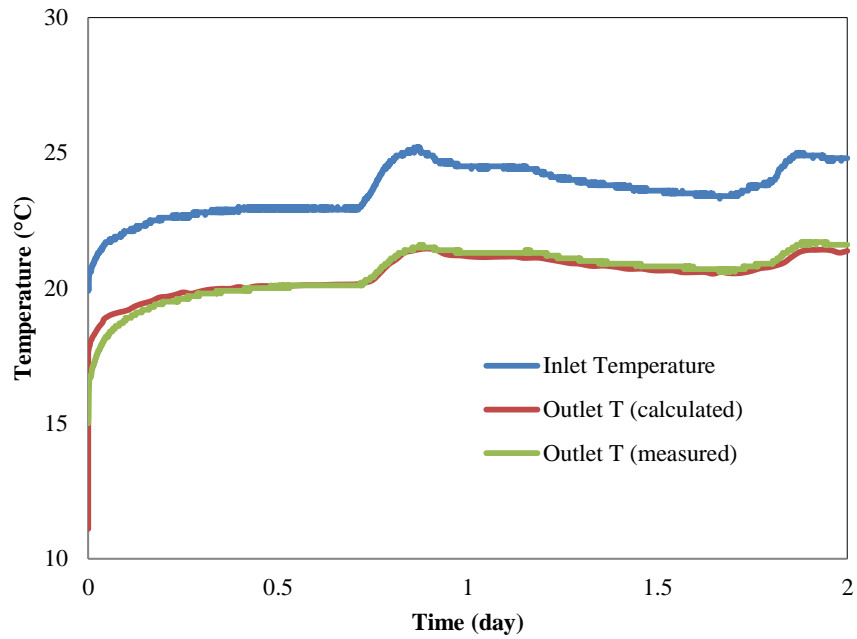
Fig. 3-34 Result of history matching to the second 10 L/min cooling test.

Fig. 3-35 shows the Darcy flux in the formation, 2 days after starting the heating test with 15 L/min of water pumping and injection in -50 m depth. This figure shows that water pumping and injection could significantly increase the groundwater flow between the GHEs and around them. Fig. 3-36 shows the temperature distribution in the formation, 2 days after starting the heating test with 15 L/min of water pumping and injection in -50 m depth. This figure shows that in the areas with strong Darcy fluxes, soil temperature dropped due to the stronger heat convection. In Figs. 3-17 and 3-18, GHE-I and GHE-P stand for injection and pumping GHEs, respectively.
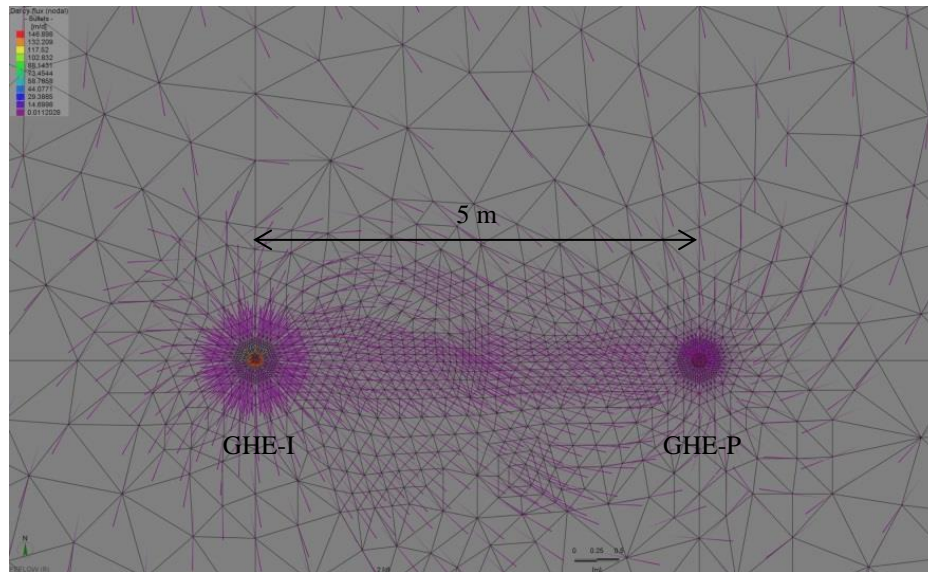
Fig. 3-35 Darcy flux (nodal) in the formation, 15 L/min case, water pumping/injection layer.
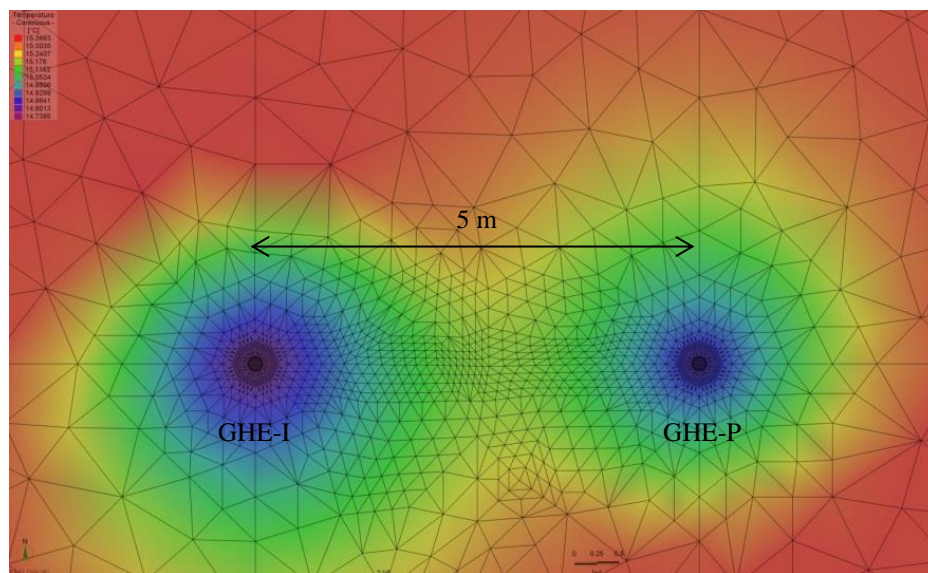
Fig. 3-36 Temperature distribution in the formation, 15 L/min case, water pumping/injection layer.

3.7 GSHP operation sensitivity analysis

3.7.1 General condition

To evaluate the effect of the operating and natural conditions on the performance of the semi-open loop GSHP system, sensitivity analysis of the numerical model was performed in heating and cooling modes. The general conditions of the sensitivity analysis were as follows:

- Circulation rate of heat medium in each GHE: 15 L/min
- Water pumping and injection rates: 0 L/min or 15 L/min
- Heating period: 30 days
- Daily operating hours: 12 hour/day or 24 hour/day

In the field test, the beneficial effect of water pumping and injection on the COP and SCOP was limited by the natural groundwater flow. Hence, the sensitivity analysis investigated two scenarios, one with groundwater flow (same as the experimental condition); the other without groundwater flow. In the presence of groundwater flow, the head gradient was set to the experimental value of 0.01. In this case, maximum groundwater flow in the domain is 15 cm/day. In order to evaluate the effect of natural groundwater flow on the system performance, the other set of simulations was performed in "No groundwater flow" condition.

3.7.1.1 Sensitivity analysis for heating operation

For cases with groundwater flow, the heat transfer rate of the GHE array (Q_{GHE}) was varied as 4, 6, and 8 kW. In the absence of groundwater flow, the maximum heat transfer rates of the GHEs were assigned to ensure the minimum temperature of the heat medium (-5 ℃). Specifically, we set:

- Base case (no pumping & injection), operating 24 hour/day: 1-2 kW
- Base case (no pumping & injection), operating 12 hour /day: 1-3 kW
- Semi-open loop mode, operating 12 or 24 hour /day: 1-8 kW

Fig. 3-37 shows the heat pump unit performance in heating operation. The system performance in the sensitivity analysis was determined from the heat pump performance curves. In each case, the outlet temperature of the GHE array (T_{out}) was calculated by the numerical model. The COP was then calculated using the performance curve in the manufacturer's catalogue:

$$COP = (0.0917 \times T_{out}) + 3.2065 \tag{3-3}$$

The heat pump power consumption W_{hp} is a function of Q_{GHE} (heat transfer rate between the GHEs and ground) and the COP:

$$W_{hp} = \frac{Q_{GHE}}{COP-1}$$

(3-4)
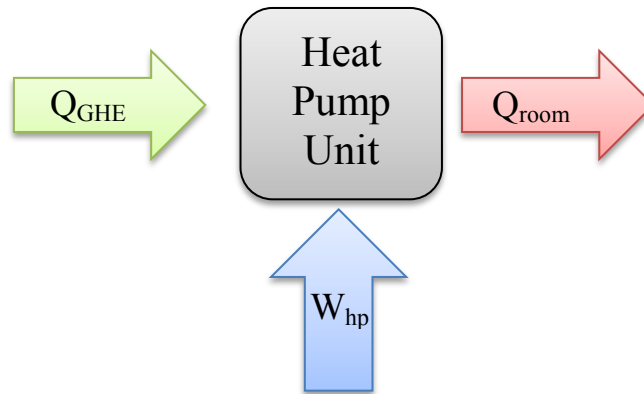
Fig. 3-37 Heat pump unit performance in heating operation

The energy delivered to the room (Q_{room}) is the sum of Q_{GHE} and W_{hp}. To obtain the SCOP, we must add the power consumptions of the circulating pump (W_{cp}) and water pump (W_{wp}) to W_{hp}, giving the total power consumption (W_{tot}). In all cases, W_{cp} and W_{wp} (for semi-open loop modes) were set to 0.19 kW (as in the test condition) and 0.05 kW, respectively. W_{wp} was lower in the sensitivity analysis than in the field test, because the water pump in the field tests was not tailored to the experimental conditions. By choosing a proper water pump with the optimum flow rate of 15 L/min, we can expect to reduce W_{wp} to its assigned value of 0.05 kW.

Figures 3-38 and 3-39 plot the minimum T_{out} values as functions of GHE heat transfer rate in the base case and semi-open loop mode, respectively, in the groundwater flow scenario. As mentioned in numerical modeling section, in the cases with groundwater flow, the hydraulic gradient is 0.01 that causes a maximum 15 cm/day of groundwater velocity in the domain. According to literature (e. g. Chiasson et al., 2000) this is considered as fast groundwater velocity condition.

The minimum T_{out} was higher in semi- open loop mode than in the base case, because water pumping and injection increased the heat advection and maintained the heat medium temperature close to the groundwater temperature. The semi-open loop mode also reduced the minimum T_{out} difference between continuous operation (24 h/day) and cyclic operation (12 h/day), because in this mode (fast groundwater condition), the heat delivered to the ground is washed away by the natural groundwater flow, which maintains the GHE temperature close to constant. Consequently, during cyclic operation, the ground can recover to its initial thermal condition, and the T_{out} is similar to that of continuous operation. In contrast, under geological conditions with slow groundwater flow, the ground has insufficient time to recover in cyclic operation, so the minimum T_{out} deviates from that of continuous mode.

The base case COP and SCOP and improvement in COP and SCOP conferred by water pumping and injection in the presence of groundwater flow are shown in Table 3-9. In the case of 12 hour/day operation with 4 kW heat transfer rate, COP was increased by 1.9%, but this improvement was not enough to compensate the water pump power consumption in the semi-open loop mode, and as a results SCOP decreased by 0.9%. The maximum enhancements of COP and SCOP were 11.5% and 8.9%, respectively. The improvement in system performance became more evident at higher heat transfer rates, because excessive heat rates rapidly deteriorate the COP in the base case, but are better tolerated by the semi-open loop system. The improvement was also higher in continuous operations than in cyclic operations, because continuous operation places heavier heat load on the GHEs.

Fig. 3-38 Minimum Tout versus heat transfer rate in the base case with groundwater flow.

Fig. 3-39 Minimum Tout versus heat transfer rate in semi-open loop mode with groundwater flow.

Table 3-9 Improvement of COP and SCOP by the application of semi-open loop (with groundwater flow).

Parameter	24 hour/day 4 kW	24 hour/day 8 kW	12 hour/day 4 kW	12 hour/day 8 kW
Base case COP	3.94	3.30	4.10	3.50
Base case SCOP	3.47	3.13	3.55	3.30
COP enhancement in semi-open loop (%)	4.8	11.5	1.9	8
SCOP enhancement in semi-open loop (%)	0.7	8.9	-0.9	5.8
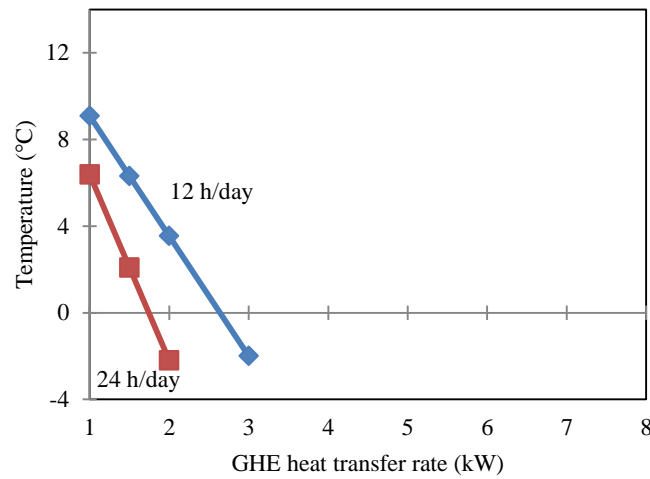
Fig. 3-40 Minimum Tout versus heat transfer rate in the base case without groundwater flow.
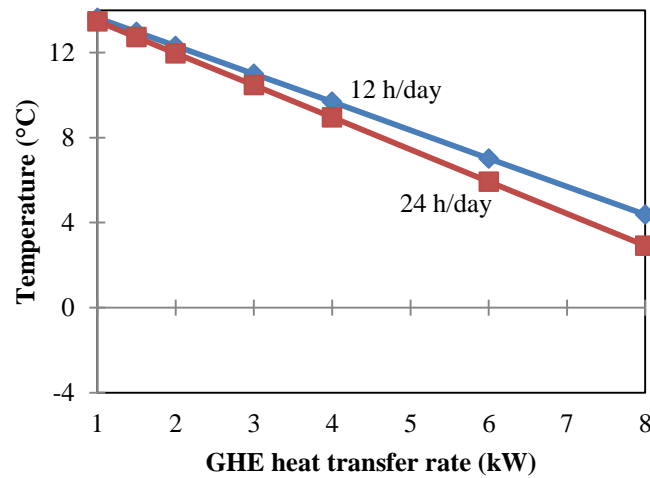
Fig. 3-41 Minimum Tout versus heat transfer rate in semi-open loop mode without groundwater flow.

Figures 3-40 and 3-41 plot the minimum T_{out} versus heat transfer rate in the base case and semi-open loop mode, respectively, without groundwater flow. As observed in the presence of groundwater flow (and for the same reasons), the minimum T_{out} was higher in semi-open loop mode than in the base case. In the base case, the minimum T_{out} reached the minimum acceptable temperature at lower heat transfer rates than in the groundwater flow scenario, because the natural advection effect was absent. The maximum acceptable Q_{GHE} in continuous and cyclic operation was 2 and 3 kW, respectively. In semi-open loop mode, however, the maximum possible Q_{GHE} was increased to 8 kW or higher. We conclude that under geological conditions with weak groundwater flows, the semi-open loop GSHP system can significantly increase the system capacity.

The values for base case COP and SCOP and improvement of COP and SCOP in the cases without groundwater flow are shown in Table 3-10. This comparison was performed only when the heat medium temperature remained above −5 ℃ (up to 2 and 3 kW during continuous and cyclic operation, respectively). The maximum COP and SCOP enhancements were approximately 40% and 20%, respectively. These simulations confirm that the semi-open loop system can increase the maximum heat transfer rate and also improve the COP and SCOP of GSHP systems, especially in locations with slow groundwater velocity.

Table 3-10 Improvement of COP and SCOP by the application of semi-open loop (without groundwater flow).

Parameter	24 hour/day 1 kW	24 hour/day 2 kW	12 hour/day 1 kW	12 hour/day 2 kW	12 hour/day 3 kW
Base case COP	3.85	3.13	4.15	3.78	3.41
Base case SCOP	2.52	2.61	2.51	2.92	2.91
COP enhancement in semi-open loop (%)	15.7	38.5	7.6	15.2	24.7
SCOP enhancement in semi-open loop (%)	-2.1	19.4	-1.3	7.1	16.5

3.7.1.2 Sensitivity analysis for cooling operation

Same as sensitivity analysis condition for heating operation, the numerical simulations for cooling operation were performed in 2 condition: one with groundwater flow (same as field tests condition), and the other one without groundwater flow. For cases with groundwater flow, the heat transfer rate of the GHE array (Q_{GHE}) was varied as 4, 6, and 8 kW. In the absence of groundwater flow, the maximum heat transfer rates of the GHEs were assigned to ensure the maximum T_{out} (40 ℃). Specifically, we set:

- Base case (no pumping & injection), operating 24 hour/day: 2, 3, 4 kW
- Base case (no pumping & injection), operating 12 hour /day: 4, 6, 8 kW
- Semi-open loop mode, operating 12 or 24 hour /day: 2-8 kW

It is necessary to note that in base case operations, with 24 hours/day condition, in "No groundwater flow" condition, that was impossible to increase the Q_{GHE} more than 4 kW. In this condition, for higher Q_{GHE}, T_{out} was exceeding the limit of 40°C, that heat pump unit is not able to work in cooling operation.

Fig. 3-42 shows the heat pump unit performance in cooling operation. The relationship between Q_{room}, Q_{GHE} and W_{hp}, are shown in equations 3-5 and 3-6.

$$Q_{GHE} = Q_{room} + W_{hp} \tag{3-5}$$

$$COP = \frac{Q_{room}}{W_{hp}} \rightarrow W_{hp} = \frac{Q_{GHE}}{COP+1} \tag{3-6}$$
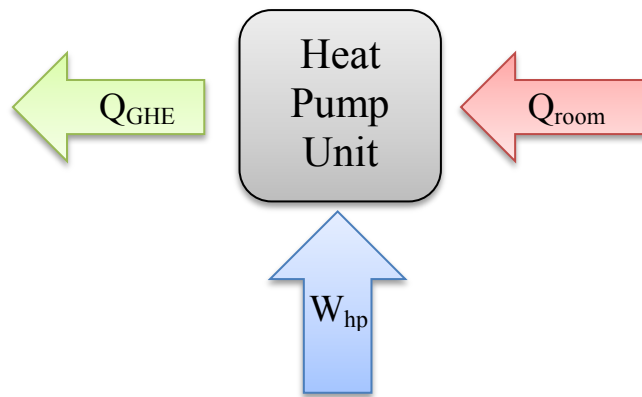
Fig. 3-42 Heat pump unit performance in cooling operation.

The system performance in the sensitivity analysis was determined from the heat pump performance curves. In each case, the outlet temperature of the GHE array (T_{out}) was calculated by the numerical model. The COP was then calculated by the formulation in the experimental GSHP manufacturer catalogue (Eq. 3-7):

$$COP = (-0.215 \times T_{out}) + 11.792 \tag{3-7}$$

After calculation of COP in each time-step of simulation, W_{hp} is calculated using Eq. 3-6. Cooling SCOP calculation has the same process as the heating SCOP calculation that was described in the previous section.

Fig. 3-43 and 3-44 show the maximum T_{out} with groundwater flow condition, for 12 hour/day and 24 hour/day operations, respectively. The maximum T_{out} was lower in semi- open loop mode than in the base case, because water pumping and injection increased the heat advection and maintained the heat medium temperature close to the groundwater temperature.

Fig. 3-45 and 3-46 show the COP and SCOP enhancement with groundwater flow condition, for 12 hour/day and 24 hour/day operations, respectively. In the some of the cases, COP was increased, but this improvement was not enough to compensate the water pump power consumption in the semi-open loop mode, and as a results SCOP decreased. The maximum enhancements of COP and SCOP were 13.1% and 6.6%, respectively. The improvement in system performance became more evident at higher heat transfer rates, because same as heating operation analysis, excessive heat rates rapidly deteriorate the COP in the base case, but are better tolerated by the semi-open loop system. The improvement was also higher in continuous than in cyclic operation, because continuous operation places heavier heat load on the GHEs.
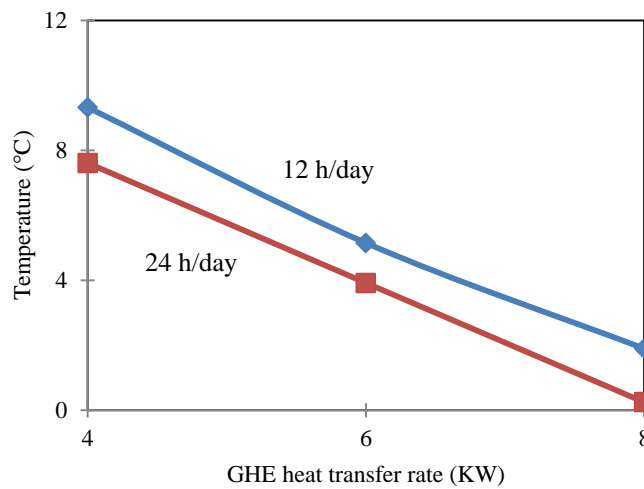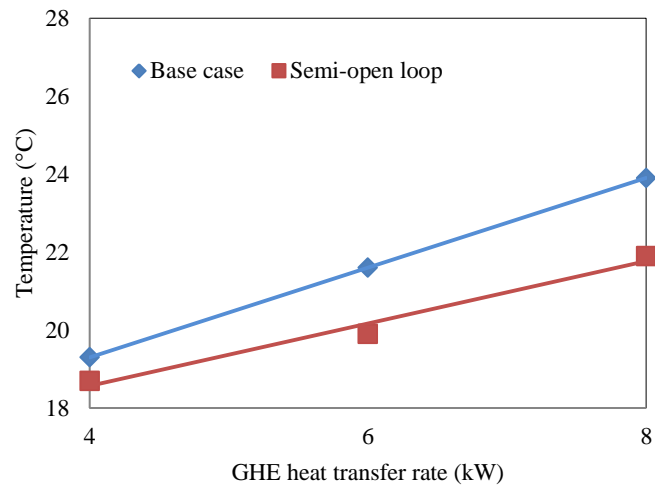

Fig. 3-43 Maximum Tout versus heat transfer rate in 12 hour/day operation with groundwater flow.
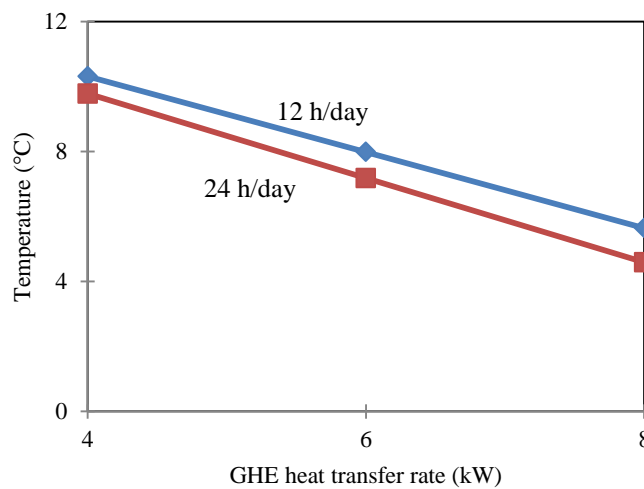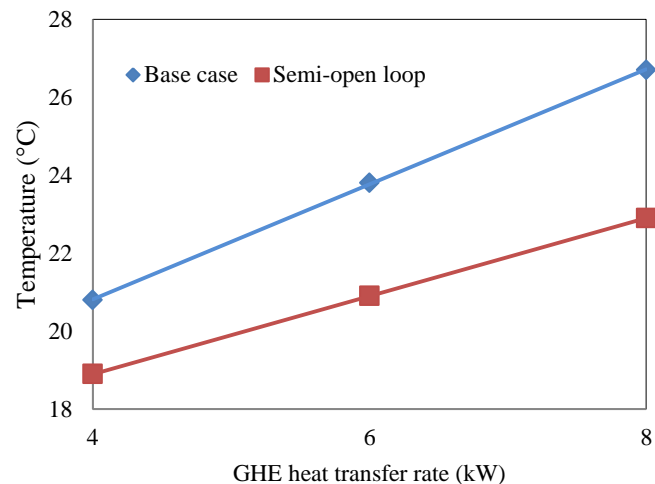

Fig. 3-44 Maximum Tout versus heat transfer rate in 24 hour/day operation with groundwater flow.
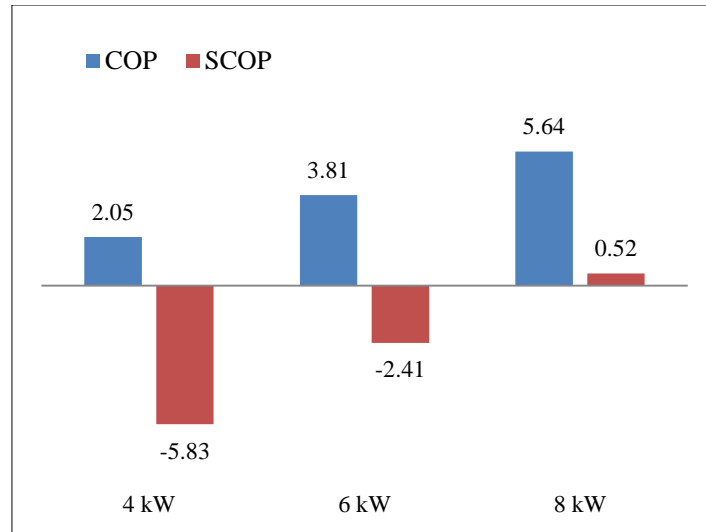
Fig. 3-45 COP and SCOP enhancement in 12 hour/day operation, with groundwater flow.
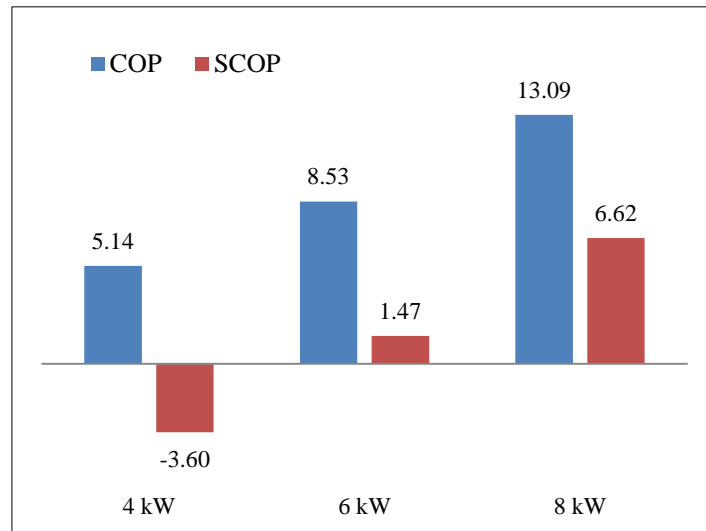
Fig. 3-46 COP and SCOP enhancement in 24 hour/day operation, with groundwater flow.

Figures 3-47 and 3-48 plot the maximum T_{out} versus heat transfer rate in for 12 hour/day and 24 hour/day operations, respectively, without groundwater flow. As observed in the presence of groundwater flow (and for the same reasons), the maximum T_{out} was lower in semi-open loop mode than in the base case. It is necessary to note that in the base case, 24 hour/day operation, in the absence of groundwater flow, it was impossible to increase Q_{GHE} more than 4 kW. In this case maximum T_{out} exceeded the limit of 40°C, that heat pump unit is not able to operate in cooling mode.

Fig. 3-49 and 3-50 show the COP and SCOP enhancement without groundwater flow condition, for 12 hour/day and 24 hour/day operations, respectively. In the case of 12 hour/day

operation with 4 kW heat transfer rate, COP was increased by 10.3%, but this improvement was not enough to compensate the water pump power consumption in the semi-open loop mode, and as a results SCOP decreased by 0.2%.

This comparison was performed only when the T_{out} remained below 40ºC (up to 4 kW during base case cyclic operation). For the 12 hour/day operation, the maximum COP and SCOP enhancements were approximately 43.5% and 31.8%, respectively. These simulations confirm that the semi-open loop system can increase the maximum heat transfer rate and also improve the COP and SCOP of GSHP systems, especially in locations with slow groundwater velocity.
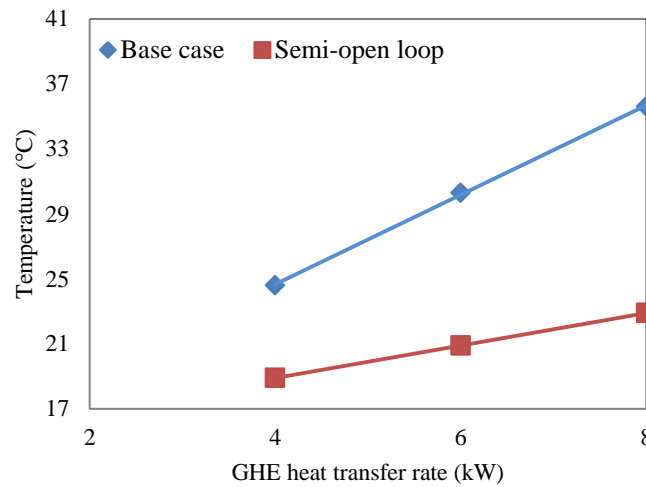
Fig. 3-47 Maximum T_{out} versus heat transfer rate in 12 hour/day operation, without groundwater flow.
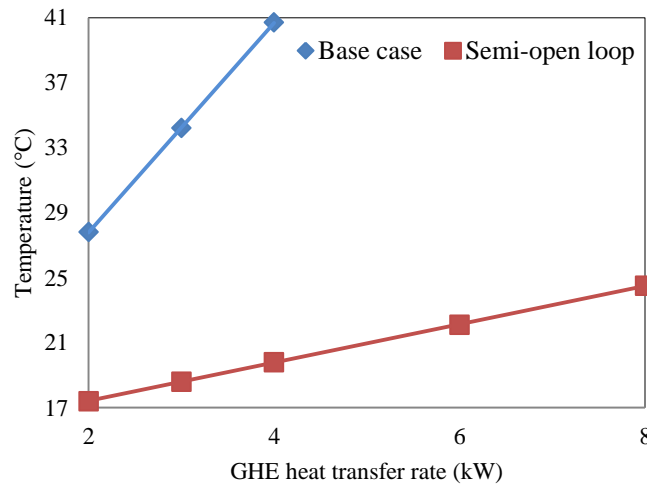
Fig. 3-48 Maximum Tout versus heat transfer rate in 12 hour/day operation, without groundwater flow.
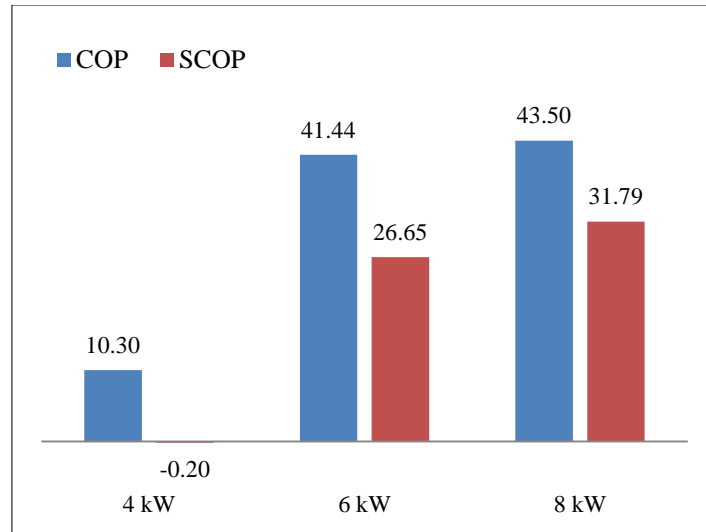
Fig. 3-49 COP and SCOP enhancement in 12 hour/day operation, without groundwater flow.
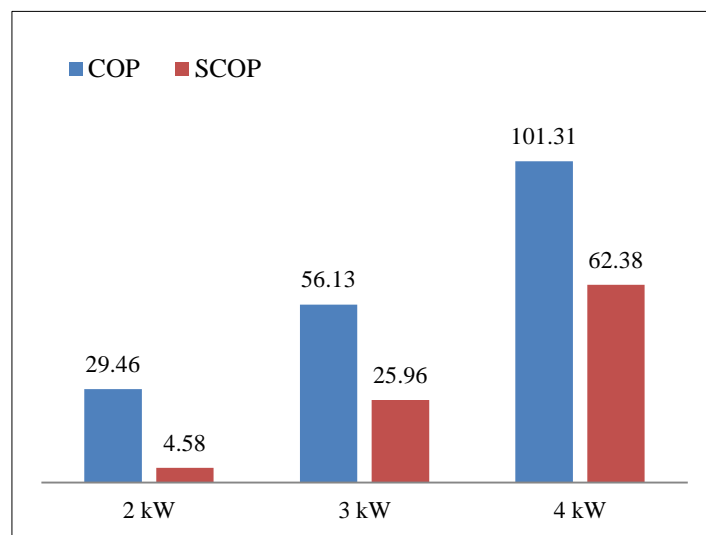
Fig. 3-50 COP and SCOP enhancement in 24 hour/day operation, without groundwater flow.

3.8 Effect of the GHE spacing on the system thermal performance

Several different parameters can affect the thermal performance of the GSHP systems. Fig. 3-51 shows the summary of the important affecting parameters (Pouloupatis et al., 2017).
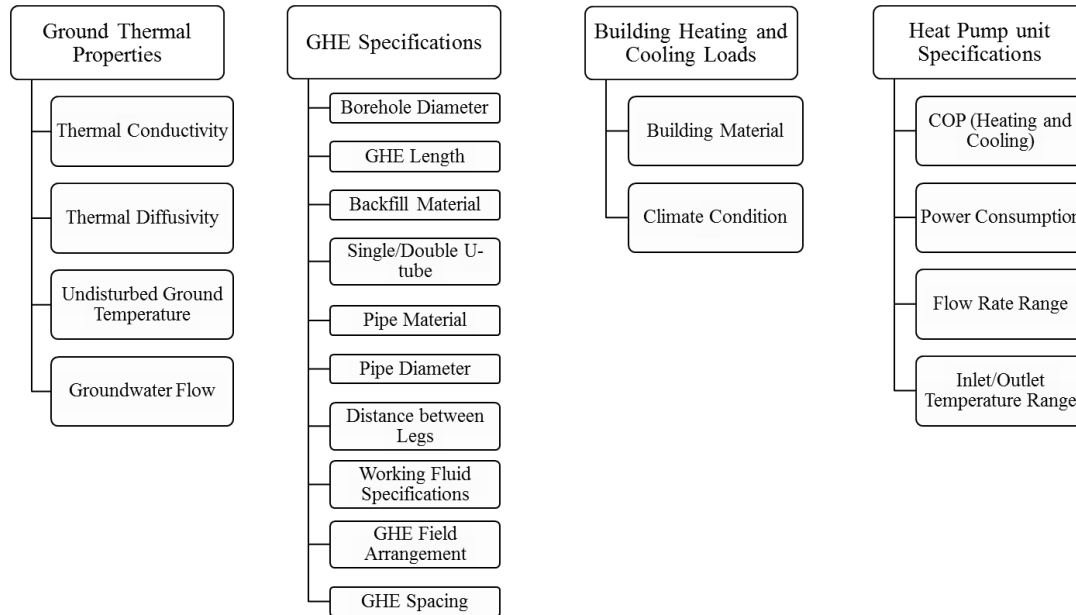
Fig. 3-51 Parameters affecting GSHP system performance.

Among the mentioned parameters in Fig. 3-35, the "GHE Spacing" parameter is one of the important factors in GSHP system design. This parameter attributes to the distance between each GHE and the surrounding GHEs. By decreasing the GHE spacing, the thermal interference between GHEs increases and can worsen the long-term performance of GSHP system, as well as ground temperature. If the spacing distance is greater than the thermal influencing radius, there is no thermal interference and the heat transfer performance of each borehole is the same as a single GHE (Yuan et al., 2016).

In the ideal case, each GHE performs as a single GHE (zero thermal interference between GHEs). However, this case is not practical because of the limited land area in reality. Based on these conditions, it is necessary to assign a minimum acceptable GHE spacing, according to other design parameters. The main objective of this section of study is to calculate the minimum GHE spacing for the introduced semi-open loop GSHP system.

In the first part, a literature review was performed on the available GSHP system standards and the published papers related to the GHE spacing topic. In the next part, a numerical model was developed based on the introduced semi-open loop GSHP system parameters. The system thermal performance is evaluated for different GHE spacing, with and without natural groundwater flow in the formation.

3.8.1 Literature review

Although BHEs are being constructed for more than half century, there is a lack of regulation from standards institutions, meaning that the choice of the procedure to use is left to the experience of the designer (Sailer et al., 2015). Most of the available GSHP standards and manuals are limited to a specific case design and just include some recommendations for the GHE spacing factor.

The Standard VDI 4640 is a German GSHP systems design standard (VDI, 2010). The assumptions in this standard are listed below.

- GHE length: 40-100 m
- Double U-tube
- Heat extraction only
- Not applicable for large number of systems existing in a limited area; this method is for small isolated systems
- Does not take into account the properties of the fill material or any fluid properties
- Neglecting the effect of groundwater flow in the formation

This standard advises for minimum 5 m GHE spacing when GHE length is between 40 m and 50 m. For longer GHEs (until 100 m) the GHE minimum spacing should be 6 m.

The Standard MCS MIS 3005 is GSHP system design standard for United Kingdom (MIS, 2013). The assumptions in this standard are listed below.

- Heat extraction only
- GHE arrangement: linear
- Applicable just for small isolated systems
- BHE diameter: 130 mm
- Single U-tube, 32 mm OD SDP-11, PE 100
- Thermal conductivity of U-tube: 0.42
- U-tube shank spacing: 52 mm center-to-center
- Thermally enhanced grout, thermal conductivity of 2.4 W/mK
- Working fluid: 25% mono ethylene glycol
- $Re > 2500$
- Neglecting the effect of groundwater flow in the formation

This standard recommends for 6 m of minimum GHE spacing, based on their assumptions and calculations.

The Chinese national standard GB 50336-2009: Technical code for ground source heat pump system (MOHURD, 2009) recommends for 3-6 m of GHE spacing to limit the thermal interference between the GHEs.

The Manual of ASHRAE (2011) is probably the most popular GSHP system design manual. The ASHRAE procedure is an analytical procedure for the calculation of the length of BHEs that is based on the proposal by Kavanaugh and Rafferty (1997). It expands the solution for a cylindrical heat source established by Ingersoll (1954) by introducing a series of factors that take into account the characteristics of the BHE, such as its geometry, disposition and materials used, as well as the thermal resistance of the ground as developed by Carslaw and Jaeger (1947) for different heat pulses (up to 10 years). Moreover, once the number and disposition of the BHEs is defined, this method allows the estimation of the change in ground temperature after a given number of years of operation, also known as temperature penalty. In this manual, the recommended minimum GHE spacing is 15ft (4.572 m).

In most of the GSHP system standards and manuals, the design parameters are limited to a specific case, and mainly the calculations are based on the analytical methods that neglect the effect of natural groundwater flow in the formation.

Bai and Che (2016) studied the effects of borehole spacing and well arrangement on soil temperature and heat flux variation. A 5×5 GHE field with different GHE spacing (3-6 m) was considered and ground temperature and heat flux during 6 months of heating period were calculated. Results showed that the greater the borehole spacing, the smaller the soil average temperature and heat flux decline, which is more favorable to long-term operation of the heat pump system.

Yuan et. al., (2016) investigated the effect of intermittent ratios and GHE spacing on the thermal interaction of multiple boreholes. In their heat transfer simulation, soil heat transfer was treated as pure heat conduction without regard to soil moisture migration. So the soil heat transfer is simplified to a two dimensional unsteady pure heat conduction problem. The calculations were performed for GHE spacing of 4, 5 and 6 m. results showed that when the distance between the holes increases, the appearance of thermal interference is delayed due to the greater heat diffusion field.

Koohi-Fayegh and A. Rosen (2012) studied the effect of system parameters such as borehole spacing as well as heat flux from the borehole wall on the transient response of two ground heat exchangers by performing analytical and a finite volume numerical solution. In their numerical simulations they assumed that the impact of groundwater advection is negligible. They changed the GHE spacing as 1, 2 and 3 m. They changed the GHE heat flux as 3.14, 3.28 and 31.41 W/m. Results of calculations showed that varying the heat flux at the borehole wall has a bigger role on the thermal interaction between the boreholes than varying borehole distances with the same ratio.

Cimmino and Eslami-Nejad (2017) developed a simulation model is to evaluate the performance of shallow solar assisted ground heat exchanger bore fields. They considered a 4×4 GHE field with GHE spacing of 1.5 and 3 m. they calculated the necessary GHE length to ensure

same minimum heat pump entering fluid temperature. Results showed that GHE length with 1.5 m spacing is 75% longer than GHE spacing with 3 m. They also mentioned at GHE spacing between 3-4 m, the thermal interference between GHEs in approaching to zero. They used the finite line source solution that ignored groundwater advection effect in its assumption.

Pouloupatis et al., (2017) investigated the influence of the temperature, thermal conductivity, specific heat and density of the ground as well as pipe diameter on the performance of GHEs using GLD software. They changed the GHE spacing from 3 to 10 m in different cases. Results showed that as the distance between the boreholes increases, the estimated ground temperature over the 50-year period decreases rapidly, reaching 0°C at a distance 10 m.

Their modelling results also showed that in some cases the distance between the boreholes could be less than 3 m. Although a short distance between boreholes can save space, too short a distance is not desirable as drilling cannot be guaranteed to be entirely vertical. The greater the depth of the borehole, the larger the deviation from vertical could be and if boreholes are too close to each other, the effectiveness of the GHEs will be reduced. Therefore, it is desirable to keep the distance between boreholes as large as practically possible, particularly for deep boreholes. For 100 m deep boreholes and a 3 m distance between them the deviation from vertical should be less than 0.5°.

Sailer et al., (2015) performed a parametric study using an analytical design procedure to point out the influence of various factors, such as borehole characteristics and thermal properties of the ground. In their calculations, using ASHRAE analytical procedure, they changed the GHE spacing form 5-20 m and presented the normalized GHE length (m/kW). Results showed that small initial decrease in length (of 5% and 7%, respectively) when spacing between boreholes increases from 5 to 8 m, while for larger values of spacing the change is negligible. This is due to a lower temperature penalty being obtained for larger values of spacing between boreholes. Indeed, the temperature penalty reduces to about 0.2°C when the borehole spacing reaches 8 m, a value which no longer affects the BHE design. Moreover, this effect is more pronounced in systems with double U-tubes as they extract more heat per unit length and, therefore, develop higher temperature penalties.

The literature review showed that the calculations in most of the published articles are based on the analytical or numerical methods that neglect the effect of natural groundwater flow. Mainly these studies are targeting the ground temperature and none of the available articles calculated the thermal performance of GSHP system in different GHE spacing scenarios.

3.8.2 Numerical modeling

In order to evaluate the effect of GHE spacing on thermal performance and heat transfer capacity of semi-open loop GSHP system, a numerical model was developed in FEFLOW. This model consists of two ungrouted vertical GHEs, with same characteristics of the GHEs in the

field tests (Table 3-1). The ground thermal and hydraulic specifications are the average of the related parameters in the validated numeral model. The model specifications are summarized as below. Figs. 3-52 and 3-53 show the 3-D and 2-D views of the numerical model.

- Model dimensions: 40 m, 60 m and 80 m.
- Mesh elements: 65,712.
- Number of layers: 16.
- Initial temperature: 15°C.
- Hydraulic conductivity in horizontal directions: 10^{-4} m/s.
- Hydraulic conductivity in vertical direction: 10^{-5} m/s.
- Soil thermal conductivity: 1.3 W/m/K.
- Soil volumetric heat capacity: 2 MJ/m^3/K.
- Porosity: 0.2.
- GHE spacing: 0.5, 1, 1.5, 2.5, 5, 10, 15 and 20 m.

The simulations were performed in 2 scenarios, with (same as the field tests condition) and without natural groundwater flow formations. The direction of the natural groundwater flow was changed in 3 cases (in Scenario#2) in order to evaluate its effect on thermal performance of the GSHP system. In each simulation, the heat pump COP and also the minimum working fluid temperature inside the GHEs were calculated and have been compared to other cases. The operational conditions in the simulations are summarized as below.

- Heating period: 180 days, continuously.
- GHE heat transfer rate, With groundwater flow: 75 W/m.
- GHE heat transfer rate, No groundwater flow: 37.5 W/m.
- GHE flow rate: 15 L/min (for each GHE, 30 L/min for system).
- Groundwater pumping and injection rate: 15 L/min.
- Relationship between COP and outlet temperature of GHE (T_{out}): same as the experimental condition COP=(0.0917* T_{out})+3.2065.

It is necessary to note that the GHE heat transfer rate in each scenario is the maximum possible heat transfer rate for the GHE, for all of the different GHE spacing in that scenario. The reason for maximizing the GHE heat transfer rate is to make the effect of GHE spacing on the average COP and also the minimum working fluid temperature inside the GHEs more obvious.
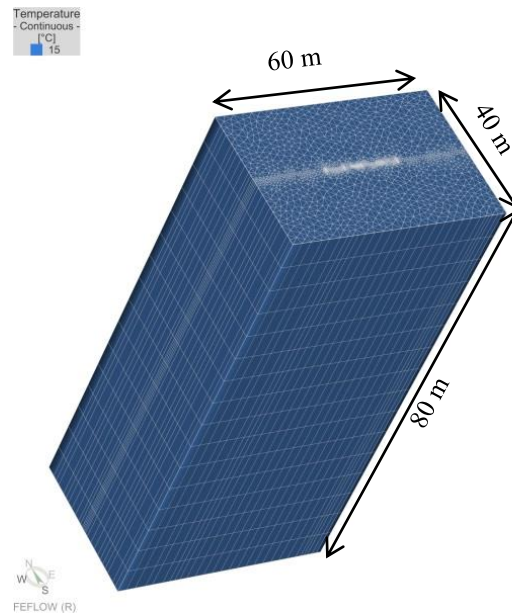
Fig. 3-52 3-D view of the numerical model, with different GHE spacing.
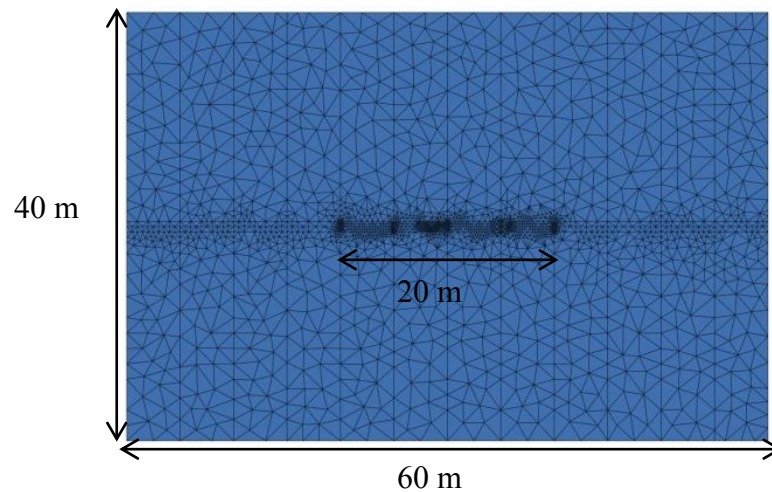
Fig. 3-53 2-D view of the numerical model, with different GHE spacing.

3.8.2.1 Results of the numerical simulation in Scenario#1

In this scenario, there is no natural groundwater flow in the formation. The simulation was performed for 6 months and the average heat pump COP and minimum working fluid temperature are calculated for different GHE spacing. The results of the calculations are shown in Figs. 3-54 and 3-55. Fig. 3-54 shows that by increasing the GHE spacing, the minimum

107

working fluid temperature increases and for the GHE spacing less than 1 m there is a possibility for freezing. When the GHEs are close, the thermal interference between the GHEs increases and the thermal efficiency of the system decreases. Fig. 3-55 shows that by increasing GHE spacing, the heat pump COP increases. The enhancement rate is high for GHE spacing less than 5 m. For the greater GHE spacing the COP has almost a steady trend. For example, the average COP in GHE spacing of 5 m is 20% higher than the case with GHE spacing of 0.5 m. However, the difference between average COP with GHE spacing of 5 m and greater GHE spacing are 1.7%, 2.3% and 2.7% for 10 m, 15 m and 20 m GHE spacing, respectively.
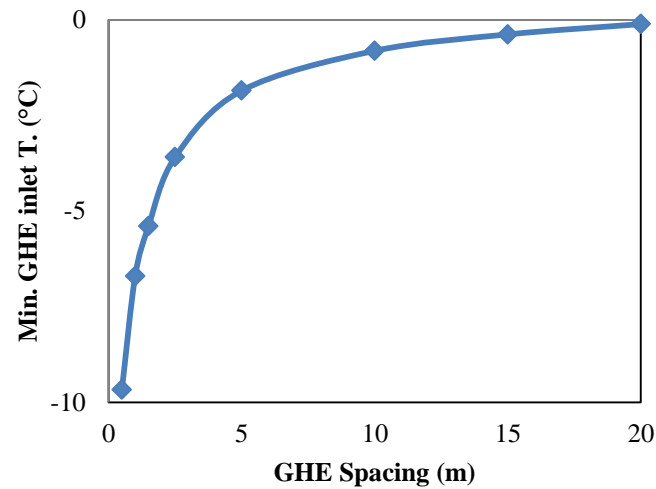
Fig. 3-54 Minimum working fluid temperature in Scenario#1, for different GHE spacing.
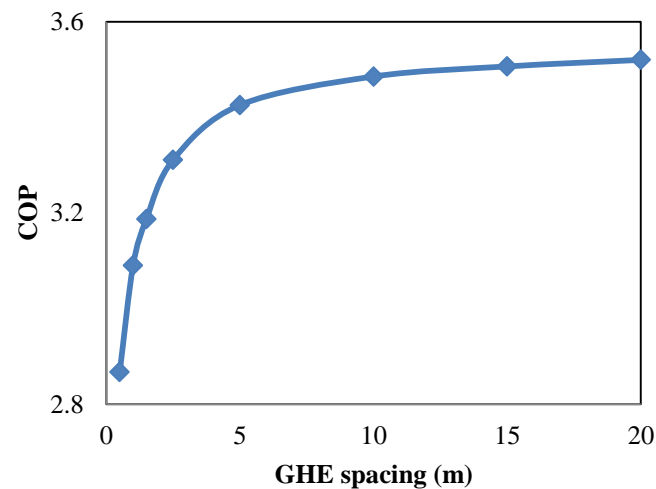
Fig. 3-55 Average COP in Scenario#1, for different GHE spacing.
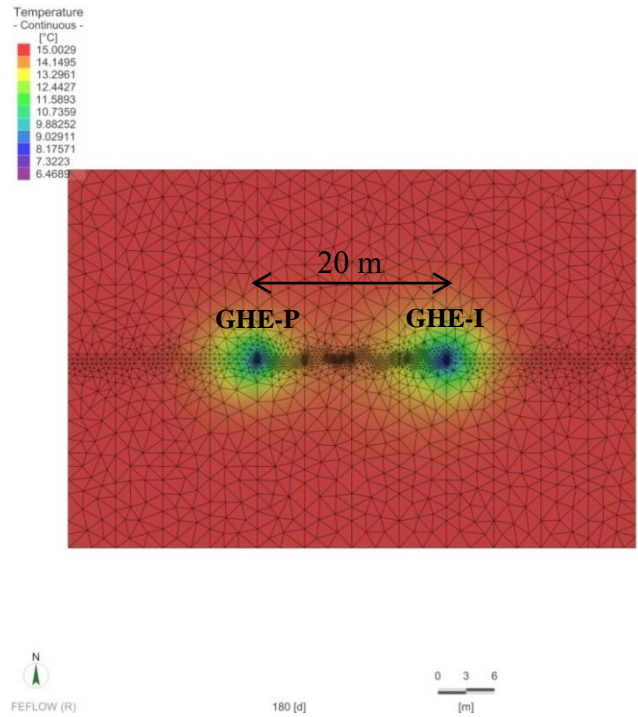
Fig. 3-56 Temperature distribution in -40 m depth in Scenario#1, GHE spacing=20 m.
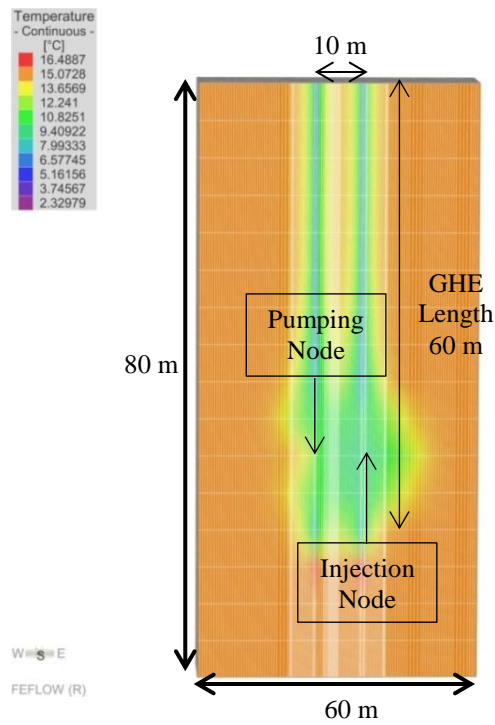
Fig. 3-57 Temperature distribution in cross-sectional view in Scenario#1, GHE spacing=10 m.

Fig. 3-56 shows the temperature distribution in -40 m depth, when the GHE spacing is 20 m. In this figure, GHE-P and GHE-I stand for the pumping GHE and injection GHE in semi-open loop GSHP system, respectively. The temperature drop is high around GHEs. However, because of long GHE spacing, the ground temperatures drop in the middle of the connecting line of the GHEs in not high after 6 months of continuous heating operation, representing a limited thermal interference between the GHEs. Fig. 3-57 shows the temperature distribution in the cross sectional view of the model for Scenario#1, after 6 months of heating operation, when GHE spacing is 10 m.

Results of the calculations showed that the greater the GHE spacing, the better GSHP thermal performance is. However, in Scenario#1 the GHE spacing of 5 m can be considered as the minimum acceptable GHE spacing for semi-open loop GSHP operation.

3.8.2.2 Results of the numerical simulation Scenario#2

In this scenario, there is natural groundwater flow in the formation, with 3 different directions:

- Vertical groundwater flow: the natural groundwater flow direction is perpendicular to the connecting line of the GHEs (Fig. 3-58).
- Groundwater flow from pumping side: the natural groundwater flow in the formation is parallel to the connecting line of the GHEs, from GHE-P side (Fig. 3-59).
- Groundwater flow from injection side: the natural groundwater flow in the formation is parallel to the connecting line of the GHEs, from GHE-I side (Fig. 3-60).

The hydraulic gradient in the formation is 0.01 for all of the cases, same as the validated numerical model for the field test. This hydraulic gradient causes a natural groundwater flow with 8.64 cm/day in the formation. The GHE heat transfer rate was set as 75 W/m; this is the maximum possible heat transfer rate for 6 months of heating operation for different GHE spacing in all of the cases.
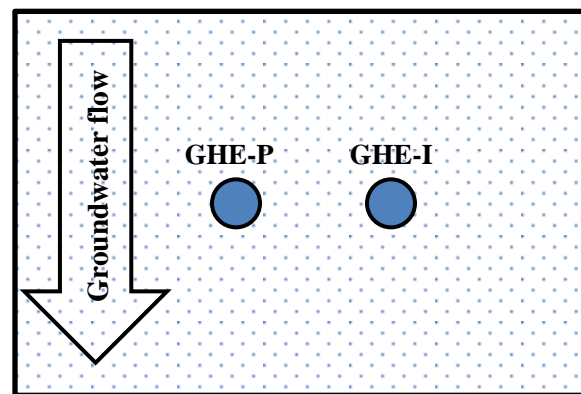
Fig. 3-58 Vertical groundwater flow, Scenario#2.
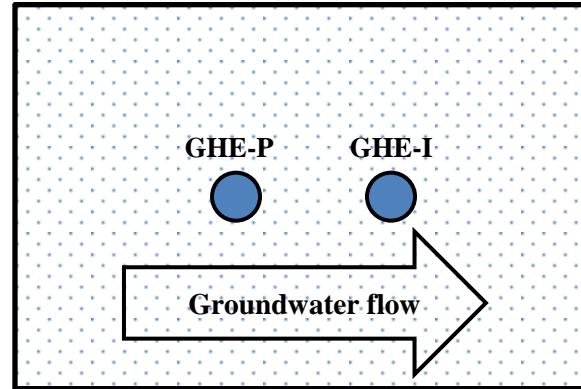
Fig. 3-59 Natural groundwater flow from pumping side, Scenario#2.
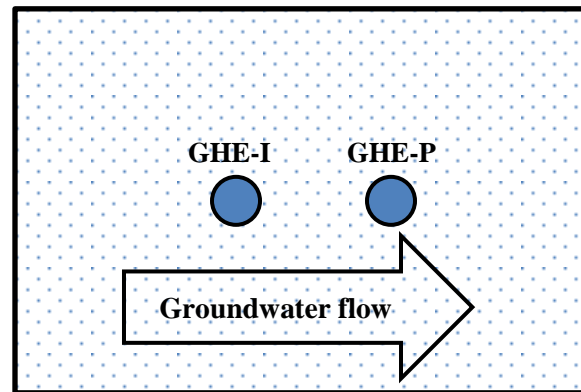
Fig. 3-60 Natural groundwater flow from injection side, Scenario#2.

Table 3-11, 3-12 and 3-13 show the results of numerical simulations for Scenario#2. The results show that by increasing the GHE spacing, the thermal performance of the semi-open loop GSHP system increases. It happens by decreasing the thermal interference between the GHEs. For example, for the case with vertical flow, the average COP in the case with 5 m GHE spacing is 7.8% higher than the case with 0.5 m GHE spacing. The average COP enhancement for the GHE spacing higher that 5 m is limited to less than 2%. Although longer GHE spacing has better impact on the system thermal performance, but in Scenaro#2, the GHE spacing of 5 m can be considered as the minimum acceptable distance between GHE-P and GHE-I.

Fig. 3-61 shows the temperature distribution after 180 days of heating operation at -40 m depth for vertical groundwater flow. The temperature distribution for the cases with groundwater flow direction from pumping and injection side are shown in Fig. 3-62 and 3-63, respectively. In all of the cases, the temperature drop around GHEs is high and expands in the direction of the natural groundwater flow in the formation, due to the convective heat transfer.

Table 3-11 Results of the numerical simulations for Scenario#2, vertical groundwater flow.

Distance between wells	0.5 m	1 m	1.5 m	2.5 m	5 m	10 m	15 m	20 m
Min working fluid temperature (°C)	-6.65	-5.67	-5.24	-4.66	-4.03	-3.51	-3.26	-3.12
Average GHE outlet temperature (°C)	-1.34	-0.39	0.04	0.62	1.28	1.76	1.96	2.05
Average of COP	3.084	3.171	3.210	3.263	3.324	3.368	3.386	3.394

Table 3-12 Results of the numerical simulations for Scenario#2, groundwater flow from pumping side.

Distance between wells	0.5 m	1 m	1.5 m	2.5 m	5 m	10 m	15 m	20 m
Min working fluid temperature (°C)	-6.65	-5.67	-5.24	-4.66	-4.03	-3.51	-3.26	-3.12
Average GHE outlet temperature (°C)	-1.34	-0.39	0.04	0.62	1.28	1.76	1.96	2.05
Average of COP	3.084	3.171	3.210	3.263	3.324	3.368	3.386	3.394

Table 3-13 Results of the numerical simulations for Scenario#2, groundwater flow from injection side.

Distance between wells	0.5 m	1 m	1.5 m	2.5 m	5 m	10 m	15 m	20 m
Min working fluid temperature (°C)	-7.5	-6.52	-6.06	-5.37	-4.6	-3.96	-3.66	-3.46
Average GHE outlet temperature (°C)	-2.11	-1.13	-0.65	0.04	0.84	1.46	1.74	1.9
Average of COP	3.013	3.103	3.147	3.210	3.284	3.340	3.366	3.381
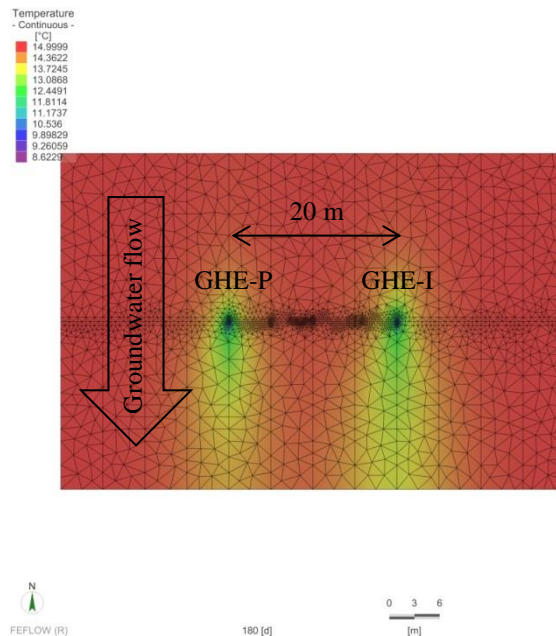
Fig. 3-61 Temperature distribution in -40 m depth in Scenario#2, vertical groundwater flow.
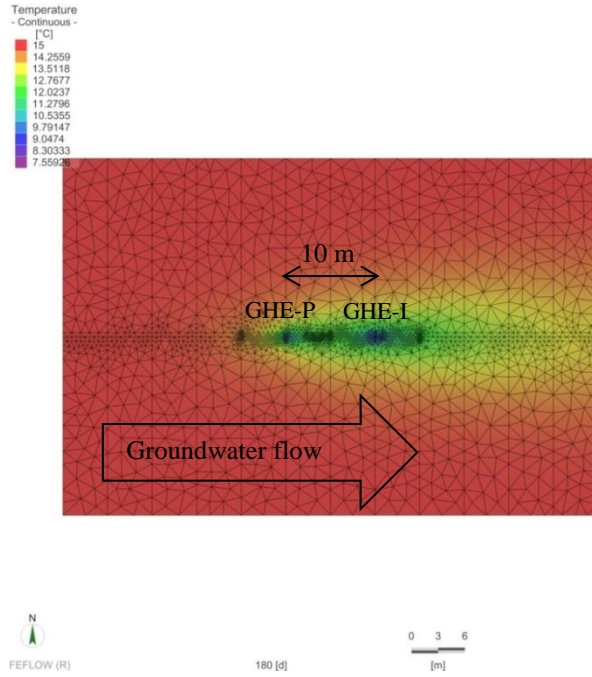
Fig. 3-62 Temperature distribution in -40 m depth in Scenario#2, groundwater flow from pumping side.
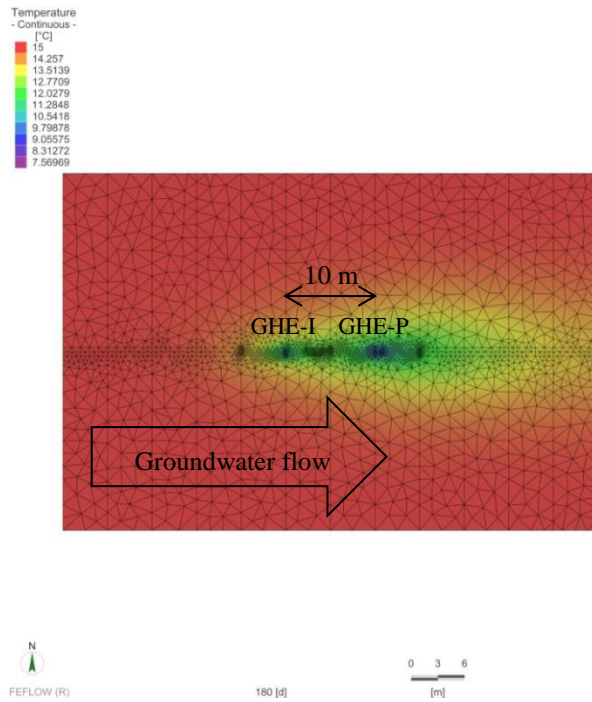
Fig. 3-63 Temperature distribution in -40 m depth in Scenario#2, groundwater flow from injection side.
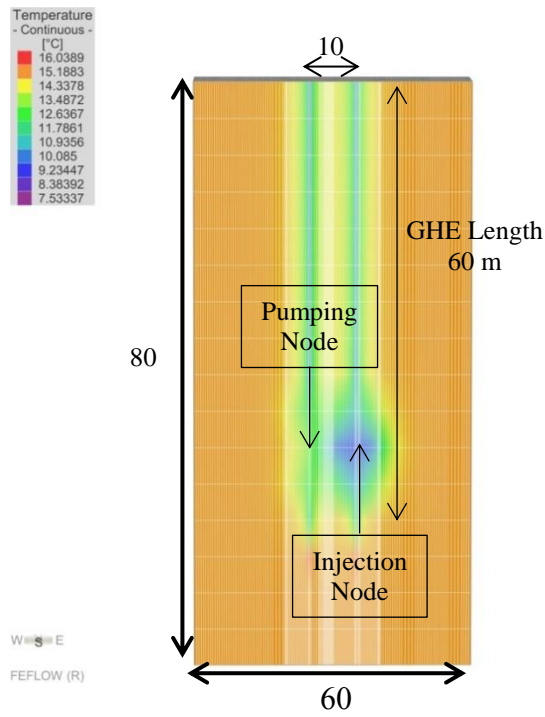
Fig. 3-64 Temperature distribution in cross-sectional view in Scenario#2, vertical groundwater flow.
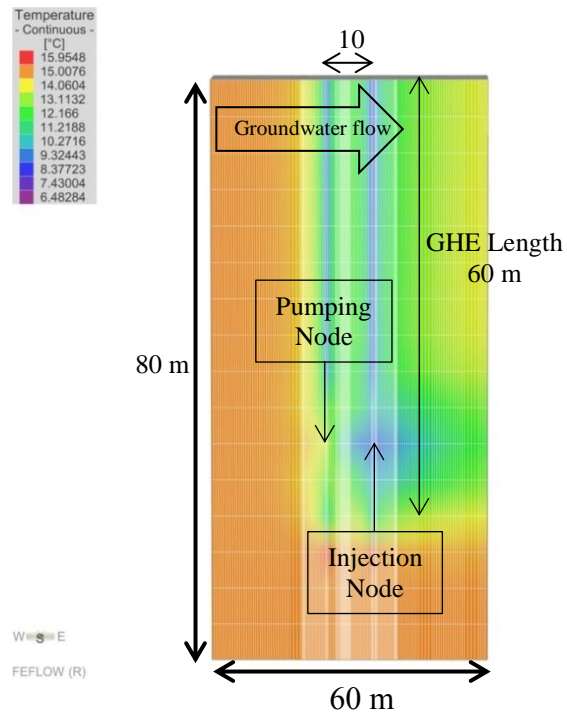
Fig. 3-65 Temperature distribution in cross-sectional view in Scenario#2, groundwater flow from pumping side.
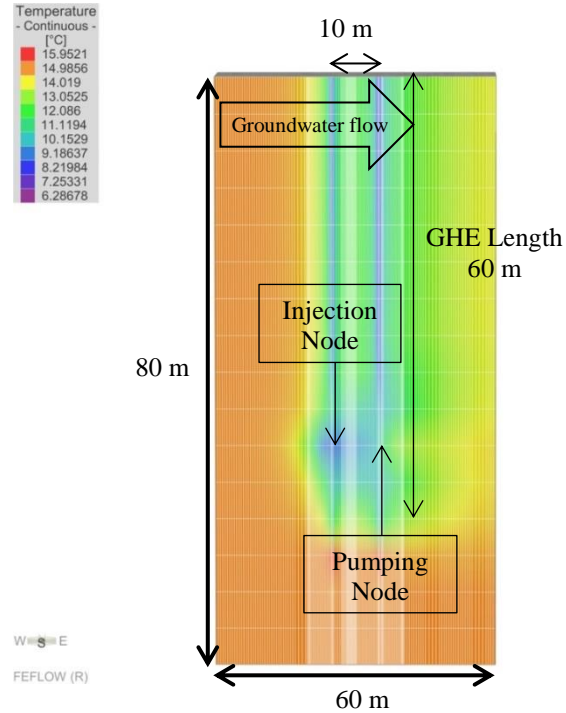
Fig. 3-66 Temperature distribution in cross-sectional view in Scenario#2, groundwater flow from injection side.

Fig. 3-64 shows the temperature distribution in the cross sectional view of the model for vertical groundwater flow after 6 months of heating operation. In this figure, the temperature drop around GHE is obvious. Figs. 3-65 and 3-66 show the same plot for the cases with natural groundwater flow parallel to the connection lines of the GHEs. The temperature drop expands in the direction of the groundwater flow. In all of the cases, the temperature drop around the injection node is high.

Figs. 3-67 and 3-68 summarize the minimum working fluid temperature and average COP for the scenarios with natural groundwater flow. By increasing GHE spacing, the thermal behavior of the system increases in all of the scenarios. However, for the case with vertical groundwater flow, the system thermal behavior is better than the cases with natural groundwater flow direction parallel to the connecting line of the GHEs. In the latter condition, the thermal interference between GHEs increases. Fig. 3-50 shows that the ground temperature is low around the injection point at GHE-I. The natural groundwater flow brings cold groundwater to heat diffusion area, when the natural groundwater flow is from the injection side. This case showed the worst thermal performance among the cases with natural groundwater flow.
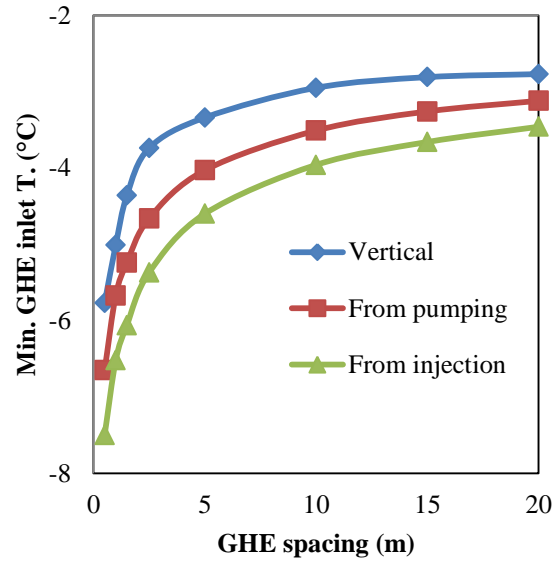
Fig. 3-67 Minimum working fluid temperature for the cases with natural groundwater flow.
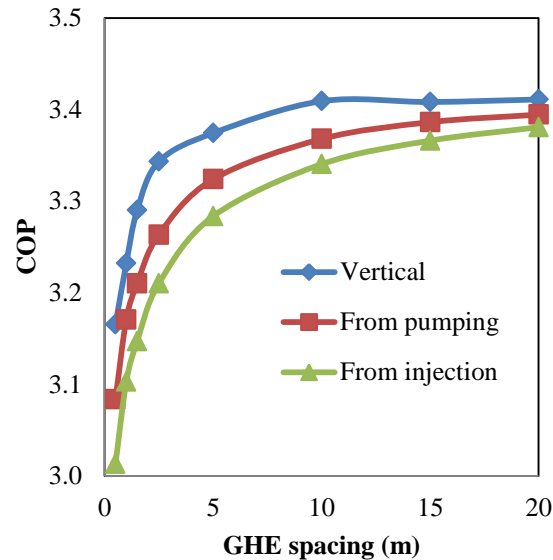
Fig. 3-68 Average COP for the cases with natural groundwater flow.

3.8.3 Summary and conclusion

Results of the numerical modeling showed the strong relationship between the GHE spacing and system thermal performance, especially when the GHEs are close. In both of the simulation scenarios, the GHE heat transfer rate was set as the maximum possible value, ensuring the prevention of the freezing during the heating operation. The maximum GHE heat transfer rate in the absence of groundwater flow was the half of the value for the scenario with groundwater

116

flow. However, in both cases, the acceptable GHE spacing is 5 m. In the formation with natural groundwater flow, it is better position the GHEs in a way that natural groundwater flow be perpendicular to the connecting line of the GHEs, or at least from the pumping GHE side in the semi-open loop GSHP system.

3.9 Conclusion

This step of study investigated the efficiency of semi-open loop GSHP systems; in which groundwater pumped from one GHE is injected into the second GHE to increase the heat advection in both GHEs. Before starting the field tests, TRTs were performed on each of the GHEs individually. Results of the effective thermal conductivity calculation and GHE temperature recovery revealed the possibility of fast groundwater flow and strong aquafer in the formation.

The analysis was performed through field tests and numerical simulations. Heating tests performed on the Akita University campus, Japan. In the field tests, the pumping and injection of groundwater at 15 L/min enhanced the COP by only 5%, and negligibly improved the SCOP. The cooling tests were performed in July-August 2016 and showed the same improvement in the COP and SCOP. The limited COP enhancement might be attributable to the possible fast groundwater flow in the testing area. The effect of groundwater flow on the performance of the semi-open loop GSHP system was discussed in the sensitivity analysis section.

The semi-open loop GSHP system was numerically modeled and validated by heating and cooling experimental data. As confirmed in the sensitivity analysis of heating operation, the COP and SCOP can be enhanced by 12% and 9% respectively under the same groundwater flow conditions as the experimental site, depending on the operational conditions. These parameters in the sensitivity analysis of cooling operation were evaluated around 13.1% and 6.6%, for COP and SCOP, respectively. In the absence of groundwater flow, the semi-open loop system was estimated to boost the COP and SCOP by 40% and 20%, respectively, for heating operations. These parameters for the cooling operation were evaluated around 101% and 62%, for COP and SCOP, respectively. The remarkable effect of water pumping and injection of system capacity enhancement was proven in the sensitivity analysis.

A numerical model was developed to evaluate the effect of GHE spacing on thermal performance of semi-open loop GSHP system. Results of the numerical simulations showed that 5 m distance between GHEs can guarantee a limited thermal interference between the GHEs.

Chapter 4: ECONOMIC ANALYSIS

4.1 Introduction

During the previous steps of this study, the thermal performance of GHE was investigated with and without water pumping and injection, by performing field tests and numerical modeling. The results showed that semi-open loop GHSP system has better thermal performance and higher ground heat exchange capacity, than normal GSHP systems.

Semi-open loop GSHP system has an additional water pump in comparison with normal GSHP system. This water pump adds an additional initial cost to the whole system. Power consumption of water pump must be added to the system power consumption. The last step of this study is going to answer to this question: in economical point of view, does it worth to add an additional water pump to GSHP system?

To answer this question, an economic analysis was performed; the results will be described in this chapter. A sample building, with characteristics similar to field test conditions was considered to calculate the hourly heating and cooling loads during a reference year, according to Akita City's metrological data. The validated numerical FEFLOW model was used to calculate the minimum necessary GHE length to meet the heating and cooling demand of the building, for different scenarios that considers different natural groundwater condition and also water pumping and injection rates. In the last step, the total saving due to water pumping and injection was calculated using cash flow diagram and considering GHE length reduction, water pump installation cost and its power consumption cost.

4.2 Heating and cooling loads calculation

In this section, the calculation procedure and the results of heating and cooling loads of a sample building is presented. In the first part, the importance of human comfort condition and the effective parameters on the buildings heating and cooling loads calculation were described. In the next part, the hourly heating and cooling loads of a sample building in Akita City was calculated based on the proposed method of Energy Conservation Standards in Japan and using metrological data of Akita City. In the last part of this section, the hourly heat transfer rate of Ground Heat Exchangers (GHEs) in the GSHP system was calculated based on the building heating and cooling loads during one year.

4.2.1 Human comfort zone

There are several factors that can affect the human comfort in a space, including:

- Dry-bulb temperature

- Humidity
- Air movement
- Air quality
- Noise level
- Adequate lighting
- Proper furniture and work surfaces

Creating thermal comfort for human is to prepare a space with suitable dry-bulb temperature, humidity and air motion that is appropriate for the activity level of residents. In this condition, the heat generation and the heat loss of human body will be balanced. According to ASHRAE Standard 55, Thermal Environmental Conditions for Human Occupancy (2013), the comfort condition is the combination of the above mentioned factors for delivering acceptable thermal comfort for 80% of the people in a space. The sample of comfort zone in psychometric chart is shown in Fig. 4-1. The main mission of a successful heating and cooling system for a building is to keep the indoor condition in the comfort area for the residences during the cold and warm seasons (e. g. point A in Fig. 4-1).
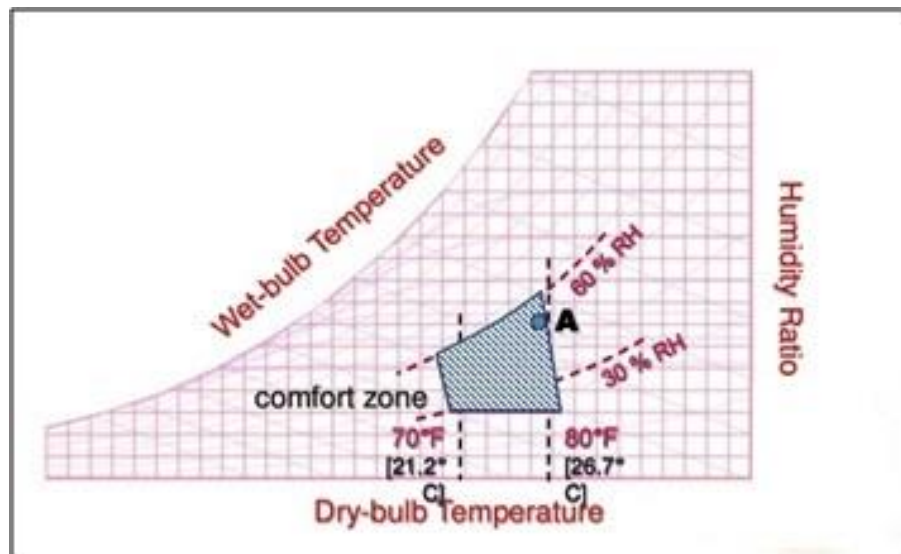
Fig. 4-1 Psychometric chart and human comfort area.

In heating and cooling system design step, if the system size overestimated, the system initial and running cost will be high. The underestimated systems will not be able to provide proper comfort condition for the residences. The first step of all heating and cooling system sizing is calculating the heating and cooling loads of the building.

4.2.2 Effective parameters on space heating and cooling loads

Calculating the cooling load for a space is more complicated in comparison with the heating load, although the heating system sizing needs more caution. The damage due to underestimating heating system size especially in GSHP systems is more serious in comparison with cooling, due to the possibility of freezing phenomenon inside the GHEs.

The space cooling load is the rate at which heat must be removed from a space in order to maintain the desired conditions in the space, generally a dry-bulb temperature and relative humidity. Some of the most important parameters in space cooling load (space heat gain during the warm season) are:

- Conduction heat gain from outdoors through the roof, exterior walls, skylights, and windows.
- Solar radiation heat gain through skylights and windows.
- Conduction heat gain from adjoining spaces through the ceiling, interior partition walls, and floor.
- Internal heat gains due to people, lights, appliances, and equipment in the space.
- Heat gain due to hot, humid air infiltrating into the space from outdoors through doors, windows, and small cracks in the building envelope.

Providing fresh air for residences during the warm season can increase the space cooling load, depends on the type of cooling and air conditioning system in the building. So, these parameters are also important in cooling load calculation:

- Heat gain due to outdoor air deliberately brought into the building for ventilation purposes.
- Heat generated by the fans in the system and possibly other heat gains in the system.

The space heating load is the rate at which heat must be added to a space in order to maintain the desired conditions in the space, generally a dry-bulb temperature. There are some differences between heating and cooling loads calculations. In usual heating load calculation:

- In general, the estimation of heating loads and system sizing assumes worst-case conditions for the space.
- No credit is given for heat gain from solar radiation through glass or from the sun's rays warming the outside surfaces of the building.
- No credit is given for internal heat gains due to people, lighting, and equipment in the space.

The main factor for heating load calculation (space heat loss during the cold season) is the conduction heat loss to the outdoors through the roof, exterior walls, skylights, and windows.

4.2.3 Heating and cooling load calculation for the sample building

During the previous parts of this chapter, it has been described that there are many important parameters that are effective in space heating and cooling load calculations. The level of accuracy and complexity in heating and cooling load calculation depends on the scopes of the study. For the complex studies, there are some well-developed commercialized software, for example, Hourly Analysis Program (HAP) that thermally models every single material and object in the building and provides a comprehensive and detailed analysis of the buildings heating and cooling loads, and also heating and cooling system power consumption over the year. But this level of complexity is out of the scopes of our study.

According to the Japan energy saving standard, published by Ministry of Land, Infrastructure, Transport and Tourism (MLIT, 2014), Japan is classified for 8 regions in energy conservation standard (see Fig. 4-2). The heating and cooling loads for the conventional buildings are calculated with Eq. 4-1 and 4-2:

$$Q_{heating} = \frac{U \times A_e \times (T_i - T_o)}{A_f} - \frac{I \times \eta}{A_f} \tag{4-1}$$

$$Q_{cooling} = \frac{U \times A_e \times (T_o - T_i)}{A_f} + \frac{I \times \eta}{A_f} \tag{4-2}$$

In these equations:

- $Q_{heating}$ and $Q_{cooling}$: Heating and cooling loads (W/m^2)
- A_e: Building envelope area (m^2)
- A_f: Building floor area (m^2)
- T_i: Room temperature (°C)
- T_o: Ambient temperature (°C)
- I: Solar radiation (W/m^2)
- U: Overall heat transfer coefficient (W/m^2/K)
- η: Average solar heat acquisition rate (W/W/m^2)

In this method, the values for U and η vary for different regions. The regions are shown in Fig. 4-2 and the values for U and η are shown in Table 4-1.

Akita City is placed in Region 4, so according to Table 4-1, the value for U is 0.75 W/m^2/K. The value for η is missing for regions 1-4 (mainly north part of Japan with low solar radiation), so the amount of solar radiation will not be considered in Eq. 4-1 and 4-2.
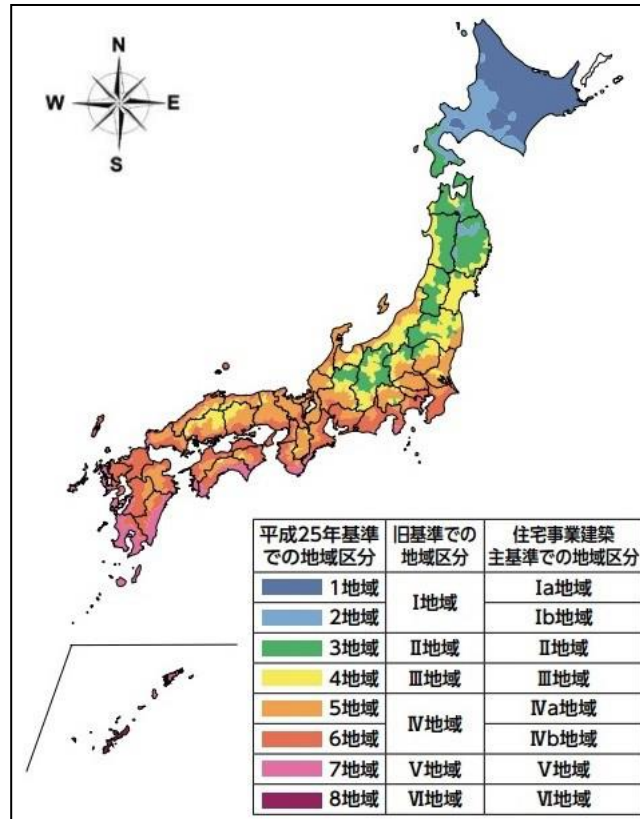
Fig. 4-2 Region classification in energy conservation standard (MLIT, 2014).

Table 4-1 U and η parameters for different regions in Japan (MLIT, 2014).

Region	1	2	3	4	5	6	7	8
U [W/(m²K)]	0.46	0.46	0.56	0.75	0.87	0.87	0.87	-
η [W/(W/m²)]	-	-	-	-	3.0	2.8	2.7	3.2

Table 4-2 Sample building dimensions (MLIT, 2014).

Total floor area A_f [m²]			**120.08**
Breakdown	Main room	[m²]	29.81
	Other rooms	[m²]	51.34
	Non-residence	[m²]	38.93
Total building envelope area A_e [m²]			**312.8**
Breakdown	Ceiling area	[m²]	67.19
	Floor area	[m²]	65.42
	Total area of wall and opening	[m²]	176.99
	Perimeter of earth floor (outside air)	[m²]	3.185
	Perimeter of earth floor (others)	[m²]	3.185

The sample building dimensions are based on the "Outline of Revision of Energy Conservation Standards", published by Ministry of Land, Infrastructure, Transport and Tourism (MLIT, 2014) and are shown in Table 4-2. The values for A_e and A_f will be 312.8 and 120.08 m^2, respectively. According to ASHRAE Standard 55 (2013), the room temperature for heating and cooling will be 22°C and 24°C, respectively. Based on the above mentioned descriptions, the heating and cooling loads per meter of the sample building in Akita City can be estimated using Eq. 4-3 and 4-4, respectively.

$$Q_{heating} = \frac{0.75 \times 312.80 \times (22 - T_o)}{120.08} \tag{4-3}$$

$$Q_{cooling} = \frac{0.75 \times 312.80 \times (T_o - 24)}{120.08} \tag{4-4}$$

The yearly average ambient temperatures (To) in Akita City for 2000-2015 are shown in Fig. 4-3 (Japan Metrological Agency online data center). The average of T_o in 2009 is very close to the trend line that has been plotted on the Fig. 4-3; so 2009 is used as the reference year for the heating and cooling load calculation. The hourly T_o for 2009 is shown in Fig. 4-4. Akita City is experiencing low T_o during the cold season, but it is not very high during the warm season, so we can expect high heating load in comparison with the cooling load.

The heating period was set as November-April (6 months), everyday 8:00-20:00. The cooling period was set as July-September (3 months) everyday 8:00-20:00. This period is similar to student office working hours during the field tests. The heating and cooling loads were calculated in hourly basis and are shown in Fig. 4-5.
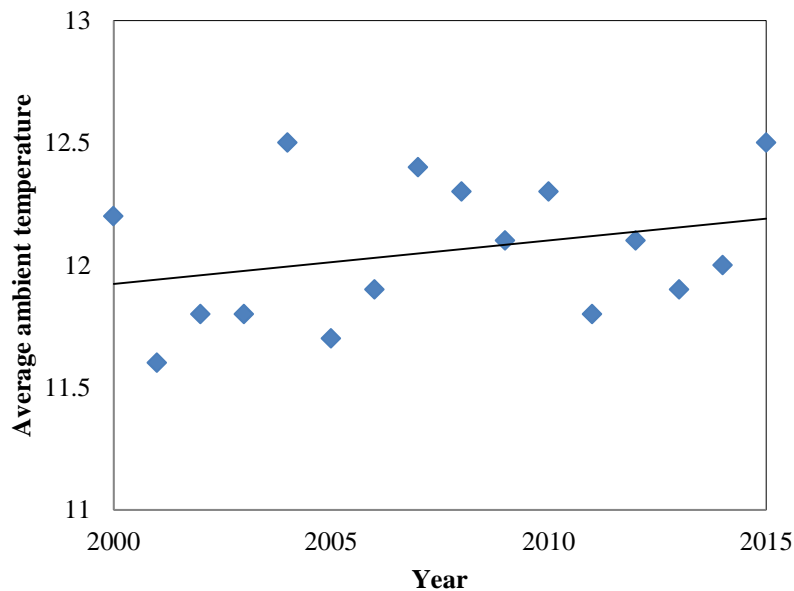
Fig. 4-3 Average ambient temperature of Akita City 2000-2015.

123
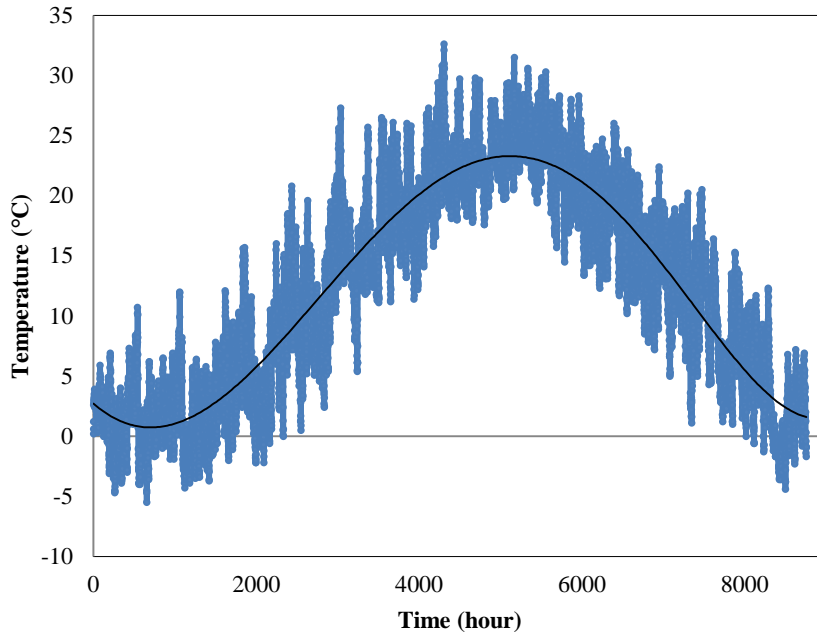
Fig. 4-4 Hourly ambient temperature of Akita City 2009.
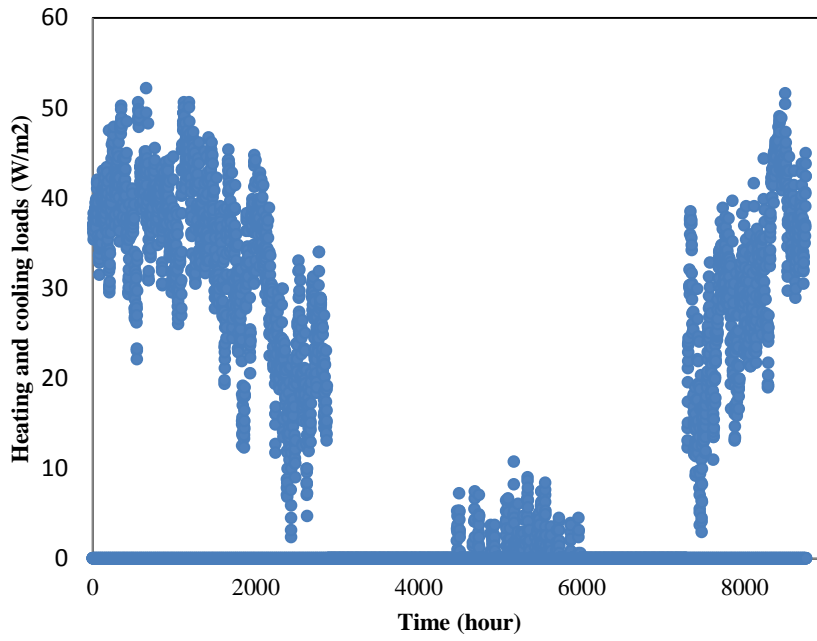
Fig. 4-5 Calculated hourly heating and cooling loads.

4.2.4 GHE heat transfer rate calculation

In order to calculate the minimum GHE length in GSHP system, the heat transfer rate between GHE and ground must be calculated. The relationship between heating and cooling load (Q_{room}), transfer rate (Q_{GHE}) and heat pump power consumption (W) for heating and cooling conditions are shown in Eq. 4-5 and 4-6, respectively.

$$Q_{GHE} = Q_{room} - W \tag{4-5}$$

$$Q_{GHE} = Q_{room} + W \tag{4-6}$$

The Coefficient Of Performance (COP) is the ratio of Q_{room} and W. In our calculation, the heating and cooling COPs were set as 3.5 and 5.5, respectively. Based on these discerptions, Q_{GHE} in hourly basis was calculated and shown in Fig. 4-6. This value is the input parameter to the validated FEFLOW numerical model to calculate the minimum necessary GHE length to meet the heating and cooling demand of the building. As it was expected, the maximum the heat transfer rate in heating operation was higher in comparison with that in the cooling operation. The maximum Q_{GHE} in heating period is around 4.5 kW, while it is around 1.5 kW in cooling period. It is necessary to note that in Fig. 4-6, heating loads have negative values, while cooling loads are positive.
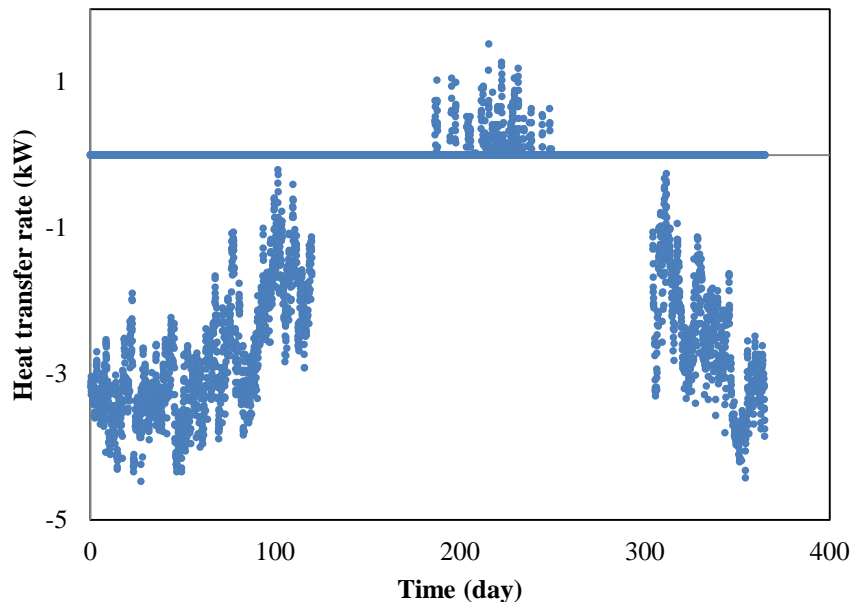
Fig. 4-6 Calculated hourly GHE heat transfer rate.

4.3 GHE length calculation

In the GSHP systems, GHE sizing is very important. Oversizing the GHE length will cause high initial cost. On the other hand, undersized systems will not be able to meet the heating and cooling demands of the building and the problems like freezing in the GHE during the cold seasons is possible.

In this study, the validated FEFLOW model with described characteristics in Chapter 3 is the tool to estimate the minimum necessary GHE length to meet the calculated building heating and cooling loads. The calculated hourly GHE heat transfer rate (for 1 year) is the input parameter to the FEFLOW model. Although in this study the heating load is dominant in comparison with cooling one and the minimum working fluid temperature will be the design parameter, but the simulation was performed for whole year.

In the field tests and also numerical model specification, the working fluid inside the GHE is the mixture of water and ethylene glycol (20% volume, freezing point: -7.9 °C). Considering the safety factor to prevent the freezing phenomenon during the cold season and also operating the heat pump in high COP ranges, the minimum working fluid temperature during the cold season was set as -0.5°C.

In order to consider the effect of natural groundwater flow and also water pumping and injection rate, 3 different scenarios were analyzed and the minimum GHE length in each scenario was calculated both for the base case (without water pumping and injection) and semi-open loop operation. After setting the minimum GHE length for base case operation, the GHE length for semi-open loop operation was set to ensure equal heat pump power consumption for base case and semi-open loop operations. In order to evaluate the long-term performance of GHEs, numerical modeling was performed for 3 years for the selected cases.

The FEFLOW model specifications were shown and described in Fig 3-17-1 and Table 3-8 in Chapter 3. The hydraulic boundary condition will be different for each scenario and will be described in the next sections.

4.3.1 GHE length in Scenario 1

In this scenario, the "No groundwater flow" condition was considered. In this scenario, the hydraulic head for both eastern and western lateral sides of model was set as -5 m. In the base case condition, there is no water pumping and injection inside the GHE wells. In semi-loop condition, the groundwater is pumped from GHE2 to GHE1 with the rate of 15 L/min. The pumping and injection node in numerical model were place 10 m higher than the bottom of the GHE. For example, if for the GHE length of 50 m, the water pumping and water injection node depth will be 40 m, inside the GHE. Fig. 3-17-4 in Chapter 3 shows the water pumping and water injection nodes inside the GHE.

The results of sensitivity analysis in chapter 3 showed that the effect of water pumping and injection on GHE heat transfer capacity in "No groundwater flow" condition is very strong, so we can expect a large GHE length difference between the base case and the semi-open loop operation in Scenario 1.

The main input parameter to the FEFLOW model is the calculated GHE heat transfer rate. Based on the model input data, GHE inlet and outlet temperatures are calculated and reported in each time step of numerical modeling. The GHE length and minimum working fluid temperature in Scenario 1 is shown in Table 4-3.

Table 4-3 GHE length and minimum working fluid temperature for Scenario 1.

Case	Water pumping and injection rate (L/min)	Total GHE length (m)	Minimum fluid temperature (°C)
1	0	120	-3.63
2	0	140	-2.34
3	0	160	-1.01
4	0	180	-0.27
5	15	120	7.52
6	15	100	6.52
7	15	80	4.96
8	15	60	2.90
9	15	40	0.82

In Table 4-3, the shaded rows are the selected cases. In Case 4, the total GHE length for base case is 180 m (2 GHEs, each with 90 m length). The minimum working fluid temperature for Case 4 is -0.27°C. In Case 9, the total GHE length for base case is 40 m (2 GHEs, each with 20 m length). The minimum working fluid temperature for Case 4 is 0.82°C.

As mentioned in Chapter 3, there is a linear relationship between T_{out} and heat pump COP. In order to have same heat pump power consumption for semi-open loop and base case operations, the average of T_{out} during the heating and cooling operations must be same for base case and semi-open loop operations. In this study, the heating season is longer and heating load is higher than the cooling one, so the average of T_{out} for the heating period will be the essential parameter for GHE sizing.

Table 4-4 shows the average of T_{out} during the heating period for the selected cases in Scenario 1. This parameter is 9.22 °C for the base case. For the semi-open loop operations, average of T_{out} is 7.38 °C and 10.69 °C for the GHE lengths of 40 m and 60 m, respectively. Leaner interpolation between two semi-open loop cases shows that GHE length for semi-open loop operation in scenario 1 will be 51 m. In Scenario 1, due to the absence of groundwater flow, the GHE length reduction rate is very high. The GHE length difference between base case and

semi-open loop operation is 129 m that shows around 72% of reduction by the water pumping and injection of 15 L/min.

Table 4-4 Average of heating T_{out} for 3 cases in Scenario 1.

Case	Water pumping and injection rate (L/min)	Total GHE length (m)	Average heating T_{out} (°C)
4	0	180	9.22
8	15	60	10.69
9	15	40	7.38

4.3.2 GHE length in Scenario 2

In Scenario 2, same as Scenario 1 there is no natural groundwater flow in the domain. It means that the hydraulic head boundary conditions are same as those used in Scenario 1. The difference between Scenario 1 and 2 is in the water pumping and injection rate for the semi-open loop operations. In Scenario 1 it was 15 L/min, while in Scenario 2 it is 5 L/min to see the effect of water pumping and injection rate in "No groundwater flow" condition. In Table 4-5 the results of numerical simulations for Scenario 2 are shown.

Table 4-5 GHE length and minimum working fluid temperature for Scenario 2.

Case	Water pumping and injection rate (L/min)	Total GHE length (m)	Minimum fluid temperature (°C)
4	0	180	-0.27
10	5	40	-1.88
11	5	50	-0.34
12	5	60	1.65

In this scenario, the GHE length for base case is same as that in Scenario 1 (180 m), because there is no difference for base cases in Scenarios 1 and 2. The minimum GHE length for semi-open loop operation is Scenario 2 is 50 m (2 GHEs, each with 25 m length).

In the same process as Scenario 1, Table 4-6 shows the average of T_{out} during the heating period for the selected cases in Scenario 2. This parameter is 9.22 °C for the base case. For the semi-open loop operations, average of T_{out} is 7.64 °C and 9.45 °C for the GHE length of 50 m and 60 m, respectively. Leaner interpolation between two semi-open loop cases shows that GHE length for semi-open loop operation in scenario 1 will be 59 m.

Comparison between Scenarios 1 and 2 shows that reducing water pumping and injection rate from 15 L/min to 5 L/min in semi-open loop operations, causes 8 m increment in total necessary GHE length. In Scenario 2, the reduction of GHE length due to water pumping and injection is 121 m (67%), which is 5% less than Scenario 1.

Table 4-6 Average of heating T_{out} for 3 cases in Scenario 2.

Case	Water pumping and injection rate (L/min)	Total GHE length (m)	Heating average T_{out}
4	0	180	9.22
11	5	50	7.64
12	5	60	9.45

4.3.3 GHE length in Scenario 3

In order to consider the effect of natural groundwater flow on the minimum necessary GHE length, a new scenario with "Slow groundwater flow" condition was analyzed. In semi-open loop GSHP system field tests and also validated FEFLOW numerical model, the hydraulic head gradient between the eastern and western lateral boundaries was set as 0.01. In that case, the maximum groundwater velocity in the domain was 15 cm/day. In Scenario 3, "Slow groundwater flow" condition was considered.

In this scenario, hydraulic head gradient between the eastern and western lateral boundaries was set as 0.001. Same as last scenarios, base case operation was modeled with no water pumping and injection. Semi-open loop operation was modeled and analyzed with 5 L/min of water pumping and injection between GHEs. In Table 4-7, the minimum calculated working fluid temperature for different GHE lengths in base case and semi-open loop open loop operations are shown.

The results of numerical modeling for Scenario 3 showed that the minimum necessary GHE length in base case operation is 110 m (2 GHEs, each with 55 m length). For the semi-open loop operation, the minimum GHE length is 40 m (2 GHEs, each with 20 m length).

Same as the previous scenarios, in order to have same average T_{out} for base case and semi-open operations, this parameter was calculated for the selected cases in Scenario 3. Table 4-8 shows that the average of T_{out} during the hearing season for base case is 9.17 °C. For the semi-open loop operations, average of T_{out} is 8.21 °C and 10.61 °C for the GHE length of 40 m and 50 m, respectively. Leaner interpolation between two semi-open loop cases shows that GHE length for semi-open loop operation in scenario 3 will be 44 m.

The calculated GHE length in the base case is 66 m longer than semi-open loop operation, so 5 L/min of water pumping and injection in Scenario 3 (Slow groundwater flow condition), can decrease the necessary GHE length by around 60%.

Table 4-7 GHE length and minimum working fluid temperature for Scenario 3.

Case	Water pumping and injection rate (L/min)	Total GHE length (m)	Minimum fluid temperature (°C)
13	0	140	2.2
14	0	120	1.36
15	0	110	0.70
16	0	100	-0.92
17	5	40	1.07
18	5	50	2.10

Table 4-8 Average of heating T_{out} for 3 cases in Scenario 3.

Case	Water pumping and injection rate (L/min)	Total GHE length (m)	Heating average T_{out}
15	0	110	9.17
17	5	40	8.21
18	5	50	10.61

4.4 Numerical simulation for 3 years of operation in selected cases

In order to evaluate the long-term performance of selected cases, the numerical modeling was performed for 3 years of operation. The minimum working fluid temperature in each year was calculated to observe the possible temperature drop in long term operation of the selected cases. In Table 4-9 and 4-10, the results of long-term numerical simulation for the selected cases are shown, for No and Slow groundwater flow conditions, respectively.

It is necessary to note that in the semi-open loop operations in Table 4-9 and 4-10, the GHE lengths are not exactly same as final calculated GHE lengths, but shorter than them (the selected semi-open loop cases in Table 4-3, 4-5 and 4-7). If the long-term operation of these cases be acceptable, their performance will be acceptable for longer GHE lengths.

Table 4-9 Min. working fluid temperature for 3 years of operation in "No groundwater flow" condition.

Case	Water pumping and injection rate (L/min)	Total GHE length (m)	Min fluid T in 1st year (°C)	Min fluid T in 2nd year (°C)	Min fluid T in 3rd year (°C)
4	0	180	-0.27	-0.29	-0.31
9	15	40	0.82	0.82	0.81
11	5	50	-0.34	-0.35	-0.36

130

Table 4-10 Min. working fluid temperature for 3 years of operation in "Slow groundwater flow" condition.

Case	Water pumping and injection rate (L/min)	Total GHE length (m)	Min fluid T in 1st year (°C)	Min fluid T in 2nd year (°C)	Min fluid T in 3rd year (°C)
15	0	110	0.70	0.69	0.68
17	5	40	1.07	1.07	1.06

The calculated results showed that the maximum of "the yearly minimum working fluid temperature" drop is for Case 4 and its value is 0.04 °C after 3 years of operation. In Case 4, the minimum fluid temperature is -0.27 °C and -0.31 °C for the first year and third year, respectively. Case 4 is the GSHP base case operation in "No groundwater flow" condition, although this value in "Slow groundwater flow condition" is 0.02 °C (Case 15). In Case 15, the minimum fluid temperature is -0.70 °C and 0.68 °C for the first year and third year, respectively.

For semi-open GSHP operations, the temperature drop in "No groundwater flow" condition is 0.01 and 0.02 °C for 15 and 5 L/min of water pumping and injection, respectively. This value in "Slow groundwater flow" condition is 0.01 °C (Case 17). In Case 17, the minimum fluid temperature is 1.07 °C and 1.06 °C for the first year and third year, respectively. The results of long-term numerical simulation show that the selected cases are trustable and the GHEs with calculated lengths are able to meet the expected heat transfer rate for long-term operation.

Results of the long-term numerical simulation showed that water pumping and injection is helpful to prevent the working fluid temperature drop in heating-dominated conditions. These results also showed that the calculated GHE lengths are suitable to meet the heating and cooling loads of the building.

4.5 Saving in semi-open loop GSHP

In this section, the economic saving of water pumping and injection in GSHP system is calculated and presented. In the first part, the capital cost saving was calculated considering: drilling cost reduction and water pumping and injection equipment cost. In the next part, the cost of power consumption of water pumping and injection process was calculated considering the parameters including: water pump working hours and power consumption, electricity price in Japan, Japan annual inflation rate and interest rate. The final semi-open loop GSHP system was evaluated considering the capital cost saving and water pump power consumption. The share of the saving to the total cost of GSHP system calculated considering the drilling cost, heat pump unit cost, distribution system cost, piping and labor cost for installation.

4.5.1 Capital cost saving

Results of GHE lengths calculation in all of scenarios showed that water pumping and injection in semi-open loop operation can decrease the necessary GHE length to meet the expected heat transfer rate. In the first step of semi-open loop GSHP system saving, the saving due to the GHE length reduction was calculated.

The drilling cost in Japan is high, in comparison with that in European and American countries as mentioned Chapter 1. In this study, the drilling and GHE installation cost is determines as 15,000 Yen/m. In Table 4-11, a summary of calculated GHE lengths for different scenarios and drilling cost saving due to the GHE length reduction are shown. Calculated results show that the maximum drilling saving happens in Scenario 1 with 1.93 million Yen. This value is 1.81 and 0.99 million Yen for Scenario 2 and 3, respectively.

Table 4-11 Drilling cost saving in different scenarios.

Scenario	Base case GHE length (m)	Semi-open loop GHE length (m)	Diff. in GHE length (m)	Diff. in GHE length (%)	Drilling cost saving (Yen)
Scenario 1	180	51	129	72%	1,935,000
Scenario 2	180	59	121	67%	1,815,000
Scenario 3	110	44	66	60%	990,000

Water pumping and injection can reduce the necessary GHE length in GSHP system and as the result, the system initial cost decreases. On the other hand, semi-open loop system contains additional component in comparison with normal GSHP system. The additional components and their costs in semi-open loop system are shown in Table 4-12. In order to prevent the possible damages to water pump in outside condition and to guarantee the long-term operation of water pump, a simple cubic casing can be installed on the water pump (water pump casing item in Table 4-12).

Table 4-12 Additional components cost in semi-open loop operation.

Item	Value
Water pump	60,000 Yen
Water pumping and injection pipe	500 Yen/m
Water pump installation	20,000 Yen
Water pump casing	10,000 Yen

The price of water pumping and injection pipe is 500 Yen/m and the length of this tube is different for different scenarios. The water pumping and injection depths inside the GHE lengths are 10 above than the bottom of the GHE, and the distance between wells is 5 m. Table 4-13

shows water pumping and injection pipe length and cost, and the total cost of additional components in semi-open loop system, for different scenarios.

Table 4-13 Capital cost of water pumping and injection for different scenarios.

Condition	Water pumping and injection pipe length (m)	Water pumping and injection pipe cost (Yen)	Total cost of additional components (Yen)
Scenario 1	35	17,500	107,500
Scenario 2	45	22,500	112,500
Scenario 3	29	14,500	104,500

4.5.2 Water pump power consumption

The water pump in semi-open loop operations is working when heat pump unit is on. According to the heating and cooling schedule, here is the working schedule of water pump during one year:

- water pump working hours in heating period: 2160 hours
- water pump working hours in cooling period: 720 hours
- water pump working hours in one year: 2880 hours

The water pump power consumption can be evaluated using the pump characteristics curves. These diagrams are providing by water pump manufacturers for the wide range of water pump performance. Unfortunately the availed data in the catalogue of water pump of the semi-open loop field tests were limited. In order to calculate the water pump power consumption, an experiment was performed on the water pump that has been used in field tests (Ebara Package Booster System, Model: 20HPAd.125). The power consumption of water pump measured for 3 flow rates: 15, 17.5 and 20 L/min. In each test, the pressure drop due to closing a valve was measured and water pump power consumption was measured after stabilizing the flow. The head loss range during this experiment was: 3.8 m to 9.9 m. The results of this experiment are shown in Table 4-14 and Fig. 4-7.

Table 4-14 Results of water pump power consumption test.

Head loss (m)	Power consumption (W) (15 L/min)	Power consumption (W) (17.5 L/min)	Power consumption (W) (20 L/min)
9.9	120	135	166
8.5	104	119	149
7.6	95	109	135
6.5	83	96	122
5.1	69	81	105
3.8	58	69	90
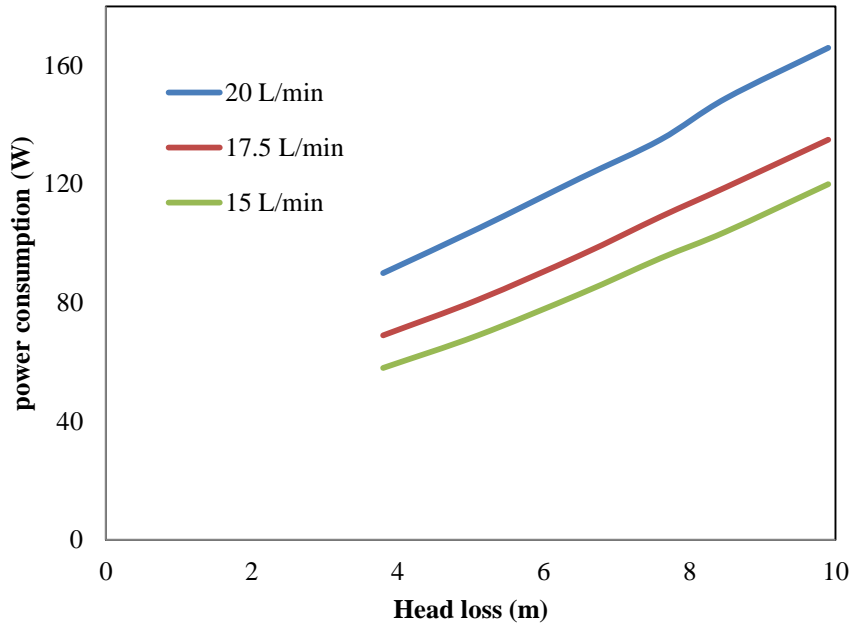
Fig. 4-7 Water pump power consumption diagram.

The head loss in the water pumping/injection pipe calculates with Eq. 4-7.

$$h_{loss} = f\frac{L}{D} \times \frac{V^2}{2g}$$ (4-7)

In this equation, h_{loss} is the head loss inside the water pumping/injection pipe due to the friction (m), f is the friction factor, L is the pipe length (m), D is the pipe diameter (m), V is the fluid velocity (m/s) and g is the gravity acceleration (9.8 m/s^2). In our calculations, D is 20.8 mm (same as field test condition).

The friction factor derives form Moody diagram (Fig. 4-8). In the friction factor calculation process, ε is the pipe roughness (m). The relative pipe roughness calculates with Eq. 4-8.

$$Relative\ pipe\ roughness = \frac{\varepsilon}{D} = \frac{0.003}{20.8} = 0.00014$$ (4-8)

Table 4-15 shows the water pumping and injection head loss for the semi-open loop operations. It is necessary to note that water/pumping and injection depth is 10 m above the bottom of the GHE.

According to Fig. 4-7, water pump power consumption in Scenario 1 will be 32 W. Because during the water pump power consumption test, it was not possible to perform the test with 5 L/min flow rate, the data of 15 L/min flow rate have been used for Scenario 2 and 3. The water pump power consumption is 21 W and 19 W for Scenario 2 and 3, respectively. Table 4-16

134

shows the summary and results of water pump power consumption cost for the first year. In our calculation, electricity price in Japan was set as 20 Yen/kWh.
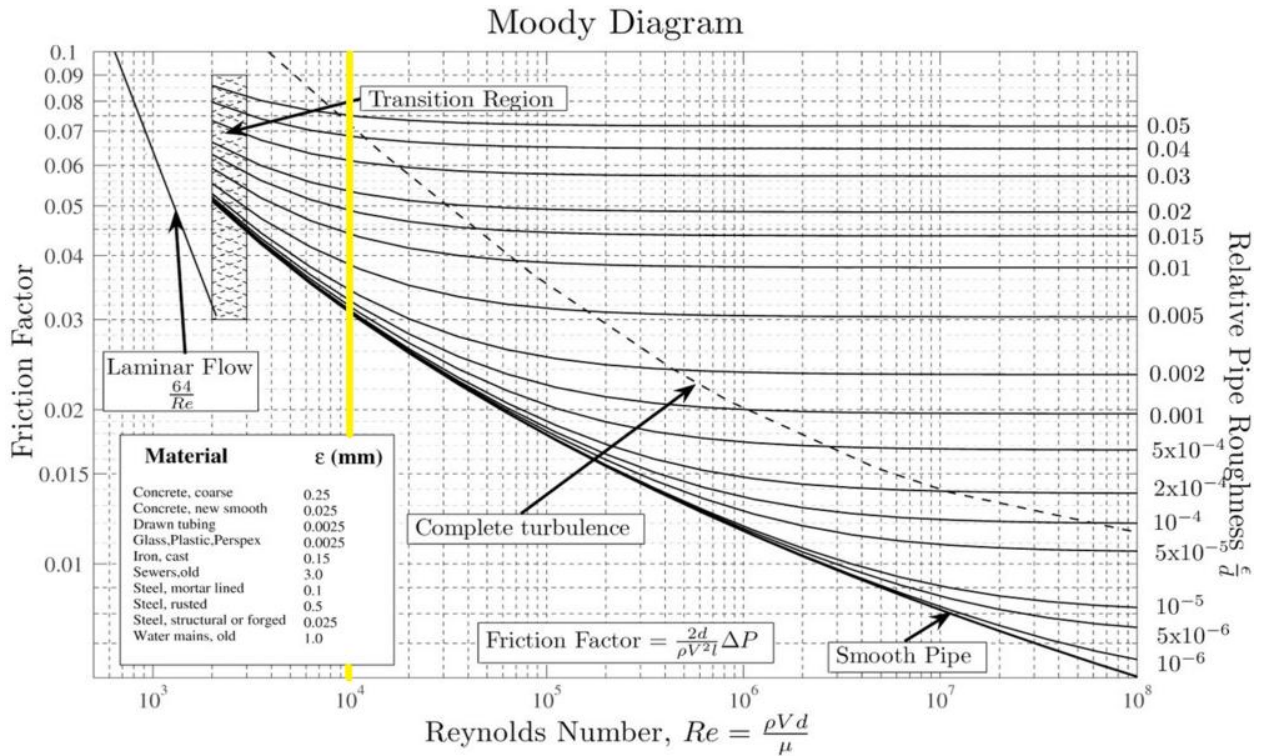
Fig. 4-8 Moody diagram.

Table 4-15 Water pumping and injection head loss for the semi-open loop operations.

Scenario	GHE length (m)	Pipe length (m)	Flow rate (L/min)	Reynolds number	f	Head loss (m)
Scenario 1	51	35	15	15,304	0.02794	1.3
Scenario 2	59	45	5	5,101	0.03734	0.25
Scenario 3	44	29	5	5,101	0.03734	0.16

In order to calculate the present value of water pump power consumption cost for 20 years of operation, there is a need to consider the "annual inflation rate" and "interest rate" factors in the economic analysis. Fig 4-9 and 4-10 show the annual inflation rate and interest rate in Japan for 2004-2014 (The World Bank online data center). Based on these data, the average of annual inflation rate of 0.19% and interest rate of 2.57% were used for the above-mentioned period.

The water pump power consumption cost over 20 years of operation can be shown using a cash flow diagram as shown in Fig. 4-11.

In Fig 4-11:

C: water pump power consumption cost for the first year

135

g: average of inflation rate in Japan (Fig 9) = 0.19%

n: project life time = 20 years

i: average interest rate in Japan (Fig. 4-10) = 2.57%

P: present value of water pump power consumption during 20 years

Table 4-16 Water pumping and injection cost for the first year in different scenarios.

Scenario	Power consumption (W)	Power consumption for the first year (kWh)	Water pumping and injection cost for the first year (Yen)
Scenario 1	32	92.2	1,844
Scenario 2	21	60.5	1,210
Scenario 3	19	54.7	1,094
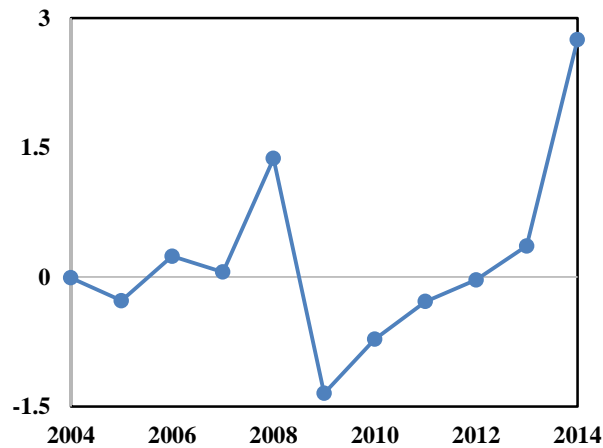
Fig. 4-9 Japan annual inflation rate (2004-2014).
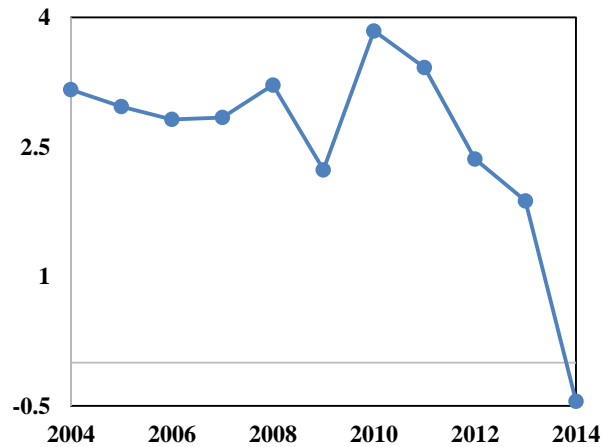
Fig. 4-10 Japan interest rate (2004-2014).
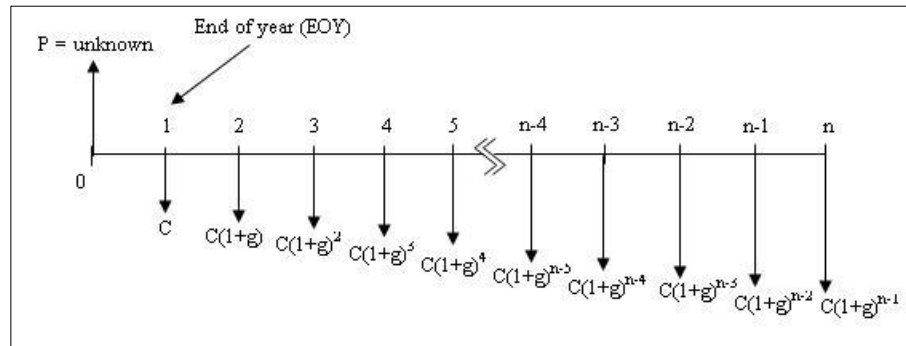
Fig. 4-11 Cash flow diagram for geometric series.

In this study, the average interest rate is higher than the average of inflation rate (i>g), so the present value of water pump power consumption for 20 years of operation calculates with Eq. 4-9:

$$P = \frac{C}{1+g} \times \frac{(1+x)^n - 1}{x(1+x)^n} \tag{4-9}$$

The relationship between x factor in Eq. 4-9, g and i is shown in Eq. 4-10:

$$x = \frac{1+i}{1+g} - 1 = \frac{1+0.0257}{1+0.0019} - 1 = 0.0237 = 2.37\% \tag{4-10}$$

The P factor calculates using Eq. 4-11:

$$P = \frac{C}{1+0.0019} \times \frac{(1+0.0237)^{20} - 1}{0.0237 \times (1+0.0237)^{20}} = 15.75 \times C \tag{4-11}$$

Eq. 4-11 shows that the present value of water pump power consumption cost for 20 years of operation is 15.75 times as much as the water pump power consumption cost of the first year of operation. Table 4-17 shows the present value of water pump power consumption cost for different scenarios.

Table 4-17 Present value of water pump power consumption cost in different scenarios.

Condition	Water pump power consumption cost for the first year (Yen)	Present value of Water pump power consumption cost for 20 years of operation (Yen)
Scenario 1	1,844	29,043
Scenario 2	1,210	19,057
Scenario 3	1,094	17,230

4.5.3 Final semi-open loop GSHP saving

Water pumping and injection has positive and negative effects of system capital and running costs of GSHP system. The calculated effects of water pumping and injection on the system capital and running costs are:

- drilling cost (positive effect)
- water pump installation cost (negative effect)
- water pump power consumption cost (negative effect)

Table 4-18 shows the calculated parameters and final saving of semi-open loop GSHP system for different scenarios.

Table 4-18 Final saving of semi-open loop operation.

Condition	Drilling cost saving (Yen)	Water pump installation cost (Yen)	Water pump power consumption cost (Yen)	Final saving (Yen)
Scenario 1	1,935,000	107,500	29,043	1,798,457
Scenario 2	1,815,000	112,500	19,057	1,683,443
Scenario 3	990,000	104,500	17,230	868,270

In order to calculate the percentage of semi-open loop saving in total cost of GSHP system in base case, the system total cost in base case GSHP system for different scenarios needs to be calculated. Here are the GSHP system capital cost in the base case operation:

- drilling cost: 15,000 Yen/m
- heat pump unit cost: 800,000 Yen
- distribution system cost: 200,000 Yen
- piping and labor cost for installation: 500,000 Yen

The heat pump unit power consumption in heating and cooling operations calculates using Eq. 4-12 and 4-13. In these equations, $Q_{heating}$ and $Q_{cooling}$ are the calculated yearly room heating and cooling loads, respectively. $W_{heating}$ and $W_{cooling}$ are the yearly heat pump power consumption for heating and cooling operations, respectively.

$$W_{heating} = \frac{Q_{heating}}{COP_{heating}} = \frac{8,984}{3.5} = 2,567 \; kWh \tag{4-12}$$

$$W_{cooling} = \frac{Q_{cooling}}{COP_{cooling}} = \frac{87}{5.5} = 16 \; kWh \tag{4-13}$$

The heat pump power consumption cost for the first year calculates using Eq. 4-14 In this equation, electricity price in Japan is set as 20 Yen/kWh.

$$Heat\ pump\ power\ consumption\ cost = \left(W_{heating} + W_{cooling}\right) \times 20 = 51{,}660\ Yen \qquad (4\text{-}14)$$

In order to calculate the present value of the heat pump power consumption cost for the 20 years of system operation, Eq. 4-11 in economic analysis section is used:

$$Present\ value\ of\ Heat\ pump\ power\ consumption\ cost = 15.75 \times 51{,}660 = 813{,}645\ Yen \qquad (4\text{-}15)$$

Table 4-19 shows the base case GSHP system cost for the conditions with and without groundwater flow. It is necessary to note that the heat pump power consumption cost is its present value for the 20 years of system operation.

Table 4-19 GSHP cost in base case operation.

Condition	Drilling cost (Yen)	Heat pump unit cost (Yen)	Distribution system cost (Yen)	Piping and labor cost (Yen)	Power consumption cost (Yen)	Total cost (Yen)
No groundwater flow	2,700,000	800,000	200,000	500,000	814,000	5,014,000
Slow groundwater flow	1,650,000	800,000	200,000	500,000	814,000	3,964,000

Table 4-20 shows the share of semi-open loop GSHP saving to the total cost of base case GSHP system for the different scenarios. In this table, "saving" factor is the saving due to the water pumping and injection and is shown in Table 4-20. The maximum saving percentage is for Scenario 1, with 38.4%. This factor is 35.7% and 22.5% for Scenario 2 and 3, respectively. The average if this factor for 3 scenarios is 30.5%.

The results of economic analysis showed the remarkable effect of water pumping and injection on GHSP system cost reduction. The introduced semi-open loop GSHP system in slow groundwater flow formations costs around two third of the normal GSHP system. The strong effect of water pumping and injection on the capital cost reduction of GSHP systems can improve the position of these systems in the market of HVAC systems.

Table 4-20 Semi-open loop operation saving.

Condition	Base case system cost (Yen)	Saving (Yen)	Saving (%)
Scenario 1	5,014,000	1,798,457	35.9
Scenario 2	5,014,000	1,683,443	33.6
Scenario 3	3,964,000	868,270	21.9

4.6 Conclusion

This chapter discussed on the economic analysis of semi-open loop GSHP system. In the first step, heating and cooling loads of a sample building in Akita City was calculated. Results showed that heating load is dominant, since the city is located in a cold region of Japan. The necessary GHE length for base case operation in different scenarios was calculated using validated numerical FEFLOW model. The GHE lengths in semi-open loop operations were calculated to ensure the same heat pump power consumption between the base case and semi-open loop operations.

Results of numerical modeling showed that water pumping and injection can decreases the GHE length in different scenarios by 60%-72%. The GHE length reduction caused 0.99-1.93 million Yen saving in drilling cost in different scenarios. Considering the capital and running cost of water pumping and injection, the final saving of semi-open loop operation was estimated as 0.87-1.80 million Yen, which is 22%-36% saving in the GSHP system cost for 20 years of operation.

Chapter 5: CONCLUSION

The increasing rate of energy consumption in the building sector, illustrates the importance of studies on reliable and clean sources of energy for heating and cooling purposes. This study is concentrated on groundwater flow rate enhancement around GHEs by introducing new semi-open loop GSHP technology.

In the first Chapter, the energy consumption demand and importance of clean and renewable energy sources were studied. The share of buildings heating and cooling energy consumption was evaluated and GSHP system was introduced as a reliable technology to meet this demand. In the literature review section, the effect of natural groundwater flow on the thermal performance of GHEs was studied and the objectives of this study were described.

In the second Chapter, the effect of water injection and pumping in a GHE under different inlet temperatures and groundwater velocities on heat exchange rate were studied by performing nine sets of TRTs. The TRT results showed that with increasing water injection/pumping rate, the average temperature of heat medium decreases. Numerical simulations were then carried out using FEFLOW 6.2 and the model was validated by the TRT data. The results of simulation were in a good agreement with TRT results.

Sensitivity studies were then performed using validated model. Water injection/pumping rates were varied from 0 to 15 L/min with two different GHE inlet temperatures. Results of simulation showed that the average heat exchange rate increased by increasing water injection/pumping rate, but was less affected in the cases with water rates higher than 5 L/min. Under the same operating conditions, the average heat exchange rate for injection was slightly higher than the pumping mode. For the case with groundwater flow, the heat exchange rate was higher than the case without groundwater flow and it was 3 times higher in the case without injection or pumping. But with increasing injecting/pumping water rate, the difference between two cases became smaller. In the case with groundwater velocity, heat exchange rate was less affected by water injection/pumping rate.

In the third Chapter the efficiency of semi-open loop GSHP systems was investigated; in which groundwater pumped from one GHE is injected into a second GHE to increase the heat advection in both GHEs. Before connection the GHEs and heat pump unit, two sets of TRTs were performed and effective thermal conductivity was calculated for each GHE. High effective thermal conductivity and fast temperature recovery after the TRTs showed the possibility of fast groundwater flow and strong aquifer in the formation. The analysis performed through field tests and numerical simulation. Heating tests performed on the Akita University campus, Japan. The pumping and injection of groundwater at 15 L/min enhanced the COP by only 5%, and negligibly improved the SCOP. The cooling tests were performed in July-August 2016 and showed the same improvement in the COP and SCOP. The limited COP enhancement might be

attributable to fast groundwater flow in the testing area. The effect of groundwater flow on the performance of the semi-open loop GSHP system was discussed in the sensitivity analysis section.

The semi-open loop GSHP system was numerically modeled and validated by heating and cooling experimental data. As confirmed in the sensitivity analysis of heating operation, the COP and SCOP can be enhanced by 12% and 9% respectively under the same groundwater flow conditions as the experimental site, depending on the operational conditions. These parameters in the sensitivity analysis of cooling operation were evaluated around 13.1% and 6.6%, for COP and SCOP, respectively. In the absence of groundwater flow, the semi-open loop system was estimated to boost the COP and SCOP by 40% and 20%, respectively, for heating operations. These parameters for the cooling operation were evaluated around 101% and 62%, for COP and SCOP, respectively. The effect of water pumping and injection of system capacity enhancement was proven in sensitivity analysis.

The developed numerical model was then modified and additional sensitivities were performed to evaluate the effect of GHE spacing on thermal performance of semi-open loop GSHP system. The GHE spacing was changed in 0.5 m-20 m range, with and without natural groundwater flow in the formation. The heat transfer rates of GHEs were set as maximum possible, preventing from freezing during the heating operation in all of the cases. Results of the numerical simulations showed that 5 m distance between GHEs is enough to ensure limited thermal interference between the GHEs in the semi-open loop GSHP system.

The last Chapter of this study was about the economic analysis of semi-open loop GSHP system. Heating and cooling loads of a sample building in Akita City was calculated. Results showed that heating load is dominant. The necessary GHE length for base case operation in different scenarios was calculated using validated numerical FEFLOW model. The GHE lengths in semi-open loop operations were calculated to ensure the same heat pump power consumption for base case and semi-open loop operations.

Results of numerical modeling showed that water pumping and injection can decreases the GHE length in different scenarios by 60%-72%. The GHE length reduction caused 0.99-1.93 million Yen saving in drilling cost in different scenarios. Considering the capital and running cost of water pumping and injection, the final saving of semi-open loop operation is 0.87-1.80 million Yen. Results of economic analysis showed that water pumping and injection will cause 22%-36% saving in GSHP system cost.

Results of comprehensive field tests and numerical modeling and sensitivity analysis showed that water pumping and injection in semi-open loop GSHP system can increase the GSHP system efficiency and heat transfer capacity of GHEs, especially in the formations with slow groundwater flow. Economic studies proved that this technology can decrease GSHP system cost and make it more competitive with conventional heating and cooling systems.

REFRENCES

Agency, U. S. E. P. (1996). BIOSCREEN. Natural attenuation decision support system, user's manual. National Risk Management Research Laboratory, Office of Research and Development.

Alcaraz, M., Garcia-Gil, A., Vazquez-Sune, E., and Velasco, V. (2016). Advection and dispersion heat transport mechanisms in the quantification of shallow geothermal resources and associated environmental impacts. Science of the Total Environment, 543, 536-546.

Al-Khoury, R., (2012), "Computational Modeling of Shallow Geothermal Systems", CRC/Balkema/Taylor and Francis, London.

Al-Khoury, R., Bonnier, P., (2006), "Efficient Finite Element Formulation for Geothermal Heating Systems. Part II: Transient", Int. J. Number. Methods Eng. 67(5), 725-745.

Al-Khoury, R., Bonnier, P., Brinkgreve, R., (2005), "Efficient Finite Element Formulation for Geothermal Heating Systems. Part I: Steady state", Int. J. Number. Methods Eng. 63(7), 988-1013.

American Society of Heating, Refrigerating and Air-Conditioning Engineers, (2013), "Standard 55-2013, Thermal Environmental Conditions for Human Occupancy". ASHREA Press.

American Society of Heating, Refrigerating and Air-Conditioning Engineers (ASHRAE), (2011), Geothermal Energy in 2011 ASHRAE Handbook – HVAC Applications, Atlanta, GA, ASHRAE 2011, 34.1-34.20.

Angelotti, A., Alberti, L., La Licata, I., and Antelmi, M. (2014). Energy performance and thermal impact of a Borehole Heat Exchanger in a sandy aquifer: Influence of the groundwater velocity. Energy Conversion and Management, 77, 700-708.

Arola, T., Eskola, L., Hellen, J., Korkka-Niemi, K., (2014), "Mapping the low enthalpy geothermal potential of shallow Quaternary aquifers in Finland". Geotherm. Energy 2 (1), 1-20.

Arola, T., Korkka-Niemi, K., (2014). "The effect of urban heat islands on geothermal potential: examples from Quaternary aquifers in Finland". Hydrogeol. J. 22, 1953-1967.

Austin W. A., C. Yavuzturk, J. D. Spitler, (2000), "Development of an In-situ System for Measuring Ground Thermal Properties". ASHREA Transactions, 106 (1): 365-379.

Austin, W.A. (1998), "Development of an in situ system for measuring ground thermal properties". MSc thesis, Oklahoma State University, Stillwater, OK, USA, 164 pp.

Bai, L., Che, W., (2016). Effects of the soil source heat pump borehole spacing and arrangement on the soil temperature of well group. Procedia Engineering, 146, 441 – 444.

Bauer, D., Heidemann, W., Muller-Steinhagen, H. Diersch, H. J., (2011), "Thermal Resistance and Capacity Models for Borehole Heat Exchangers. Int. J. Energy Res. 35(4), 312-320.

Bayer, P., Saner, D., Bolay, S., Rybach, L., Blum, P., (2012). "Greenhouse gas emission savings of ground source heat pump systems in Europe: a review". Renew. Sustain. Energy Rev. 16, 1256-1267.

Berberich H., N. Fisch, E. Hahne, (1994), "Field Experiments with a single Duct in Water Saturated Claystone". Proceeding of 6th International Conference on Thermal Energy Storage, Calorstock94, August 22-25, 1994, Espoo, Finland.

Bernier, M., (2006), "Closed-loop Ground-couple Heat Pump System", ASHRAE Journal, September 2006.

Bloomberg New Energy Finance. 2013. "Japan Eyes Smart Meters, Fuel Cells to Tackle Climate Change",.http://about.bnef.com/bnefnews/japan-eyes-smart-meters-fuel-cells-to-tackle-Climate-change/.

Boyd, T. L., Sifford, A., and Lund, J. W., (2015), "The United States of America Country Update 2015", Proceedings, Proceedings World Geothermal Congress 2015 Melbourne, Australia, 19-25 April 2015.

Burkhard Sanner, Göran Hellström, Jeff Spitler and Signhild Gehlin, (2005), Proceedings World Geothermal Congress 2005, Antalya, Turkey, 24-29 April 2005.

Canadian GeoExchange Coalition, (2010), "The State of the Canadian Geothermal Heat Pump Industry 2010", www.geoexchange.ca.

Carslaw H. S. and J. C. Jaeger, (1959), "Conduction of Heat in Solids, Second Edition". Oxford University Press, Great Britain.

Carslaw, H. S., and Jaeger, J. C., (1947). Conduction of Heat in Solids, Oxford, UK, Clarendon Press 1947.

Chen, J., Xia, L., Li, B., and Mmereki, D. (2015). Simulation and experimental analysis of optimal buried depth of the vertical U-tube ground heat exchanger for a ground-coupled heat pump system. Renewable Energy, 73, 46-54.

Chiasson, A. C., Rees, S. J., and Spitler, J. D. (2000). A Preliminary Assessment Of The Effects Of Ground-Water Flow On Closed-Loop Ground Source Heat Pump Systems. ASHRAE Transactions, 106, 380-393.

Chinese Ministry of Housing and Urban-Rural Development (MOHURD), 2009. Technical code for ground-source heat pump system (GB 50336-2005). Beijing Standard Press of China 2009.

Choudary A., (1976), "An approach to determine the thermal conductivity and diffusivity of a rock in situ" PhD thesis, OSU.

Cimmino, M., Eslami-Nejad, P., (2017). A simulation model for solar assisted shallow ground heat exchangersin series arrangement. Energy and Buildings, (2017, in press).

Cleasson J., G. Hellstrom, (2000), "Analytical Studies of the Influence of Regional Groundwater Flow on the Performance of Borehole Heat Exchangers". Proceeding Terrastock 2000, Stuttgart, Germany, August 28-September 1, 2000.

Deerman J. D. and S. P. Kavanaugh, (1991), "Simulation of Vertical U-tube Ground-coupled Heat Pump Systems Using the Cylindrical Heat Source Solution". ASHRAE Transactions 1991, vol. 97 (1), pp. 287-295.

DHI-WASY (2015). FEFLOW 6.2 - User's Manual. DHI-WASY GmbH, Berlin.

Diana Ürge-Vorsatz, Luisa F. Cabeza, Susana Serrano, Camila Barreneche, Ksenia Petrichenko, (2015), "Heating and cooling energy trends and drivers in buildings", Renewable and Sustainable Energy Reviews 41; 85–98.

Diao, N., Li, Q., and Fang, Z. (2004). Heat transfer in ground heat exchangers with groundwater advection. International Journal of Thermal Sciences, 43, 1203-1211.

Diersch H. G., (2014), "FEFLOW, Finite Element Modeling of Flow, Mass and Heat Transport in Porous and Fractured Media", Springer.

Eklöf, C. and Gehlin, S., (1996), "TED - a mobile equipment for thermal response test", MSc-thesis 1996:198E, LuTH, 62 p.

Eskilson P., (1987), "Thermal Analysis of Heat Extraction Boreholes", Lund-MPh-87/13., Department of Mathematical Physics, Lund Institute of Technology, Sweden.

European Geothermal Energy Council, (2015), "Developing Geothermal Heat Pumps in Smart Cities and Communities", www.regeocities.eu.

Farabi Asl, H., Fujii, H., and Kosukegawa, H. (2015). Heat Exchange Rate Enhancement in Ground Heat Exchangers by Water Injection and Pumping. In "Geothermal Resources Council Transactions", Reno, Nevada, U. S. A.

Fujii, H., Itoi, R., Fujii, J., and Uchida, Y. (2005). Optimizing the design of large-scale ground-coupled heat pump systems using groundwater and heat transport modeling. Geothermics, 34, 347-364.

Fujii, H., Kosukegawa, H., and Onishi, K. (2015). Effect of Water Injection into a Ground Heat Exchanger Drilled in a Low-λ Formation. In "World Geothermal Congress", Melbourne, Australia.

Gehlin, S. (1998) "Thermal response test. In situ measurements of thermal properties in hard rock". Licentiate thesis, Luleå University of Technology, 1998:37, 73 pp.

Gehlin, S. and Nordell, B., (1997), "Thermal Response Test – a Mobile Equipment for Determining Thermal Resistance of Borehole", Proc. Megastock '97, 103-108.

Gehlin, S., (2002) "Thermal response test – Method development and evaluation". Doctoral Thesis 2002:39, LuTH.

Gehlin, S.E.A. and Hellström, G., (2003), "Influence on thermal response test by groundwater flow in vertical fractures in hard rock". Renewable Energy, 28, 2221–2238.

Gehlin, S.E.A., Hellström, G. and Nordell, B., (2003), "The influence of the thermosiphon effect on the thermal response test". Renewable Energy, 28, 2239–2254.

Gustafsson, A.M. and Westerlund, L. (2010), "Multi-injection rate thermal response test in groundwater filled borehole heat exchanger". Renewable Energy, 35, 1061–1070.

Gustafsson, A.M., (2006), "Thermal Response Test–Numerical simulations and analyses". Licentiate thesis, Luleå University of Technology, 2006:14, 118 pp.

Gustafsson, A.M., Westerlund, L. and Hellström, G., (2010), "CFD modelling of natural convection in a groundwater-filled borehole heat exchanger". Applied Thermal Engineering, 30, 683–691.

Hellstrom G., (1994), "Fluid to Ground Thermal Resistance in Duct Ground Heat Storage", Proceeding Calorstock94, Espoo, Finland, August 22-25, 1994, pp:373-380.

Hellström, G., (1991),"Ground Heat Storage, Thermal Analysis of Duct Storage Systems", I. Theory. 262 p., LTH.

Hellström, G., (1997), "Thermal response test of a heat store in clay at Linköping, Sweden". Proc. Megastock97, 115-120.

Huber, H., and Arslan, U. (2015). The Influence of the Darcy Velocity of Groundwater Flow on the Effective Thermal. In "World Geothermal Congress 2015", Melbourne, Australia.

Ingersoll L. R. and H. J. Plass, (1948), "Theory of the Ground Pipe Heat Source for the Heat Pump". ASHVE Transactions vol. 54 p. 339-348.

Ingersoll, L. R., (1954). Heat conduction with engineering, geological, and other applications, Rev. edition. Madison, Wisconsin, University of Wisconsin Press 1954.

Ingersoll, L.R., (1948), "Heat conduction–With engineering and geological application". McGraw Hill Book Company, New York, USA, 278 pp.

International Energy Agency, (2012). Energy technology perspectives 2012. Paris: OECD/IEA; 2012.

Japan External Trade Organization (JETRO), "Attractive Sectors", https://www.jetro.go.jp/uk/Invest_in_Japan/Attractive_Sectors/

Japan Metrological Agency online data center, http://www.jma.go.jp/jma/indexe.html

Japan Ministry of Environment, (2010), "Overview of the Bill of the Basic Act on Global Warming Countermeasures", http://www.env.go.jp/en/earth/cc/bagwc/overview_bill.pdf.

Japan Ministry of Environment, (2013), "Japan's Climate Change Policies", http://www.env.go.jp/en/focus/docs/files/20130412-68.pdf.

Katsura, T., Nagano, K., Hori, S., and Okawada, T. (2009). Investigation of groundwater flow effect on the thermal response test resultInvestigation of groundwater flow effect on the thermal response test result. In "11th Energy Conservation Thermal Energy Storage Conference Effstock 2009", Stockholm.

Kavanaugh, S. P, and Rafferty, K. D., (1997), Ground-Source Heat Pumps: Design of geothermal systems for commercial and institutional buildings. ASHRAE 1997.

Kjellsson E., Hellstrom G., (1997), "Laboratory Study of the Heat Transfer in Water-filled Borehole with a Single U-pipe", Proceeding 7th International Confrence on Thermal Energy Storage, Megastock97, Sapporo, Japan, 18-20 June 1997, pp. 509-514.

Kjellsson E., Hellstrom G., (1999), "Laboratory Study of the Heat Transfer in Water-filled Borehole with a C-pipe" Preliminary report 1999-06-09, Lund University of Technology, Sweden.

Koohi-Fayegh, S., Rosen M. A., (2012). Examination of thermal interaction of multiple vertical ground heat exchangers. Applied Energy, 97, 962–969.

Laitinen, A., Tuominen, P., Holopainen, R., Tuomaala, P., Jokisalo, J., Eskola, L., Sir_en, K., (2014). "Renewable Energy Production of Finnish heat Pumps. Final report of the SPF-project. VTT Technical Research Centre of Finland". VTT Technology. report 164. http://www.vtt.fi/inf/pdf/technology/2014/T164.pdf.

Lee, J.Y., (2009). "Current status of ground source heat pumps in Korea". Renew. Sustain. Energy Rev. 13, 1560-1568.

Liebel, H.T., Huber, K., Frengstad, B.S., Ramstad, R.K. and Brattli, B., (2011), "Temperature footprint of a thermal response test can help to reveal thermogeological information". Norges geologiske undersøkelse Bulletin, 451, 20–31.

Lim, K., Lee, S., and Lee, C. (2007). An experimental study on the thermal performance of ground heat exchanger. Experimental Thermal and Fluid Science, 31, 985-990.

Lindholm, G. F., and Vaccaro, J. J. (1988). Region 2, Columbia lava plateau (Chapter 5). The geology of North America, The Geological Society of America, Inc., O-2, hydrogeology.

Lund, J. and Tonya L. Boyd, (2015), "Direct Utilization of Geothermal Energy 2015 Worldwide Review", Proceedings World Geothermal Congress 2015 Melbourne, Australia, 19-25 April 2015.

MARI IWATA, (2013), "Japan Retreats in CO2 Emissions Cut Target", The Wall Street Journal, http://www.wsj.com/news/articles/SB10001424052702303789604579199063912364466.

Mattinen, M.K., Nissinen, A., Hyysalo, S., Juntunen, J.K., (2014). "Energy use and greenhouse gas emissions of air-source heat pump and innovative ground source air heat pump in a cold climate". J. Ind. Ecol. 19 (1), 61-70.

Microgeneration Installation Standard, (2013). MIS 3005 Issue 4.0. Requirements for contractors undertaking the supply, design, installation, set to work, commissioning and handover of microgeneration heat pump systems, London, Microgeneration Installation Standard 2013.

Japan Ministry of Land, Infrastructure, Transport and Tourism, (2014), "Japan energy saving standard". Available online: http://www.mlit.go.jp/common/001082964.pdf.

Japan Ministry of Land, Infrastructure, Transport and Tourism, (2014), "Outline of Revision of Energy Conservation Standards". Available online: https://www.mlit.go.jp/common/001012880.pdf.

Mogensen P., (1983), "Fluid to Duct Wall Heat Transfer in Duct System Heat Storage", Proceeding International Conference on Sustainable heat Storage in Theory and Practice. Stockholm, Sweden, June 6-8, 1983, p. 652-657.

Molina-Giraldo, N., Blum, P., Zhu, K., Bayer, P., and Fang, Z. (2011). A moving finite line source model to simulate borehole heat exchangers with groundwater advection. International Journal of Thermal Sciences, 50, 2506-2513.

Niibori, Y., Iwata, Y., Ichinose, S., and Fukaya, G. (2005). Design of the BHP System Considering the Heat Transport of Groundwater Flow. In "World Geothermal Congress 2005", Antalya, Turkey.

Nikishov, G. P., (2010), "Programming Finite Elements in Java", Springer.

Nordell B., (1994), "Borehole Heat Store Design Optimization", Doctoral Thesis, Division of Water Resources Engineering, Lulea University of Technology, Sweden.

Pouloupatis, P. D., Tassou, S. A., Christodoulides and P., Florides, G. A., (2017). Parametric analysis of the factors affecting the efficiency of ground heat exchangers and design application aspects in Cyprus. Renewable Energy, 103, 721-728.

Remund C. P. (1999), "Borehole Thermal Resistance: Laboratory and Field Studies", ASHRAE Transactions, 105(1): 439-445.

Renewable Energy Policy Network for 21st century, (2016), "Renewables 2016, Global Status Report", REN21, 2016.

Rybach, L., and Eugster, W. J. (2010). Sustainability aspects of geothermal heat pump operation, with experience from Switzerland. Geothermics, 39, 365-369.

Sailer, E., Taborda, D. M.G., and Keirstead, J., (2015). Assessment of Design Procedures for Vertical Borehole Heat Exchangers. PROCEEDINGS, Fortieth Workshop on Geothermal Reservoir Engineering Stanford University, Stanford, California, January 26-28, 2015.

Sanner B., M. Reuss, E. Mands, (2000), "Thermal Response Test Experiences in Germany". Proceeding Terrastock 2000, Stuttgart, Germany, August 28-September 1, 2000, pp. 177-182.

Shonder, J.A. and Beck, J.V., (1999), "Determining Effective Soil Formation Thermal Properties from Field Data Using a Parameter Estimation Technique". ASHRAE Transactions, 105(1), 458-466.

Signorelli, S., Bassetti, S., Pahud, D. and Kohl, T., (2007), "Numerical evaluation of thermal response tests". Geothermics, 36, 141–166.

Spitler, J.D., Rees, S. and Yavuzturk, C., (1999), "More Comments on In-situ Borehole Thermal Conductivity Testing". The Source 3-4/99.

Spitler, J.D., Yavuzturk, C. and Rees, S.J., (2000), "In Situ Measurement of Ground Thermal Properties". Proc. Terrastock2000, 165-170.

Stephenson, D. A., Fleming, A. H., and Mickelson, D. M. (1988). Glacial deposits (Chapter 35). The geology of North America, The Geological Society of America, Inc., O-2, hydrogeology.

Stijn Lambrecht, "The Clean Energy Sector in Japan", EU-Japan Center for Industrial Cooperation, February 2014.

Sundberg J., (1988), "Thermal Properties of Soils and Rocks", PhD Thesis, Paul. A57. Department of Geology. Chalmers Technical University. Goteborg 1988.

The World Bank online data center, http://data.worldbank.org/

U. S. Department of Energy, (2001), "Ground Source Heat Pumps Applied to Federal Facilities-Second Edition", U. S. DOE, https://energy.gov/eere/office-energy-efficiency-renewable-energy.

U. S. Energy Information Administration online data services, available at: http://www.iea.org/statistics/

U. S. Energy Information Administration, "International Energy Outlook 2016", U. S. Department Of Energy, May 2016.

U. S. Energy Information Administration, "Short-term Energy Outlook (STEO)", U. S. Department Of Energy, November 2016.

Ürge-Vorsatz D, Petrichenko K, Staniec M, Eom J. (2013), "Energy use in buildings in a long-term perspective", Curr Opin Environ Sustain; 5(2):141–51.

Verein Deutscher Ingegneure, (2010). VDI 4640 – Blatt 1. Thermal use of the underground. Fundamentals, approvals, environmental aspects. Düsseldorf, Verein Deutscher Ingegneure 2010.

Wang, D., Lu, L., Zhang, W., and Cui, P. (2014). Numerical and Analytical Analysis of Groundwater Influence on the Pile Ground Heat Exchanger with Cast-in Spiral Coils. Energy Procedia, 61, 1784-1788.

Wang, H., Qi, C., Du, H., and Gu, J. (2009). Thermal performance of borehole heat exchanger under groundwater flow: A case study from Baoding. Energy and Buildings, 41, 1368-1373.

Weeks, J. B., and Gutentag, E. D. (1988). Region 17, High plains (Chapter 20). The geology of North America, The Geological Society of America, Inc., O-2, hydrogeology.

Witte H, J. L. (2001), "Geothermal Response Tests with Heat Extraction and Heat Injection: Application in Research and Design of Geothermal Ground Heat Exchangers", European workshop of Geothermal Response Test, EPFL, October 25-26, 2010, Lausanne, Switzerland.

Witte, H. J. L., and van Gelder, A. J. (2006). Geothermal Response Tests using controlled multi-power level heating and cooling pulses (MPL-HCP): quantifying ground water effects on heat transport around a borehole heat exchanger. In "Ecostock, The 10th International Conference on Thermal Energy Storage", New Jersey, U.S.A.

Yasukawa, K., Sasada, M., 2015. "Country Update of Japan: Renewed Opportunities", Proceedings World Geothermal Congress 2015 Melbourne, Australia, 19-25 April 2015.

Yavuzturk C, J. D. Spitler, S. J. Rees, (1999), "A Transient Two-dimensional Finite Volume Model for the Simulation of Vertical U-tube Ground Heat Exchangers". ASHREA Transactions, 105 (2): 465-474.

Yuan, Y., Cao, X., Wang, J. and Sun, L., (2016). Thermal interaction of multiple ground heat exchangers under different intermittent ratio and separation distance. Applied Thermal Engineering, 108, 277–286.

Zanchini, E., Lazzari, S., and Priarone, A. (2012). Long-term performance of large borehole heat exchanger fields with unbalanced seasonal loads and groundwater flow. Energy, 38, 66-77.

Zervantonakis, I.K. and Reuss, M., (2006), "Quality requirements of a thermal response test". Proceedings of the 10th International Conference on Thermal Energy Storage 'Ecostock2006', Stockton, NJ, USA, 7 pp.

Zogg, M., (2008). "History of Heat Pumps, Swiss Contributions and International Milestones. final report". Swiss Federal Office of Energy. www.zogg-engineering.ch/publi/HistoryHP.pdf.

Acknowledgement

Foremost, I would like to express my gratitude to my Ph. D. advisor, Prof. Hikari Fujii for his contentious support and kind guidance during my 3 years of studying in Akita University. The technical staff of Energy Resources Engineering laboratory, Mr. Kosukegawa had important role in providing the necessary equipment for conducting the field tests. Besides my advisor, I would like to acknowledge the rest of my thesis committee for their time and also insightful comments for improving the current work: Prof. Tadao Imai, Prof. Tsukasa Ohba and Prof. Makoto Tago.

I was very lucky to have two Iranian collogues during my Ph. D. studies in Japan. Prof. Jalilinasrabadi supported me in different levels of my life in Akita City, covering all the range from personal to academic and technical aspects. My dear fiend Mr. Mohammadzadeh Bina helped me a lot and I am really thankful.

I had the chance to find new friends for the last 3 years; I am really thankful for their help and support to have a better life in Japan. Finally I would like to thank my Father, Mother and Sisters for their care and love; this work is dedicated to my Family.